AA.
2018
2019

Politecnico di Milano

School of Industrial and Information Engineering

Master degree in Materials Engineering and Nanotechnology

In collaboration with Institut National Polytechnique de Toulouse

Systematic characterization of the ageing process of PEDOT

Correlation between chemical and electronic degradation

Supervisor: Prof.ssa Chiara BERTARELLI

Supervisor at INP-ENSIACET: Nicolas CAUSSE

Author: Amedeo PEZZOLI

ID.905882

Academic Year: 2018-2019

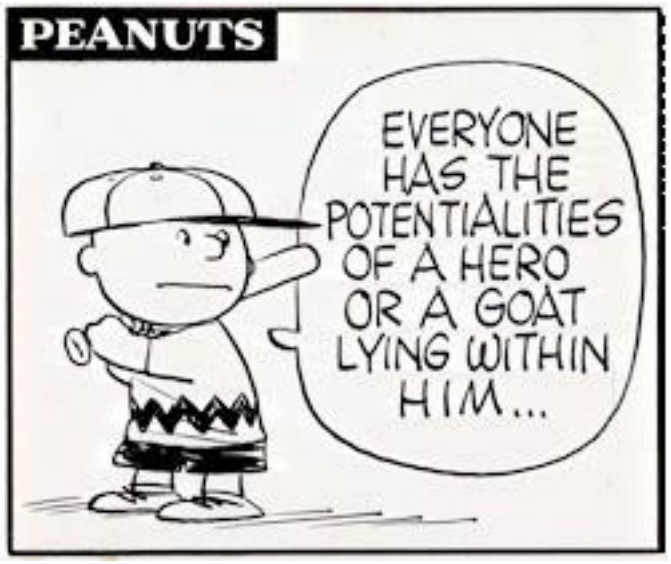

Charlie Brown – Charles M. Schulz

Acknowledgements

I would like to thank my colleagues Milad, Nicolas, Olivier, Brigitte, Hugues and Constantin at Institut National Polytechnique de Toulouse for the opportunity of working with them, their professionality and their help in achieving the results reported in this thesis. My family and my girlfriend Daniela, who never let me alone during my period abroad. My flatmate Alessandro, who won my fantasy football league for me while I was away. The European Union that, in the darkest moment in recent history, where divisions and nationalism are rampaging, allows us students to discover the world and open our minds through the Erasmus program.

Table of Contents

List of figures **5**

List of tables **7**

Abstract **8**

Sommario **8**

Keywords **9**

Sintesi estesa **10**

Chapter I: Introduction **15**

I.1.Inception of conductive polymers 15

I.2.Thesis 15

I.3.Objectives 16

I.4.Characterization choices 16

Chapter II: PEDOT, an overview **17**

II.1.Polymer conductivity 17

II.2.Polythiophene (PT) 17

II.3.First synthesis and polymerization reaction 18

II.4.Structural characteristics 19

II.5.Deposition-application: reciprocal influences 20

II.6.Ageing 25

Chapter III: Experimental section **27**

III.1.Deposition 27

III.2.Rinsing and storage 28

III.3.Analysis schedule 29

III.4. Schedule construction 29

III.5.Characterization 30

Chapter IV: Results and discussion **33**

IV.1.Profilometry 33

IV.2.Microscopy 33

IV.2.1.Optical microscopy 33

IV.2.1.1.$FeCl_3$ temperature effect 35

IV.2.1.2.N_2 flow rate effect 36

IV.2.1.3.Time effect 37
IV.2.2.AFM 38
IV.2.3.SEM 39
IV.2.4.EDS 41
IV.2.5.Microscopy conclusions 42
IV.3.Conductivity 43
IV.3.1.Time evolution 43
IV.3.2.Daily comparison 47
IV.4.Raman spectroscopy 48
IV.4.1.Acquisition optimization 48
IV.4.2.Raman spectroscopy of PEDOT 49
IV.4.3.Raman spectroscopy of impurities and contaminants 50
IV.4.4.Raman of PEDOT 52
IV.4.4.1.Low wavenumbers 52
IV.4.4.2.High wavenumbers 55
IV.4.5.Raman conclusions 63
Chapter V: Conclusions and perspectives 65
Bibliography 69

List of figures

Figure 1. The Diaz mechanism: a series of oxidation and deprotonation steps leading to the oxidative polymerization of conjugated PEDOT(27) 18
Figure 2. PEDOT's benzoid and quinoid structures (42) 20
Figure 3. VPP process involving (a) deposition of the oxidant solution (onto the substrate, black) commonly containing an Fe^{3+} salt in a solvent (typically an alcohol such as ethanol) with possible additives, (b) exposure of said oxidant to monomer vapor at a given temperature (T) and pressure (P), where oxidant/monomer is transported/condensed at the interface to initiate polymerization, and (c) washing away excess oxidant and monomer to yield a CP thin film(72) 21
Figure 4. Demonstrations of the advantages of oCVD. Conformality of micron-sized trenches in silicon coated with conductive PEDOT by (a) spin-casting $Fe(III)Cl_3$ and EDOT monomer, followed by in situ polymerization, (b) oCVD using $Fe(III)Cl_3$ as the oxidant, and (c) oCVD using the $CuCl_2$ as the oxidant. The oCVD coatings are clearly more conformal. The film morphology is dependent upon the choice of oxidant, with CuCl2 deposited PEDOT showing more uniform thickness between top and bottom of the trench(43) 22
Figure 5. Standard reactor configuration for oCVD, showing the substrate above the sources for oxidant and monomer. Films form as oxidant evaporates and reacts with EDOT monomer(70) 23
Figure 6. Schematic representation of the 10x10 silicon substrate after deposition. KAPTON® is used to provide a thickness step for profilometry measurements 27
Figure 7. Optical micrographs of all the samples immediately after deposition. a) 175-10 A-NR b) 175-10 A-R c) 200-10 A-NR d) 200-10 A-R e) 240-10 A-NR f) 240-10 A-R g) 175-50 A-NR h) 175-50 A-R i) 175-100 A-NR l) 175-100 A-R. Scale: 4 µm 35
Figure 8. Time evolution of 175-10 A-NR at Day 0(a), Day 1(b), Day 2(c) and Day 90(d). Scale: 4 µm 37
Figure 9. Set of reactions responsible for dopant neutralization in PEDOT thin films deposited via oCVD with $FeCl_3$ as oxidant(68) 37
Figure 10. AFM micrograph of 175-10 A-NR 38
Figure 11. AFM micrograph of 175-10 A-R 38
Figure 12. 3D rendering of figure 10. 39
Figure 13. SEM micrographs of: 40
Figure 14. EDS micrographs of 175-10 A-NR for a) Oxygen; b) Iron; c) Sulphur; d) Silicon. 42
Figure 15. Conductivity evolution for non-rinsed samples 43
Figure 16. Conductivity evolution for rinsed samples 45
Figure 17. Day 20 conductivity for all investigated samples 47
Figure 18. Day 90 conductivity for all investigated samples 47
Figure 19. Schematic of a PEDOT molecule with nomenclature for C-atoms identification(117) 49
Figure 20. Raman spectrum of PEDOT. Reported wavenumbers are related to the bands attributed to PEDOT(37) 49

Figure 21. Raman spectrum of pure Fe(III)hydroxide pigment provided by Winsor and Newton. λ_0 = 647,1 nm; integration time = 4s; accumulations = 100(122) 50
Figure 22. Raman spectra of Fe_3O_4 Magnetic Nanoparticles collected using 0.35mW after exposure for 7 min to different laser powers: (A) 0.35mW; (B) 0.66mW; (C) 2.58mW; (D) 4.93mW; (E) 8.85 mW(125) 51
Figure 23. Raman spectra (785 nm) of goethite obtained with: (a) a Renishaw inVia Reflex Raman microscope using 40 mW at the sample (PD = $8*10^4 Wcm^{-2}$) and (b) a portable Raman DeltaNu using ($4*10^2 Wcm^{-2}$)(123).....51
Figure 24. Raman spectra of: I) hem1 obtained in different experimental conditions: (a) with a portable Raman DeltaNu (785 nm and PD = $4*10^2 W\ cm^{-2}$); (b) with a Renishaw inVia Reflex Raman microscope (785 nm and PD = $4*10^3 W\ cm^{-2}$) and (c) with a Renishaw System 3000 (514.5 nm and PD = $1.4*10^3 W\ cm^{-2}$). II) Raman spectra of hem2 obtained (a) with a Renishaw inVia Reflex Raman microscope at PD = $8*10^4 W\ cm^{-2}$ (operating at 785 nm), and with a portable Raman DeltaNu at low laser power where (b) and (c) are different spots (123).....51
Figure 25. Raman spectrum of a) $FeCl_3$ powder before employment in the polymerization; b) $FeCl_3$ powder after employment in the polymerization. Excitation wavelength = 532 nm; accumulation time = 5s; accumulations = 3 52
Figure 26. Spectrum of 175-50 A-NR, white optical domain. Excitation length = 532 nm; accumulation time = 5s; accumulations = 3.....52
Figure 27. Spectra of 200-10 N-NR, white optical domain. Excitation length = 532 nm; accumulation time = 5s; accumulations = 3.....53
Figure 28. Spectra of 200-10 N-R, white optical domain. Excitation length = 532 nm; accumulation time = 5s; accumulations = 3.....54
Figure 29. Spectra of 175-10 A-NR, brown optical domain. Excitation length = 532 nm; accumulation time = 5s; accumulations = 3.....55
Figure 30. I) From a to e: shift of the 1430 cm^{-1} band when increasing the temperature from 47 °C to 100 °C(75); II) shift of the same band when increasing the temperature from 100 °C to 180 °C(38,70) 56
Figure 31. Spectra of 200-10 N-NR, white optical domain. Excitation length = 532 nm; accumulation time = 5s; accumulations = 3.....57
Figure 32. Spectra of 200-10 N-R, white optical domain. Excitation length = 532 nm; accumulation time = 5s; accumulations =.....58
Figure 33. Spectra comparison between 175-10 A-NR and 175-10 A-R at a) Day 0; b) Day 20; c) Day 90.....60
Figure 34. Spectra comparison between 175-10 A-NR and 175-10 N-NR at a) Day 20; b) Day 90.....62

List of tables

Table 1. Investigated values for the process parameters 27
Table 2. Complete list of the deposited films. 28
Table 3. List of days when resistance measurement and Raman spectroscopy were performed 29
Table 4. Thicknesses (nm) of the PEDOT films in different conditions. Standard deviation ~10% 33
Table 5. Comparison of the shift of the main bands of PEDOT and their attribution. (29,37,119) 50

Abstract

Poly(3,4-ethylenedioxythiopene)(PEDOT) is the conductive polymer attracting the most attention from researchers in the last years, as its electronic, mechanical and chemical properties allow its application in several fields, from biomedicine to thermoelectricity. Being insoluble, completely dry techniques are necessary for thin films' deposition; among these, oxidative Chemical Vapor Deposition (oCVD) has received a lot of interest in the recent past. Its main drawback is, however, the employment of oxidants, $FeCl_3$ in this work, that are unstable under atmospheric condition. The same oxidants also act as dopant in the deposited thin film, doping being necessary for PEDOT to show metallic properties. The long-term stability of these films has never been subject of an in-depth study, a necessity for the application in devices with an extended life expectancy. This work aims to find the best deposition conditions for oCVD PEDOT and to characterize with a systematic approach its electronic and chemical properties in a time frame of 90 days, finding their cause-effect correlations. The influence of two different process parameters (oxidant temperature and carrier gas flow rate) is studied, in parallel with the one of a post-deposition rinsing cycle and of storage in oxidative atmosphere (air) and neutral atmosphere (argon). The electronic performance of the samples is evaluated through sheet resistance measurements and its evolution is correlated to their chemical properties which are investigated via Raman spectroscopy.

Sommario

Il poly(3,4-ethylenedioxythiopene)(PEDOT) è il polimero conduttore che ha attirato di più l'attenzione dei ricercatori negli ultimi anni, sicchè le sue proprietà elettriche, meccaniche e chimiche ne permettono l'applicazione in diversi campi, dalla biomedicina alla generazione di energia termoelettrica. Data la sua insolubilità, la deposizione di film sottili è particolarmente complicata e richiede tecniche che non facciano uso di solventi; tra queste la oxidative Chemical Vapor Deposition (oCVD) ha ricevuto molto interesse nel recente passato. La sua falla più grande, tuttavia, è quella di necessitare di agenti ossidanti, $FeCl_3$ in questo lavoro, i quali agiscono anche, una volta completata la deposizione, come dopanti all'interno del film sottile, una necessità se si vuole ottenere PEDOT dal carattere metallico. La longevità di questi sistemi molto complessi non è mai stata studiata nel dettaglio, nonostante sia fondamentale conoscerla se si vuole procedere con l'applicazione del materiale in dispositivi con un'aspettativa di vita medio-lunga. Questa tesi si pone l'obiettivo di trovare le condizioni migliori per la deposizione di film sottili di PEDOT tramite oCVD e di procedere a una caratterizzazione sistematica delle proprietà elettriche e chimiche del materiale in una finestra di tempo di 90 giorni, trovando i rapporti causa-effetto che le legano. L'influenza di due parametri di processo (temperature dell'ossidante

e flusso del gas di trasporto), in parallelo con quella dell'applicazione di un ciclo di lavaggio post-deposizione e di stoccaggio in atmosfera ossidante (aria) e neutra (argon). La performance elettrica dei campioni è valutata tramite la misurazione della resistenza superficiale ed è correlata alle proprietà chimiche, misurate a loro volta tramite spettroscopia Raman.

Keywords

PEDOT

oCVD

$FeCl_3$

Thin film

Long-term ageing

Raman spectroscopy

Conductivity

Sintesi estesa

Il PEDOT è un polimero che al suo stato pristino ha proprietà semiconduttive; quando viene depositato in forma di film sottile, possono essere introdotti dei dopanti, allo scopo di ottenere film dal comportamento metallico, ossia conduttivi. Il termine "dopanti" è prestato dalla chimica dello stato solido ma questi sono, in realtà, coppie redox che hanno lo scopo di ossidare o ridurre le catene del polimero, aumentandone la densità di portatori di carica. Nel caso in studio in questa tesi, questi sono contro-anioni $FeCl^{4-}$, che attirano a se un elettrone della catena, creando una buca e favorendo la riorganizzazione della struttura del PEDOT da benzoide (non conduttiva) a quinoide (conduttiva) (Figure 2) la quale è caratterizzata da una superiore coniugazione, ossia da una migliore sovrapposizione degli orbitali π della catena, che aumenta la mobilità dei portatori di carica. Questo duplice effetto positivo è quindi alla base dell'applicazione di questo polimero in applicazioni che richiedono conduttività elevate. Si crea quindi un problema intrinseco di questi dispositivi: nonostante il PEDOT sia in sè molto stabile, la presenza di questi contro-anioni è fondamentale per le sue proprietà ma essi non sono, a loro volta, stabili qualora siano presenti in contemporanea ossigeno e acqua nell'ambiente. Essi vanno incontro alle reazioni presentate in Figure 9, dove si vede come vengano neutralizzati formando idrossido di ferro(II) e cloro molecolare. La liberazione di un elettrone va inoltre a neutralizzare le buche presenti lungo la catena, con un'ulteriore diminuzione della conduttività. Si può notare inoltre come la presenza residua di $FeCl_3$ dalla reazione abbia un effetto catalitico per queste reazioni. Lo studio dell'effetto del processo di lavaggio con metanolo serve proprio a quantificare l'efficacia nel contrastare questo ultimo effetto, mentre l'analisi dell'evoluzione dei campioni in atmosfera neutra serve a valutare quanto i film si degradino spontaneamente e quanto si degradino per via delle interazioni con l'ambiente esterno appena descritte. Idealmente, si vuole trovare una degradazione nulla in queste condizioni, ad attestare una stabilità perfetta dei film. Prima di procedere con la caratterizzazione è stato necessario ideare l'intera analisi, visto che prima d'ora non era mai stato svolto uno studio sulla degradazione del PEDOT in condizioni naturali, ma solo in condizioni di invecchiamento accelerato dalla temperatura. È stato creato un calendario (Table 3) che permettesse la comparazione dei film nonostante fossero stati deposti in giornate differenti e sono state pensate le tecniche da utilizzare al fine di ottenere le informazioni necessarie: ai fini di trovare quali condizioni permettessero la deposizione di film sottili di PEDOT con le proprietà migliori, sono state usati il microscopio ottico, il Microscopio a Forza Atomica (AFM), il Microscopio Elettronico a Scansione (SEM) e, in parallelo a quest'ultimo, la spettroscopia EDX/EDS (Energy-dispersive X-ray spectroscopy), per valutare la loro morfologia, e misure di resistenza superficiale, per valutare la loro conduttività; ai fini di correlare l'evoluzione della conduttività con l'evoluzione del film a livello chimico-strutturale è stata utilizzata la spettroscopia Raman, che ci permette di

valutare l'evoluzione dei singoli legami molecolari. Gli spettri Raman della struttura benzoide e di quella quinoide sono differenti, seppur lievemente, e ciò permette la loro identificazione e relativa quantificazione.
La deposizione è stata svolta su wafer di silicio da 10 cm di diametro, separati in quattro spicchi così da permettere di avere quattro diversi campioni da ognuno. Così facendo, è stato possibile avere da una singola deposizione tutti i campioni necessari per investigare ognuna delle condizioni di deposizione prescelte, potendo partire da caratteristiche comuni per diversificare le condizioni di lavaggio e quelle di stoccaggio. Una lista completa dei campioni e delle loro caratteristiche è disponibile in Table 2.
I risultati hanno mostrato morfologie molto diverse per le varie condizioni di deposizione (Figure 7): un film trasparente omogeneo di PEDOT è stato deposto in tutte le condizioni (eccezion fatta per la temperature dell'ossidante di 240 °C, troppo calda e quindi caratterizzata da suo eccessivo quantitativo) e risulta sormontato da "isole" colorate di dimensioni fortemente variabili. Tali isole risultavano poi venire rimosse efficacemente dal processo di lavaggio; ricordando che il PEDOT non è solubile in alcun solvente, tanto meno in metanolo, si intuisce come tali conformazioni non siano composte da PEDOT, se non parzialmente. L'interesse si è quindi concentrato sull'identificare la composizione di esse e sul giustificarne l'esistenza. Dall'analisi AFM è stato possibile scoprire (Figure 12) che le isole sono caratterizzate da uno spessore di molto superiore a quello del film omogeneo di PEDOT sottostante e che hanno una natura viscoelastica, visibile dai segni di trascinamento in Figure 10. Le immagini SEM hanno evidenziato come la loro morfologia sia diversa (Figure 13) da quella del film di PEDOT sottostante ma non solo: quella dei film lavati con metanolo risulta molto più fine rispetto a quelli che non hanno subito lo stesso trattamento e si avvicina molto a quella del film di $FeCl_3$ puro deposto come riferimento. Questo porta alla conclusione che il film omogeneo di PEDOT sia deposto in seguito alla reazione con dell'ossidante che ha raggiunto il substrato prima rispetto al monomero, avendo il tempo di creare una copertura uniforme. A quel punto l'EDOT comincia ad arrivare al substrato, dove reagisce per formare il polimero, sino a formare un film sottile. Mentre ciò accade, altro $FeCl_3$ continua a raggiungere la superficie del film ma, essendo EDOT presente nell'atmosfera del reattore, non ha tempo di organizzarsi in maniera ordinata e finisce per formare le isole descritte in precedenza. Tali isole non risultano ricche di PEDOT perchè vi è $FeCl_3$ in eccesso, il quale finisce col non reagire e, una volta estratto dal reattore, attira a sè l'umidità presente nell'aria, data la sua natura fortemente igroscopica (visibile sotto forma di gocce azzurre in Figure 8a). Sempre nella stessa figura si vede come nel giro di due giorni tali gocce scompaiano, lasciando spazio alle isole marroni menzionate prima (comunque già presenti anche immediatamente dopo la deposizione). A conferma di questa analisi, in Figure 14 sono presentate delle micrografie EDS, dove si vede come le isole siano ricche in ferro e ossigeno, mentre non contengono tracce di zolfo, il quale, essendo presente solo nel PEDOT, chiarisce la loro natura non polimerica. Questa analisi è stata svolta per sottolineare come sia necessaria una rivalutazione del metodo di

introduzione dell'ossidante nel reattore, così da permettere la deposizione di film sottili già dalle proprietà perfezionate, eliminando la necessità dello step di lavaggio, non solo rendendo più facile e veloce il processo, ma anche permettendo ad un fabbricatore su larga scala di non dover utilizzare solventi pericolosi per l'ambiente.
Passando all'analisi della prestazione elettronica, si può notare come un alto rapporto EDOT/$FeCl_3$ (Table 2) sia desiderabile per avere una conduttività superiore. Questo è dovuto al fatto che si creano film più sottili composti da catene più lunghe, piuttosto che da catene corte che limitano la lunghezza di coniugazione e quindi la mobilità dei portatori di carica. La conduttività più alta misurata è di 264 S/cm, bassa se comparata con quelle di PEDOT prodotto con altre tecniche, ma bisogna considerare che l'obiettivo dello studio non era quello di ottenere un valore alto, bensì di valutarne l'evoluzione. Tale evoluzione è proprio il fulcro della discussione svolta attorno a Figure 15 e Figure 16:

- i film non sottoposti a lavaggio stoccati in aria incorrono in un forte degrado dopo soli 10 giorni
- quelli non lavati stoccati in atmosfera neutra resistono fino al giorno 20, per poi mostrare un degrado improvviso ma più ridotto, per poi tornare stabili dal giorno 45 in poi
- quelli lavati resistono anche loro fino al giorno 20 ma poi incorrono in un drastico degrado, ancora superiore rispetto a quelli non lavati, indiscriminatamente dalla loro atmosfera di stoccaggio
- guardando Figure 17 si vede come i film non lavati stoccati in atmosfera neutra siano i migliori dopo 90 giorni per ognuna delle condizioni di processo investigate.

Questi trend sono attesi, considerando le conoscenze trasmesse da alcuni studi sul degrado accelerato del PEDOT e dei meccanismi di degrado presentati in Figure 9, tuttavia non è facile spiegare perchè i film stoccati in atmosfera neutra degradino comunque e tantomeno perchè quelli lavati con metanolo soffrano un degrado più intenso.
Viene in soccorso la spettroscopia Raman: guardando Figure 32 si può vedere come la banda a 1312 cm^{-1} aumenti di intensità col passare dei giorni. Essa non è relativa a PEDOT, substrato o altre impurità conosciute, nè può essere attribuita con certezza. Essa è ritenuta responsabile dell'alto degrado di questi campioni ma ulteriori analisi sono necessarie.
Facendo un passo, indietro, è stata analizzata tramite spettroscopia Raman, la zona di spettro tra 100 cm^{-1} e 500 cm^{-1}, dove gli ossidi di ferro hanno le loro bande. In seguito a una approfondita ricerca, gli spettri dei principali ossidi sono stati trovati (da Figure 21 a Figure 24), fatta esclusione per $Fe(OH)_2$. Essi sono stato comparati con gli spettri ottenuti in questa tesi per la polvere di $FeCl_3$ e per questa stessa polvere, però dopo il suo utilizzo nel reattore (Figure 25). Differenze significative sono state trovate tra la polvere pre- e post-reazione, significative di una alterazione dell'ossidante avanzato all'interno del suo crogiolo che in teoria non avrebbe dovuto reagire in alcun modo con l'EDOT nel reattore in quanto non sublimato. In ogni caso, le due bande caratteristiche di questa polvere post-reazione

non sono compatibili con alcuno degli ossidi di ferro presentati. Tali bande sono poi state trovate all'interno dello spettro Raman delle isole marroni discusse in precedenza e sono quindi state attribuite a $Fe(OH)_2$. Esse sono anche risultate presenti nei film lavati con metanolo, mentre non ne è stata trovata traccia all'interno dello strato trasparente di PEDOT dei film non lavati. Questo è indicativo del fatto che le isole marroni fungono da "centro di aggregazione" per $Fe(OH)_2$ nei film non lavati: l'idrossido prodotto dalla neutralizzazione dei contro-anioni $FeCl^{4-}$ evacua il film uniforme di PEDOT e per ridurre l'energia superficiale tende ad accumularsi attorno a queste strutture ricche di impurità. È noto infatti che il PEDOT ha caratteristiche idrofobe ed è quindi plausibile che tale idrofobia si traduca in una repulsione anche per $Fe(OH)_2$, un composto dalle caratteristiche ioniche simili ad H_2O. Per contro, nei film lavati con metanolo, questi centri di aggregazione non sono presenti, perciò $Fe(OH)_2$ non ha modo di aggregarsi e rimane presente in maniera uniforme in tutto il film, risultando visibile in Figure 28.

SI rivolge ora l'attenzione allo studio della parte di spettro tra 1200 cm^{-1} e 1700 cm^{-1}, dove il PEDOT ha le sue bande principali, la cui attribuzione è visibile in Table 5. Dallo studio della grande quantità di lavori disponibili in letteratura sulla spettroscopia Raman del PEDOT, è stato possibile capire l'effetto che la transizione da struttura quinode a struttura benzoide ha sullo spettro di un film sottile di polimero. Tale effetto consiste in un redshift della banda principale attorno a 1430 cm^{-1} (che è il risultato della somma di una banda intorno a 1410 cm^{-1} attribuita alla struttura quinoide e una a 1440 cm^{-1} attribuita a quella benzoide), accompagnato da un aumento dell'intensità ed un blueshift della banda a 1508 cm^{-1}, propria della struttura benzoide. Solo alcuni degli spettri ottenuti in questo lavoro vengono presentati, in quanto oggetto della discussione sono i trend comuni ai film con condizioni di stoccaggio o lavaggio comuni. In Figure 31 si può vedere quello di un film non lavato e stoccato in atmosfera neutra. Salta subito all'occhio come la banda principale sia molto spostata verso i 1440 cm^{-1} della banda della struttura benzoide, rispetto ad alcuni dei valori presentati in Table 5, a spiegare la scarsa conduttività già dal momento della deposizione dei film prodotti per questa tesi. Tale banda durante l'intera durata dello studio incorre in cambiamenti notevoli, con un progressivo raffinamento del picco, sintomo di una uniformazione dell'ambiente in cui vibrano i legami della banda stessa. Questo può essere spiegato se si considera che, con l'eliminazione progressiva dei contro-anioni si ha un'uniformazione delle catene verso la struttura benzoide, con un conseguente numero sempre maggiore di legami C=C che vibrano alla stessa frequenza. Una differente spiegazione è data dalla possibile reazione nel tempo degli oligomeri presenti in superficie, a formare catene più lunghe a struttura benzoide. Questo non è improbabile se si va a vedere il confronto diretto tra film non lavato e lavato presentato in Figure 33: si può vedere come i due spettri si assomiglino sempre di più con il passare dei giorni. Se si considera che con il lavaggio in metanolo gli oligomeri superficiali sono eliminati insieme alle altre impurità, si capisce come sia logico pensare a una eliminazione progressiva di tali oligomeri nel film non lavato, a favore della formazione di più stabili catene lunghe, dovuta

a una polimerizzazione attivata dal poco $FeCl_3$ intrappolato nei nanopori del film di PEDOT e dalla temperatura. Guardando alla comparazione tra film stoccati in aria e film stoccati in argon di Figure 34, si può invece notare come non solo la banda centrale subisca un redshift minore nei film stoccati in atmosfera neutra, coerentemente con il loro degrado più ridotto, ma anche come tutte le bande risultino generalmente più larghe, sintomo della presenza di diversi ambienti di vibrazione per uno stesso legame, che causano la presenza di frequenze leggermente diverse con conseguente allargamento dei picchi. L'esistenza di questi diversi ambienti è attribuita alla ridotta neutralizzazione dei contro-anioni in atmosfera neutra, con conseguente distorsione delle catene caratterizzate da una natura parzialmente benzoide e parzialmente quinoide. Tutto ciò è coerente con le misure di conduttività analizzate al capitolo IV.3.

Questa tesi ha il potenzialep per diventare un riferimento nell'ambito della caratterizzazione elettrochimica del PEDOT, visti i suoi molteplici caratteri di novità. Queste novità aprono anche alla sua citazione in ricerche future sulla durabilità di dispositivi basati sul PEDOT. La necessità di studiare più nel dettaglio alcune tematiche qui solo presentate come evidenza sperimentale, senza possibilità di approfondimento, dimostra la possibilità di sviluppare nuove ricerche utilizzando questa come punto di riferimento.

Chapter I: Introduction

I.1. Inception of conductive polymers

Conductive polymers' (CPs) history starts in the 1950s with the synthesis of charge-transfer complexes salts, in which the polymer molecules are paired with a halogen. In order to witness the first all-polymeric conductor, the scientific community had to wait Bolto *et al.*, in 1963, year in which they released a paper describing the never before seen conductive properties of polypyrrole(1); pyrrole black (later known as polypyrrole) had been known since 1916, when it was first reported as a deposit on the walls of pyrrole containers. Another early discovered conductive polymer is polyacetylene, a synthesis of which has been known since 1958 thanks to Giulio Natta, which made use of Ziegler-Natta catalysts; the material would go unnoticed until the 1970s due to its insolubility and unremarkable properties. As a third example, poly(p-phenylene sulfide), now well known for its conductivity, had been commercialized since 1970 under the name Ryton® as a thermoplastic, with no regard to its electrical properties. These three examples shed light on the fact that polymeric materials were widely regarded as insulators and not deemed necessary in the still green electronic industry, therefore their electrical properties were often overlooked. One could say that conductive polymers are "rediscovered" materials, their role in the field of electronics being discovered much after their first synthesis. To testimony this, Hideki Shirakawa, the pioneer of conductive polymers chemistry together with Alan J. Heeger and Alan G. MacDiarmid, received the Nobel Prize in chemistry in the year 2000, for the work they conducted starting from 1977(2,3). As mentioned above, the first real effort in characterization of the electrical properties of a conductive polymer was conducted on polyacetylene, which attracted lots of attention from researchers thanks to its high conductivity values, up to 38 S/cm when doped with iodine(3) and 560 S/cm with AsF_5(2) by Shirakawa's group. At the time much effort was devolved to the formation of as ordered and oriented films as possible: a primitive ordering method like tensile stretching of as-prepared cis-rich films already provided an order of magnitude increase in conductivity, lighting up the scientific interest. In the coming years, though, polyacetylene had been relegated as a scientific research topic, since its very limited shelf life, due to its tendency to oxidize, made it useless for most applications.

Interest had shifted to the search of new, more stable, conductive polymers and this sparked the research on polythiophenes, a new group of polymers based on the thiophenic ring, of which poly(3,4-ethylenedioxythiopene) (PEDOT) is member.

I.2. Thesis

This thesis interjects itself in this still fresh field of research: indeed, while PEDOT:PSS has been widely studied and applied in many different fields, thanks to its great thermoelectric properties(4), transparency and antistatic capabilities, from transparent electrodes(5,6) to

thermoelectric generators(7) and photovoltaic cells(8). PEDOT as a standalone material has not been studied as deeply: its well-known insolubility makes its application less straightforward, which explains why it has been paired with PSS in the first place. Thanks to the invention of new deposition processes which do not require a solvent, *e.g.* CVD in all its facets, PEDOT is on the rise and is proving more and more to be a viable material for organic conductive systems. Among the numerous papers discussing its electronic properties, there is a distinct lack of discussion about its longevity and chemical reactivity in application conditions; this thesis aims to fill this void, providing an extensive and systematic characterization of the electrical conductivity and chemical composition of chlorine doped thin films of PEDOT deposited via oxidative Chemical Vapor Deposition (oCVD) on silicon wafers. The ageing period spans 3 months and it has been accomplished with conductivity measurements, profilometric measurements, Raman scattering analysis and optical, SEM, AFM and EDS imaging. To provide further insight, the influence of storage atmosphere and methanol rinsing is studied, thanks to a carefully organized deposition and characterization program.

I.3.Objectives

The objective of the study was to quantify the evolution of conductivity of Cl^- doped PEDOT thin films deposited via oCVD on Si wafers during a period of 90 days, correlating it to changes in the deposition parameters, storage conditions and structural and chemical changes that the samples may undergo over time. An additional objective was to establish a correlation between conductivity and Raman spectra, with the aim of providing an intuitive way of determining which film would have the best electrical performance from the analysis of the RAMAN spectrum.

I.4.Characterization choices

In order to understand the changes that the films would go through, it was necessary to use characterization methods that would allow for their morphological, structural, chemical, compositional and electrical description. For the first two, optical, SEM and AFM imaging was used to provide a complete vision of the film at various scales, paired with the profilometry measurements; all of this was also to assess the influence of different deposition parameters. For the chemical description, Raman scattering analysis was used, even though the correlation between the spectra and the final properties is not universally agreed upon. EDS was used to assess the compositional uniformity of the films along the surface: this is especially important since the oCVD deposition process employed, proved unable to deposit uniform layers. To quantify the electrical conductivity, a 4-point probe was used, to obtain the macroscopic conductivity of the thin film, in order to not factor in the local lack of uniformity.

Chapter II: PEDOT, an overview

II.1. Polymer conductivity

Before delving into the discussion regarding specific conductive polymers (CPs), it is wise to describe their mechanism of conduction, which is based on conjugation. CPs conductivity derives from the alternation of single and double bonds: this arrangement induces what is referred to as conjugation, a condition in which the main chain carbons' p orbitals overlap with one another across the σ bond between them. This promotes delocalization of the π electrons along the whole extension of the conjugation (called conjugation length); effectively, these electrons do not belong to any specific carbon atom or bond, they have high mobility and therefore promote conductivity. Conjugation length becomes the main factor influencing conductivity. For conjugation to exist and extend it is mandatory that every contiguous atom possesses a p orbital perpendicular to the plane of the molecule, therefore it is not instrumental to have perfect single-double/triple bond alternation, but it is sufficient for an atom along the chain to have a lone pair in a p orbital positioned in the correct plane, *e.g.* oxygen in PEDOT.

II.2. Polythiophene (PT)

Embraced the conductive polymers revolution but let down by the failure of polyacetylene, the scientific community began searching for a new polymer that could succeed where its predecessor failed, allowing for a successful commercialization; the candidates were polyaniline, polypyrrole and polythiophene. Since their inception in 1980 by Yamamoto *et al.*(9), oligothiophenes and, later, polythiophenes attracted a lot of attention from the scientific community thanks to their stability, electronic properties and ease to manufacture. A strong interest has been sparked by the newly born field of disposable and flexible electronics and by the increasing interest in green energy in the last decade(10-13). Application in these areas had very specific requirements that traditional semiconductors could not answer, such as flexibility, transparency and, most importantly, limited cost. Among the known conductive polymeric materials, *i.e.* polyacetylene, polypyrrole and polyphenylene, polythiophene showed the most promise, thanks to a long list of advantages, including but not limited to high electrical conductivity, thermal and chemical stability, properties tunability and accessible manufacturing(14). Undoped polythiophene conductivity can vary from 2 to 5 eV, depending on the extension of the conjugation and the nature of the substituents on the backbone(14,15). This wide bandgap variation is the cause of a peculiar optical property of PT, as well: its emission wavelength when at the excited state varies from green to red, allowing for applications where coloration is necessary. When doped, instead, the formation of two polaronic states between the π and π* bands, leads to absorption in the IR region and transparency(16,17). The tunability of

the material properties lead to the create of multiple derivatives, where one of the carbons of the thiophenic ring is attached not to a hydrogen but a side group R of varying nature. A very deep review of these materials has been carried out by Nielsen and McCulloch(18). Among them, the focus of this thesis is poly(3,4-ethylenedioxythiophene) (PEDOT).

II.3.First synthesis and polymerization reaction

A dialkoxy substituted PT, precursor of PEDOT was first synthetized by Daoust and Leclerc(19), while the synthesis of bicyclic ethylenedioxythiophenic polymer was carried out via electrochemical transfer to the polymer by Heywang *et al.* and chemical polymerization by Jonas *et al.* at Bayer Corporate Research laboratories in 1992(20,21). Even if similar to the dialkoxythiophenes subgroup, these ethylenedioxythiophenes behaved differently: they showed remarkable conductivities and better longevity, making quickly clear that a "tremendously stable, highly conductive polymer"(22) was possible. The polymerization of EDOT has a mechanism similar to the one for pyrrole proposed by Diaz(23-25) and follows a series of oxidation and deprotonation steps(26), visible in Figure 1(27). The first step is the oxidation of the monomer, generating a radical cation characterized by multiple resonance forms. Two of these then combine forming a neutral dimer. Here the role of the substitution in 3,4-position comes into play: β is blocked, the dimer once again oxidizes, forming a radical which can form bonds only in positions 2,5. This grants the chain improved planarity that helps the formation of π-conjugated oligomers; said conjugation decreases the oxidation potential and this favors the growth of the already-formed chains over the formation of new ones. The final neutral chains are further oxidized with creation of a positive charge along the backbone, one every three of four chain segments. A counter-anion binds to the chain to balance this charge(27). The role of the oxidant is crucial, therefore its oxidation strength is an important factor when specifying the polymerization reaction condition: it has to be high enough to drive the reaction but, at the same time, it can not be too much, since that would cause undesirable bond cleavage in the monomer, leading to imperfections disrupting conductivity(28).

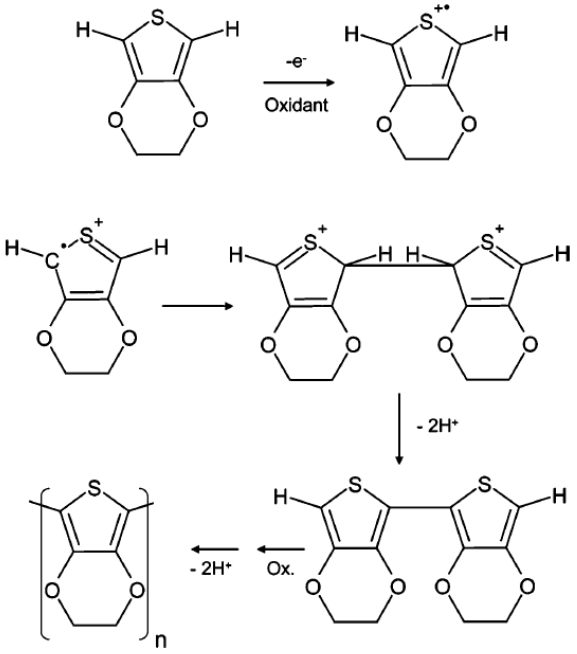

Figure 1. The Diaz mechanism: a series of oxidation and deprotonation steps leading to the oxidative polymerization of conjugated PEDOT(27)

II.4.Structural characteristics

The charges introduced during the polymerization are not sufficient to grant as-deposited poly(3,4-ethylenedioxythiopene) sufficient conductivity: it has a bandgap of around 1.6 eV(29) which, although low compared to other members of the polythiophene group, is still too high to allow a conductive behavior. To mend this, it is commonly doped during film deposition, with maximum reported conductivities way above 1000 S/cm. It has been reported that at an increase in doping percentages corresponds an increase in conductivity, thanks to the incorporation of counter ions along the polymer backbone: these do not impair electron mobility, since they do not interrupt conjugation, while increasing the number of carriers. Its particularly low bandgap has proven advantageous also for electro-optical applications: unlike most polymers that, once doped, see their bandgap fall into the visible region and become opaque, PEDOT turns transparent, making it viable for usage in organic photovoltaics(30), as transparent antistatic coating(31) and technologies where transparent electrodes could be useful, in general. As mentioned, unlike other polymers, PEDOT's backbone is linear, due to the presence of the alkylenedyoxy substituents in positions 3 and 4, which prevent β coupling, and of the oxygen atoms, which stabilize the polymer when oxidized and act as electron donors(29). The aforementioned properties stem from the ones of EDOT, in particular its low oxidative potential, wide anodic potential, molecular symmetry and low steric inhibition(32). These factors explain why PEDOT is very stable(33) and insoluble in most solvents.

Going back to PEDOT doping, since Shirakawa's group findings on doping of polyacetylene in 1977(2), it has been clear that, in order to have a conductive polymer, it would be necessary to alter its energetic equilibrium: these materials, in their pristine state, have a wide gap between Highest Occupied Molecular Orbital (HOMO) and Lowest Unoccupied Molecular Orbital (LUMO), limiting the number of carriers available to conduction. Doping of PEDOT, first reported in 1994(22), can be both n-type or p-type(34-36), unlike any other polymer but the material's reduced form (present when n-type doped) is not stable in humid and oxygenated environments, making it useless for most applications. Its other drawback is the lower conductivity caused by the presence negative polarons alone as charge carriers, while the n-type doped form possesses positive polarons, bipolarons and free holes(34). The term doping is borrowed from condensed matter physics and consists of the introduction along the chain of atoms or molecules that act as an oxidant in a redox pair with the main chain: they attract electrons, becoming counter-anions, while a positive charge is created along the chain; this is beneficial because conduction in PEDOT is carried out by positive charge carriers, as they have much higher mobility when compared to electrons. The counter-anions also create energy states in the previously forbidden energy gap, effectively reducing it and allowing for a further increase in the number of carriers. Doping is not an easy procedure: first of all, problems of steric hindrance and stability (internal energy) limit the doping percentages (number of dopant atoms per unit chain

length, around 35%); second, doping tends to be inhomogeneous, with strongly doped sections being followed by almost pristine ones, lowering overall performance; third, counter-anions are prone to neutralization in certain conditions, degrading over time the electrical conductivity of the sample; fourth, the choice of the dopant makes a big difference with regards to final properties, with conductivity variations even of several

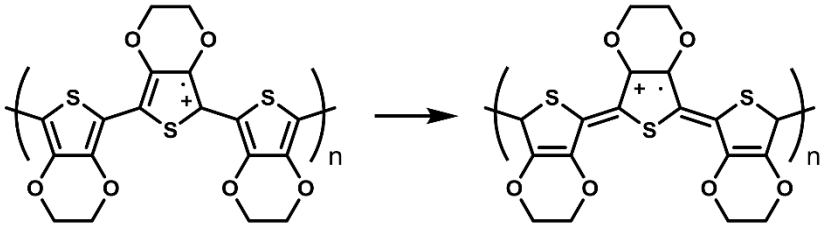

Figure 2. PEDOT's benzoid and quinoid structures (42)

orders of magnitude. For this very reason, many studies have focused on doping with different dopants(35,37), using different oxidants during deposition(38), with multiple dopants(39), dopant exchange after deposition(40) or the synthesis of PEDOT copolymers(41).

In PEDOT, doping induces a transition from benzoid structure to quinoid structure (Figure 2)(42): this contributes to the extention of the conjugation length, critical to increase hole mobility and, consequentially, conductivity. Benzoid structure is typical of pristine PEDOT, which is only a semiconductor, while quinoid structure should, ideally, be the only structure present in metallic PEDOT, however this is impossible, due to the steric hindrance and internal energy problems mentioned above.

II.5. Deposition-application: reciprocal influences

Even if this research is focused on more theoretical aspects, it is worth mentioning some practical applications of poly(3,4-ethylenedioxythiopene), so the reader can comprehend the importance of the material. The applications have been strictly related to the deposition techniques available at the time, therefore they are presented together, each with their own limitations which pushed (and keep pushing) researchers to find alternative practices. In the history of PEDOT, insolubility has been the first big hurdle to overcome, causing more than a few problems to researchers trying to envision its application. Until the late 2000s, solution techniques (most notably spin coating) were the only methods known for a quick and reliable deposition of thin polymeric films. For this very reason, PEDOT:PSS, a polymeric mixture of ionomers, was developed. The spin coating solution is composed of EDOT monomer, dissolved in an aqueous polystyrene sulfonate solution and then an oxidant is added, promoting its polymerization to PEDOT. The result, once the oxidant is evaporated, is a uniform copolymeric thin film, with electronic properties worse than PEDOT (conductivity at most 10 S/cm(43)). Solved the solubility issues and able to make use of PEDOT's properties, technological applications followed swiftly. It was first used (and still is) for antistatic coatings in the movie/photography industry. Nowadays it is

also used as: a thermoelectric material (ZT~0,42) in composite thermoelectric generators(4,7,44-48); an electrolyte in polymer electrolytic capacitors; in composites in supercapacitor electrodes(49-52); in Organic PhotoVoltaics (OPVs) as a transparent electrode(53). In many other fields studies are investigating the usage of PEDOT:PSS, *e.g.* for molecule sensing(54,55), water filtration(56) or fuel cells(57,58).

Eventually, the necessity for standalone PEDOT arose, when thinner and more uniform films started to be required for more technological applications, more complex shapes had to be covered and nanostructured composites entered the scene. The race to so-called *in situ* PEDOT had started. Nowadays, *in situ* PEDOT polymerization can be carried out mainly in three ways: electropolymerization(59-61), Vapor Phase Polymerization (VPP)(62-67) and oxidative Chemical Vapor Deposition (oCVD)(27,30,38,40,41,68-71). Going into detail, electropolymerization, as devised by Diaz *et al.*(23) for polypyrrole, relies on the application of bias between two electrodes to extract electrons from the monomer, initiating the polymerization(72). It provides some control over film thickness, morphology and properties such as conductivity and can be used to produce nanocomposites with enhanced properties(73). Its main shortcoming is the necessity to adopt a conductive substrate, to which the solubility of the monomer in a solvent which also has to contain the desired anionic doping salt is added. The final film can show uniformity problems as well, if large scale production is required.

VPP and oCVD are the most popular ones in the family of chemical vapor deposition processes. Among the others, Plasma Enhanced CVD(74) and pulsed laser deposition(75) are somewhat used.

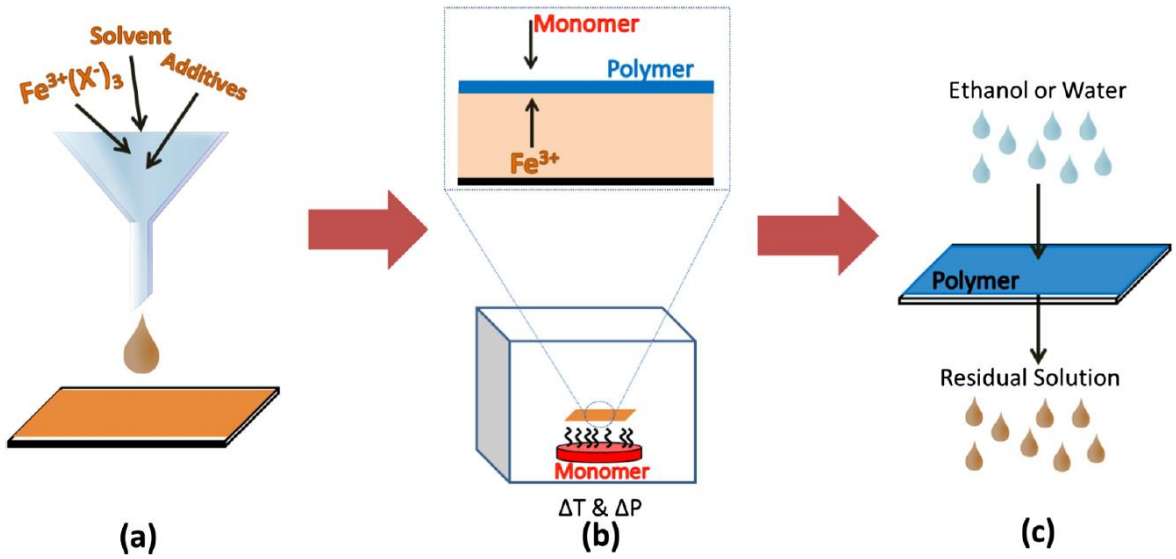

Figure 3. VPP process involving (a) deposition of the oxidant solution (onto the substrate, black) commonly containing an Fe^{3+} salt in a solvent (typically an alcohol such as ethanol) with possible additives, (b) exposure of said oxidant to monomer vapor at a given temperature (T) and pressure (P), where oxidant/monomer is transported/condensed at the interface to initiate polymerization, and (c) washing away excess oxidant and monomer to yield a CP thin film(72)

"Over the past decade, the VPP process has fast become a popular process by which to produce 'state of the art' ICPs for a host of different potential applications"(72). In VPP (Figure 3)(72), the polymerization occurs at the vapor-liquid interface between, where the

liquid component is an oxidant solution cast on the surface of the substrate, subsequently exposed to a monomer-rich atmosphere. A washing (rinsing) step is required to rid the thin film of the excess reactants. This is its main disadvantage: rinsing has to be carried out with some sort of solvent, from methanol to strong acids, in the case of PEDOT, and these can cause serious problems when handled, even more when they need to be disposed of. This causes problems when willing to apply VPP to an industrial level, even if it has large advantages, especially over electropolymerization: the procedure is simple and allows to utilize a variety of substrate-monomer combination; as long as the substrate can be cast

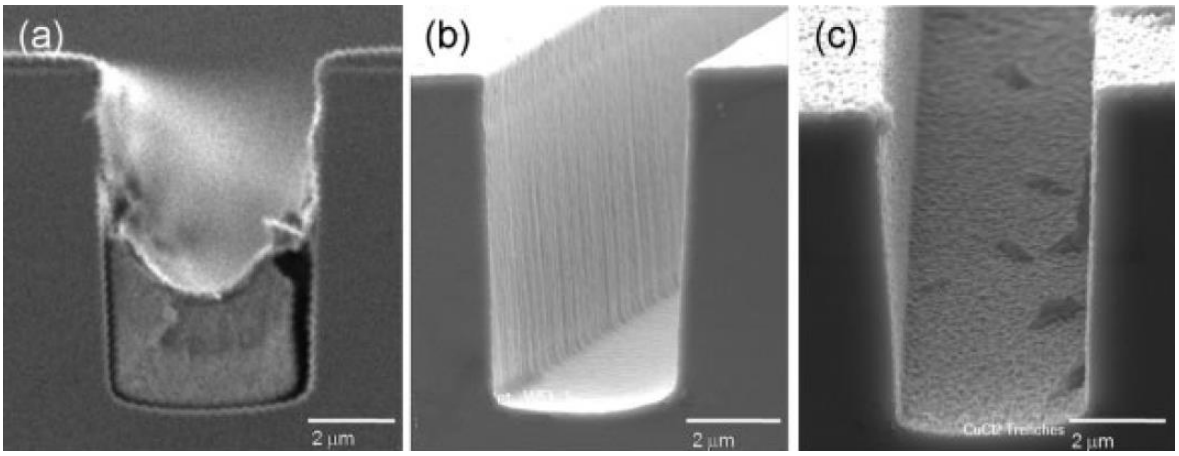

Figure 4. Demonstrations of the advantages of oCVD. Conformality of micron-sized trenches in silicon coated with conductive PEDOT by (a) spin-casting Fe(III)Cl_3 and EDOT monomer, followed by in situ polymerization, (b) oCVD using Fe(III)Cl_3 as the oxidant, and (c) oCVD using the $CuCl_2$ as the oxidant. The oCVD coatings are clearly more conformal. The film morphology is dependent upon the choice of oxidant, with CuCl2 deposited PEDOT showing more uniform thickness between top and bottom of the trench (43)

with the oxidant solution and the monomer vaporized, coatings of both soluble and insoluble polymers can be deposited; properties can be easily manipulated with the addiction of additives in the oxidant solution(72). To express the potential of this method, it is sufficient to say that tinkering with these additives led to the deposition of PEDOT nanowires with conductivity above 7000 S/cm(76).

OCVD started as a laboratory-size limited technique, due to the need for extreme vacuum and limited reactor sizes but it is becoming more and more popular with the development of better performing pumps that allow for the upscaling of the reactor's size; it allows for extremely conformal (Figure 4)(43) deposition even on textile fibers or paper substrates(27,38,77) and for incorporation of dopant in the film during deposition, avoiding a succeeding doping step. The advantages of this process are related to the absence of a liquid solvent: wetting and solution effects are avoided, allowing for a better control of the nanostructure of the final product and a more conformal coverage of complex shapes, while also allowing to deposit thin films on materials that would deteriorate when in contact with a liquid, these can be heat sensitive as well, since substrate temperatures rarely get above 150 °C(43). When an initiator is used, the process is called initiated chemical vapor deposition(iCVD), even the most delicate substrates can be coated(43) and polymers from radical polymerization can be deposited. A drawback of these techniques is the difficulty to deliver the oxidant in gaseous form, although it has been partially solved

when $FeCl_3$ is used: the direction of a carrier gas stream on the surface of the heated crucible where the solid oxidant sublimates favors the mobility of the particles and helps them reach the substrate. This causes the problems visible in Figure 4: films deposited using $FeCl_3$ suffer from the intrinsic directionality the carrier gas flow imposes on the diffusion of the oxidant, therefore the thickness of the final product will be higher on surfaces oriented properly, while it will be lower in harder to reach areas. Another downside, similarly to VPP, appears after the deposition: a rinsing step is necessary to remove all impurities (EDOT, oxidant, by-products) left in the thin film but this procedure is seldom efficient. Researchers have focused on looking for better rinsing solutions(40) or removing the rinsing step by changing the oxidant(38,77,78) but nowadays the most used solvent remains methanol which, although it yields poor results, at least is non-toxic. Having mentioned oxidants, it has to be said that iron(III) chloride ($FeCl_3$) is the more widespread, since it yields films with good conductivity, thanks to a more efficient incorporation in the chains, but it causes contamination by iron oxides, is very hydrophilic, causing water absorption, and its counter-anion ($FeCl^{4-}$) has a tendency to oxidize, causing conductivity to decline(68). The research has focused on looking for alternative oxidants, like I_2, Br_2 and V_2O_5, with not good enough results to dethrone $FeCl_3$(40,41,68,77,78).

The maximum conductivity ever obtained for PEDOT deposited via oCVD is 6259 S/cm through a combination of processing method, dopant selection, polymerization rate control, and post deposition solvent treatment (70,79-82). *"oCVD PEDOT thin films with ultrahigh electrical conductivity and high carrier mobility show great promise for novel high-speed organic electronics with low energy consumption and better charge carrier transport."*(82).

Going into detail on the oCVD process, a typical reactor configuration, used in this work as well, can be seen in Figure 5(70): the scheme of the standard arrangement for *"evaporation of a solid material onto an inverted substrate"*(43) is the result of trial and error since, in a previous paper(27), positioning the oxidant crucible above the substrate had caused significant transfer of oxidant macroparticles on the thin film. The peculiarity of this technique is the fact that all the reactants (oxidant and monomer in the scenario investigated here) are introduced in gas phase. The reaction happens in high vacuum (P = 13 Pa in this work), to prevent contamination and formation of byproducts. In order to reach the gas phase, $FeCl_3$ solid powder is positioned in a heated crucible inside the reactor, while EDOT monomer is heated in a bubbler on the side and then introduced in the reactor via heated pipes. One of the main advantages of oCVD is the possibility to coat heat-sensitive substrates, thanks to a cooling system integrated into the

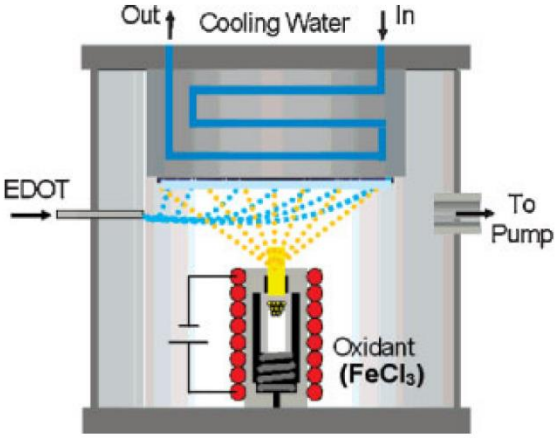

Figure 5. Standard reactor configuration for oCVD, showing the substrate above the sources for oxidant and monomer. Films form as oxidant evaporates and reacts with EDOT monomer(70)

substrate holder. It is believed that, once introduced in the reactor, monomer and oxidant react at the surface of the substrate and not in the whole reactor but, it is worth noticing how the exact mechanism of deposition is not understood, yet. In particular, the reaction process is not universally agreed upon and the catalytic role of the substrate still has to be proven.

The development of these techniques, which allows deposition in many different forms, sizes and compositions, together with the very appreciated properties of PEDOT, opened to its application in a wide range of fields. It is important to understand that most of PEDOT's applications are not as a standalone material but as a composite with, for example, metal oxides or textile fibers, since its chemical properties allow for stability in most environments, including electrolytic solutions or human fluids, but its mechanical ones are not sufficient to guarantee resistance to mechanical stresses; therefore PEDOT is paired with another material with the aim of refining the properties of both to obtain a more well-rounded device.

The first application ever envisioned was in the field of electronics, in particular in capacitors, with the first patent by Jonas *et al.* being issued in 1988: this was due to the extremely high capacitance values (with a theoretical maximum of 400 $\mu F/cm^2$) that PEDOT can reach(83). Since then more research has been focused on the topic, with application both as solid electrolyte(84,85) and as one of the electrodes(53). The usage in other electronic devices was proposed later, with applications in batteries, where the hybrid electrical-ionic conductivity of Conductive Polymers (CPs) allows for faster charge and discharge times compared to traditional devices(69,86) and transistors, where electrical-ionic transport provides higher transconductance at moderate bandwidths compared to their field-effect based counterparts(80,87). Studies on thermoelectrical applications stemming from the high capacitance mentioned above followed swiftly(88-90). Given the world's very strong interest on renewable energy, it is not a surprise to see that PEDOT is being tested for different roles in OPVs: as a counter-electrode for the regeneration of I^{3-} ions in Dye Sensitized Solar Cells (DSSCs)(91,92), as a hole conductor in DSSCs(93), as a transparent electrode(94), as a Lead substitute in Lead-free Perovskite Solar Cells (PSCs)(12,95) and as a thermoelectric material in wearable (flexible) solar cells(10). PEDOT established itself in the discipline of sensors for environment monitoring, food and drug analysis and health care(32,96) thanks to its fast electron transfer rate, nanostructures with large surface area, hydrophobic interaction and ability to synthetically control electrochemical redox properties. In the recent years, the biomedical field opened its doors to PEDOT applications thanks to its biocompatibility, chemical stability and non-toxicity: the polymer has been tested for both drug delivery(97) and wound care and tissue regeneration(11,98,99).

Discussing the production pathways mentioned in this chapter, electrodeposition, being limited to conductive substrates, focuses on the production of devices that are either composites to be used in the field of electronics and the one of sensors(100-103) or complex nanostructured PEDOT(60,61,104,105). VPP, instead, is used mostly to deposit thin films, with varying degrees of conductivity(62-65).

II.6.Ageing

For most of the applications mentioned above, it is important to assess the longevity a device based on PEDOT thin films can have. Considering that the material itself is chemically stable, what is meant here with stability is the ability of the thin film (or nanostructure) to maintain its as-deposited conductivity value, since that is the most important property for 99% of the systems employing PEDOT.

All the studies relative to ageing focus on thermal ageing, intending accelerated ageing at a defined temperature, higher than the atmospheric one. Thanks to the well-known structural properties of polymers, this allows to obtain information that span a longer time with respect to the investigation period length; these are, however, only reliable when discussing the structure of the polymeric system investigated: indeed, when discussing conductivity degradation, one can not only attribute it to structural deterioration of the polymer, but also to its chemical degradation. Studying at a higher temperature than the one of application alters the degradation pathways the material can follow (energetically unfavored reactions can be activated by the higher thermal energy) and leads to a corruption of the results, which would not reflect the actual behavior of the material during application. While structural properties have been investigated at ambient temperature(106), electronic behavior has been studied only, as far as the writer found, in conditions of accelerated thermal ageing(5,107-112). The chemical degradation is believed to be related to the neutralization of $FeCl^{4-}$ counter-anions, as suggested elsewhere(68), and its kinetics would indeed be altered by the temperature variations.

The results obtained under thermal ageing are coherent, all showing similar trends of conductivity decrease and, although in a limited form for the reasons mentioned above, they are comparable with the ones at ambient temperature this study provides; going in depth on the influence of storage atmosphere as has been done in other papers(107,113), provides further common points and comparison avenues.

To conclude, the lack of characterization of the ageing of conductive polymers derivates from the fact that the criterium used to judge the quality of a CP thin film has always been conductivity and PEDOT makes no exception, with studies focusing mostly on this property, disregarding other important factors, including stability (intended as the film's retention of the maximum conductivity over time).

Chapter III: Experimental section

III.1. Deposition

PEDOT thin films were deposited on round silicon wafers (d=10 cm) via oCVD. They were divided into four corners with KAPTON® tape as shown in Figure 6. The chosen oxidant was $FeCl_3$, due to its known efficiency, low toxicity, availability and the willingness to utilize a completely dry process. The reaction was organized as follows: after the introduction of the solid oxidant in the crucible, the reactor was shut and the pressure adjusted and then maintained at 13 Pa by a couple of vacuum pumps, in the meantime EDOT was being evaporated at 70 °C in a bubbler to the side. Once the pressure reached the desired value, the oxidant crucible was heated to the target temperature and only after the EDOT inlet was open, allowing for the reaction to start. A directed flux N_2 was used as a neutral carrier, allowing for a larger amount of reactants to reach the substrate, where the reaction takes place. The main focus of the research was to verify the effect of ageing on PEDOT, therefore some process parameters were changed in order to analyze which deposition conditions yielded the most conductive film and which ones allowed said conductivity to be maintained for a longer period of time. In particular, the parameters were:

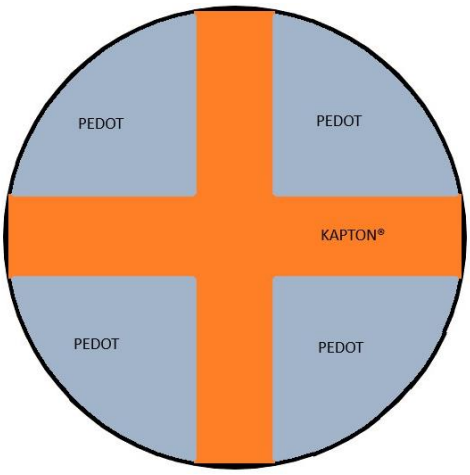

Figure 6. Schematic representation of the 10x10 silicon substrate after deposition. KAPTON® is used to provide a thickness step for profilometry measurements

- Oxidant crucible temperature, which changes the quantity of $FeCl_3$ in the reactor
- N_2 flow rate, which changes the EDOT quantity in the reactor: since the inlet is shared between N_2 and EDOT and it has limited throughput, a fixed amount of gas can pass through it, if the amount of N_2 increases, the amount of EDOT lowers.

The two parameters were investigated separately: when varying the temperature, flow rate was fixed at one of the analyzed values and vice versa. The fixed temperature was 175 °C and the fixed N_2 flow rate was 10 sccm. These two values, the lowest in their categories were chosen because from previous depositions realized with the same setup, it was clear that the higher the EDOT/$FeCl_3$ ratio in the reactor, the higher the quality of the films.

Table 1. Investigated values for the process parameters

Process parameter	Condition 1	Condition 2	Condition 3
N_2 flow rate (sccm)	10	50	100
$FeCl_3$crucible T (°C)	175	200	240

III.2.Rinsing and storage

The four corners shown in Figure 6 were then separated by cutting to allow for the study of two more parameters:

- Rinsing: allows to study the effect over time of impurities and superficial contamination. Done in methanol because of its non-toxicity and ready availability, regardless of its poor rinsing effect(40).
- Storage: allows to evaluate the influence of moisture and oxidative atmosphere on the long-term conductivity. Done in air (humid, oxidative) and Argon (neutral). It is worth noting that, in order to perform the required analyses over time, the samples had to be removed from the glove box where they were stored, exposing them for less than two hours at a time to the atmosphere.

After the cutting, two of the samples would be rinsed and two would not, then one of each would be stored in a sample holder left in standard atmospheric conditions and the others would be stored in a sample holder and put in a glove box filled with Argon. The rinsing protocol followed consisted of 15 minutes of immersion in MeOH, followed by forced drying with blown air. The introduction of these two parameters brings us to four and a total of twenty samples. Such an in-depth analysis in unparalleled in the field of PEDOT and sets this study as a future reference in the field. This large number of samples requires a clear-cut nomenclature system, but it is not easy to keep it concise. Presented below is the chosen solution:

$FeCl_3$ crucible T-N_2 flow rate-Storage (A=air, N=neutral)-Rinsing (R=rinsed, NR=non-rinsed)

Example: sample deposited with $FeCl_3$ temperature of 175 °C, N_2 flow rate of 10 sccm stored in air and rinsed:

175-10 Air-Rinsed. Shortened: 175-10 A-R

Table 2. Complete list of the deposited films.

$FeCl_3$ Crucible T	N_2 Flow rate	EDOT/$FeCl_3$	Storage	Rinsing	Name
175	10	0.57	Air	Non-rinsed	175-10 A-NR
175	10	0.57	Air	Rinsed	175-10 A-R
175	10	0.57	Argon	Non-rinsed	175-10 N-NR
175	10	0.57	Argon	Rinsed	175-10 N-R
200	10	0.43	Air	Non-rinsed	200-10 A-NR
200	10	0.43	Air	Rinsed	200-10 A-R
200	10	0.43	Argon	Non-rinsed	200-10 N-NR
200	10	0.43	Argon	Rinsed	200-10 N-R

240	10	0.13	Air	Non-rinsed	240-10 A-NR
240	10	0.13	Air	Rinsed	240-10 A-R
240	10	0.13	Argon	Non-rinsed	240-10 N-NR
240	10	0.13	Argon	Rinsed	240-10 A-R
175	50	0.14	Air	Non-rinsed	175-50 A-NR
175	50	0.14	Air	Rinsed	175-50 A-R
175	50	0.14	Argon	Non-rinsed	175-50 N-NR
175	50	0.14	Argon	Rinsed	175-50 N-R
175	100	0.08	Air	Non-rinsed	175-100 A-NR
175	100	0.08	Air	Rinsed	175-100 A-R
175	100	0.08	Argon	Non-rinsed	175-100 N-NR
175	100	0.08	Argon	Rinsed	175-100 N-R

III.3.Analysis schedule

Since the main focus is the evaluation of the degradation over the span of 90 days, it was necessary to develop a calendar that would allow the samples to be compared with each other. Since deposition takes up to four hours, it was impossible to deposit all the films in the same day. To maintain coherence, it was decided to also characterize them in a staggered way. Since the most dramatic changes were expected in the first days, the analyses were organized to be more frequent up to Day 10 from the deposition and then more and more rare up to 90 days. To clarify, Day 0 is deposition day, while the X^{th} day after deposition is referred as "Day X". Table 3 shows all the investigated days; the * signifies that only some samples were analyzed on that day.

Table 3. List of days when resistance measurement and Raman spectroscopy were performed

Day 0	Day 1*	Day 2*	Day 3	Day 7	Day 10	Day 20	Day 45	Day 70	Day 90

III.4. Schedule construction

The table presented above is the result of a complex process, not to be taken as granted: given the total lack of research in this field, an established procedure to characterize PEDOT films over time does not exist. It was deemed necessary to contain the amount of analyses, limited to the ones already described, due to the very thick schedule that would make impossible to elaborate and obtain information from the collected data, while at the same time not sacrificing the quality of the research. After attempting to foresee the possible evolution the films could incur, the two main characterization techniques (Raman and sheet resistance measurement) were considered in-depth enough to provide a good understanding of the evolution. As it came out, they monopolized the focus during most of the months of research, not leaving time for much more detailed analyses; when they did not prove sufficient, discussion ensued, leading to the decision to perform one of the *una*

tantum measurements discussed later in this chapter. The other side of the organization involved deciding when to perform the characterization. Common sense and studies on accelerated degradation(6,20,68,111,112) led to believe that the early days after deposition were the ones where the strongest evolution would occur, making frequent characterization crucial for the study. What differentiates this study from others, though, is the analysis of the material on the long term, over the span of 90 days. This length was agreed on as a long enough time frame to allow most, if not all, of the evolution to occur while keeping its encumbrance manageable. In light of these considerations, the schedule in Table 3 was chosen and applied to all films. It is a bold claim but, hopefully, the choices made here could be followed by future studies on the matter and could impose as a standard in the community or, at least, inspire others to investigate further the ageing of PEDOT in atmospheric conditions and application conditions, a crucial step towards its technological application.

III.5.Characterization

In order to judge the evolution incurred over time, Raman spectroscopy and resistance measurement were chosen to be performed following the calendar mentioned above. These would allow to establish a correlation between the conductivity changes and the chemical changes in the film, allowing the study to not only assess the evolution, but also to explain it. Raman was performed with a Horiba Jobin-Yvon LabRam HR800 spectrometer and a 532 nm laser wavelength with 8 mW power density, 10% filter and 600 line/mm grating. Sheet resistance was calculated with the voltage values obtained with a Signatone S-302-4 four-point probe with 1 mm probe spacing, collecting voltage data in 7 different points of the film while an oscillating I of 100 nanoamperes was imposed. This machine provided the value of the voltage result of the alternating current flowing through the film; these two values were then inserted into the formula below to obtain the sheet resistance:

$$R_s = 4.4516 \frac{V}{\Delta I}$$

Calculated the sheet resistance and measured the average thickness with a DektakXT stylus profiler, the average conductivity was obtained as follows:

$$\sigma = \frac{1}{R_s t}$$

Thickness was measured at the end of the 90 days because of two main reasons:

- Profilometry takes a long time to be accurate and could not be performed in neutral atmosphere, it would have caused unacceptable contamination of the films if performed at Day 0 and over time.
- A change over time of the thickness is not expected for a solid film, making the risk of contamination for the sake of accuracy not worth.

III.Experimental section

Some *una tantum* analyses were performed to further increase the understanding of the evolution behavior: optical micrographs were obtained with a BX Olympus microscope embedded in the Raman spectroscope with up to 100x magnification; Scanning Electron Microscopy (SEM) and Energy Dispersion X-ray Spectroscopy (EDS) were performed with a Helios NanoLab 600i; Atomic Force Microscopy (AFM) micrographs were done with a Agilent Technologies AFM/STM 5500 (PicoPlus) microscope.

Chapter IV: Results and discussion

IV.1. Profilometry

EDOT to $FeCl_3$ ratio efficiency can be linked to the thickness of the samples, results of which are shown in Table 4. The measurements are the result of averaging of multiple acquisitions where the standard deviation was 10%. For the purpose of the study, it is assumed that all four corners of the film (Figure 6) have equal thickness and storing in argon has no effect on it.

Table 4. Thicknesses (nm) of the PEDOT films in different conditions. Standard deviation ~10%

Thickness(nm)	**175-10**	**200-10**	**240-10**	**175-50**	**175-100**
Non-rinsed	41	48	278	54	73
Rinsed	34	46	162	24	33

First, the dramatic increase in thickness at high $FeCl_3$ crucible temperature is attributed to a large excess of the latter on the substrate, which damages the properties of the film. In general, an increase in thickness is visible when depositing with lower EDOT/$FeCl_3$ ratio and not rinsing, this confirms the non-PEDOT nature of the compounds originating this extra thickness that then get rinsed away by methanol. Since rinsing removes contaminants, oligomers and impurities, it can be said that the conditions met for the 200-10 films are the ones that produce less byproduct, leading to a thicker PEDOT layer, formed by long and stable chains. It is known, however, that PEDOT sees a sharp decrease in conductivity when the thickness is above 25 nm(41), then a proper balance has to be found.

IV.2. Microscopy

IV.2.1. Optical microscopy

The results will be here presented starting from the macro-vision to then go more and more in detail, down to the nanoscale. To start, optical micrographs are presented in Figure 7. These were taken immediately after deposition, if the sample did not require rinsing, or immediately after rinsing. On the left, from top to bottom are the 175-10 A-NR, 200-10 A-NR, 240-10 A-NR, 175-50 A-NR and 175-100 A-NR and, on the right, their rinsed counterparts. Before any analysis, it is worth noticing how, being these images taken immediately after deposition, there is no storage parameter influence.

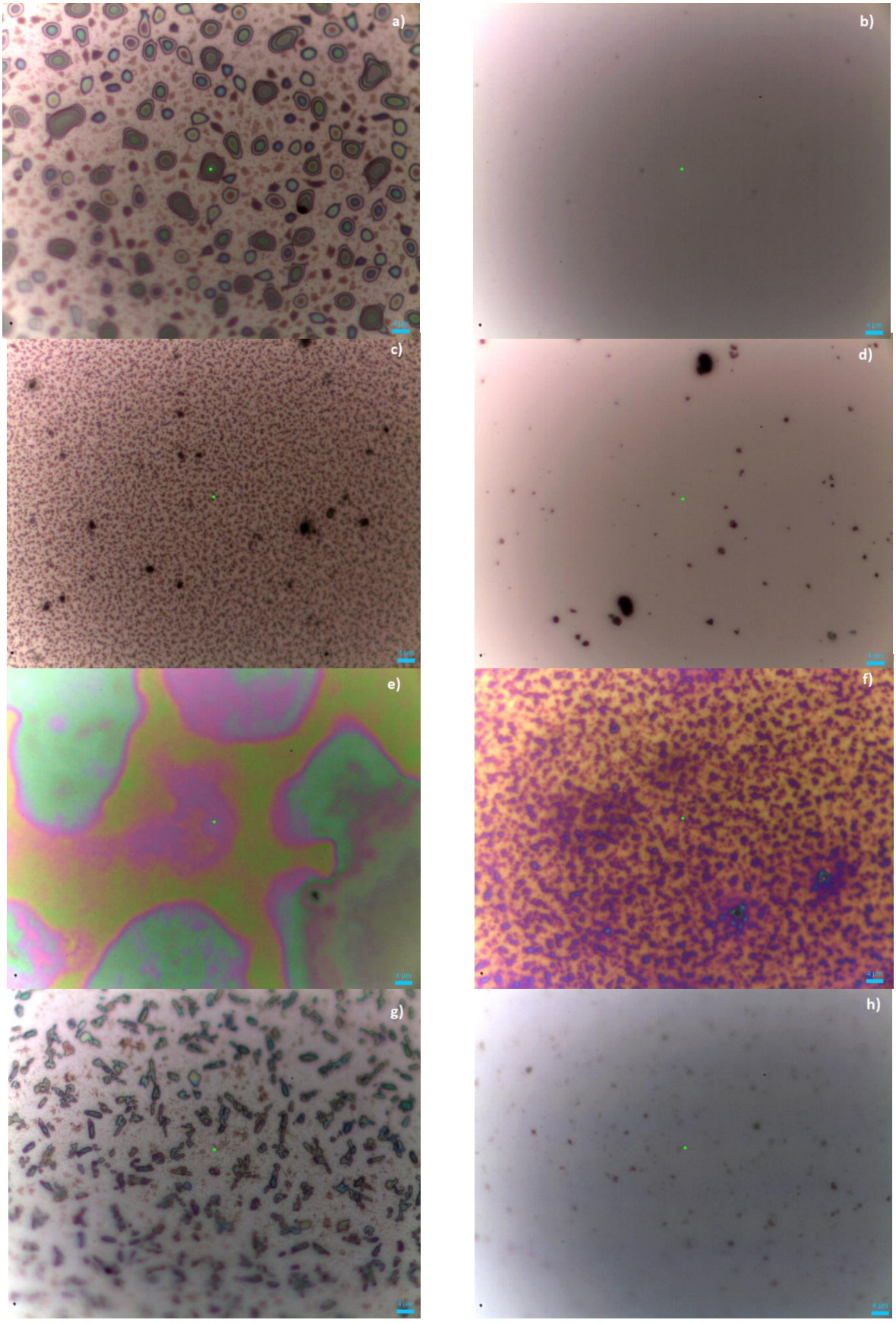
a)
b)
c)
d)
e)
f)
g)
h)

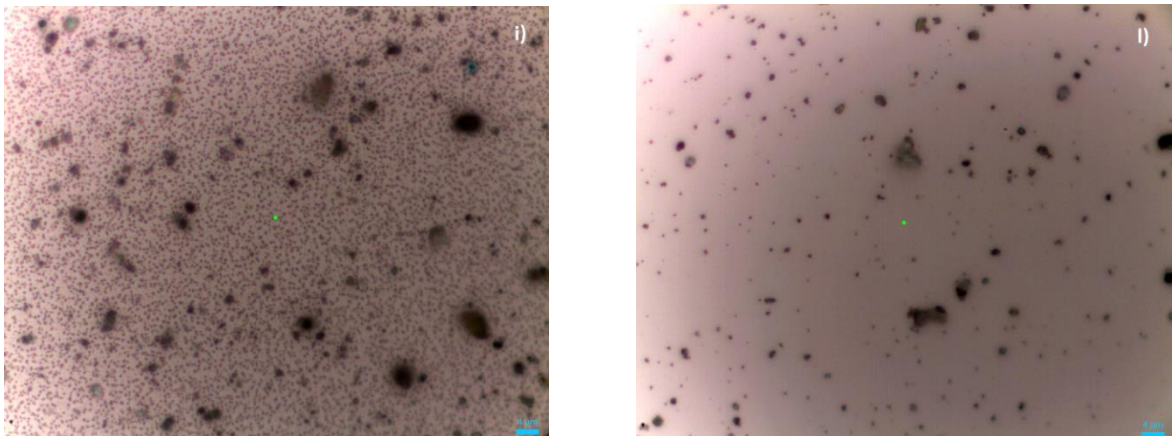

Figure 7. Optical micrographs of all the samples immediately after deposition. a) 175-10 A-NR b) 175-10 A-R c) 200-10 A-NR d) 200-10 A-R e) 240-10 A-NR f) 240-10 A-R g) 175-50 A-NR h) 175-50 A-R i) 175-100 A-NR l) 175-100 A-R. Scale: 4 µm

IV.2.1.1.$FeCl_3$ temperature effect

Studying the first 3 couples, we can investigate the influence of the oxidant crucible temperature. As a reminder, an increase in temperature (here from Figure 7a to 9e) causes and increase in the oxidant available in the reactor. First thing first, notice how the 240-10 A-NR and 240-10 A-R samples (Figure 7e,f) are different: they were ruined by an excess of $FeCl_3$ reaching the substrate: they were very inhomogeneous, with poor quality PEDOT, poorly attached to the substrate (to the point where the rinsing step almost removed the thin film). For these reasons, they can not be compared with the other films and therefore will not be investigated further. This is a result in itself, since it provides for a temperature ceiling above which $FeCl_3$ ceases to be a good oxidant for oCVD of PEDOT. Focusing on the other two temperatures, a pattern can be identified: a homogeneous transparent PEDOT film (white) lies below a plethora of islands of a different chemical nature. In particular, at the lower temperature, these domains are larger and come in different colors and sizes. When analyzing them with the Raman spectroscope, the blue-green domains suffered from burning, meaning they are not composed of PEDOT, which is stable under irradiation. Their presence is attributed to $FeCl_3$ that, being very hygroscopic, causes water adsorption on the surface. The brown domains are, instead, attributed to iron oxides impurities, caused once again by unreacted $FeCl_3$ and absorbed water, which react after extraction from the reactor and into the atmosphere. The presence of the underlying uniform transparent PEDOT layer, the wide size distribution and inhomogeneous scattering of these domains can be explained by a sub-optimal flow of $FeCl_3$ towards the substrate:

- At the start of the deposition, the crucible is heated and $FeCl_3$ starts to sublimate; since EDOT is not present in the reactor yet, the oxidant is allowed to reach and coat the substrate uniformly.
- Once EDOT is introduced, it reaches the substrate and reacts with the present adsorbed $FeCl_3$ to form a uniform layer.

- Above this layer, $FeCl_3$ keeps reaching the now coated substrate but can not form a uniform layer because it keeps reacting with EDOT.
- Once the catalyzing effect of the substrate can not be felt through the thickness of the already formed thin film, $FeCl_3$ can not react anymore and remains on the surface.
- When the system is extracted from the reactor and exposed to air, unreacted oxidant starts to react once again but with water, to form iron oxides.

These islands are completely different in the 200-10 A-NR film: their small size and homogeneous distribution would seem incoherent, since a higher temperature provides a larger amount of oxidant to the surface of the film, which should coalesce to form even bigger islands. Yet, it is necessary to keep in mind that a higher temperature could also favor a more homogeneous delivery of oxidant, since its sublimation would be more favored and less influenced by local fluctuations of temperature in the crucible or by turbulences in the carrier gas flow. As mentioned in chapter II.5, oCVD is not fully understood and this is one example of why. Sustaining the theory of islands formed above a uniform layer is the effect of rinsing: in both conditions, we can see a total disappearance of the colored domains. This confirms the fact that they are not composed (for the most part) of PEDOT, since it is not soluble in methanol. Small very faint spots remain visible in Figure 7b, due to impurities embedded in the PEDOT film, while large black ones remain in Figure 7d, most likely coming from the crucible itself losing cohesion when heated. This is sustained by the fact that at higher temperatures more particles are visible.

IV.2.1.2.N_2 flow rate effect

The effect an increase in carrier gas flow rate (Figure 7a,b,g,h,l,l) has is similar to the one between that an increase in temperature provokes, visible in Figure 7a and Figure 7c. This time, the reduction in size of the domains lying above the uniform layer is attributed to the stronger N_2 flow rate which, yes, carries more $FeCl_3$ towards the substrate but limits its residence time close to the substrate, limiting adsorption and coalescence into the big clusters seen in Figure 7a. In the rinsed samples black particles are present in larger amount than in the previous ones, this is attributed to the stronger gas flow being able to sustain the movement of more particles towards the substrate. This implies that the crucible breaks down even at 175 °C. unlike discussed earlier, but the lower number of particles needs a stronger flow rate to contaminate the substrate enough to be visible. This problem needs to be addressed in future research, with the development of a more stable crucible.

IV.2.1.3.Time effect

The last analysis on optical micrograph is the one related to time evolution. The 175-10 A-NR sample (Figure 7a) showed a remarkable visual change in the first two days (Figure 8). Two main effects are visible:

- The round, light-blue domains gradually disappear
- Light brown, dark brown and deep blue domains appear and increase in size

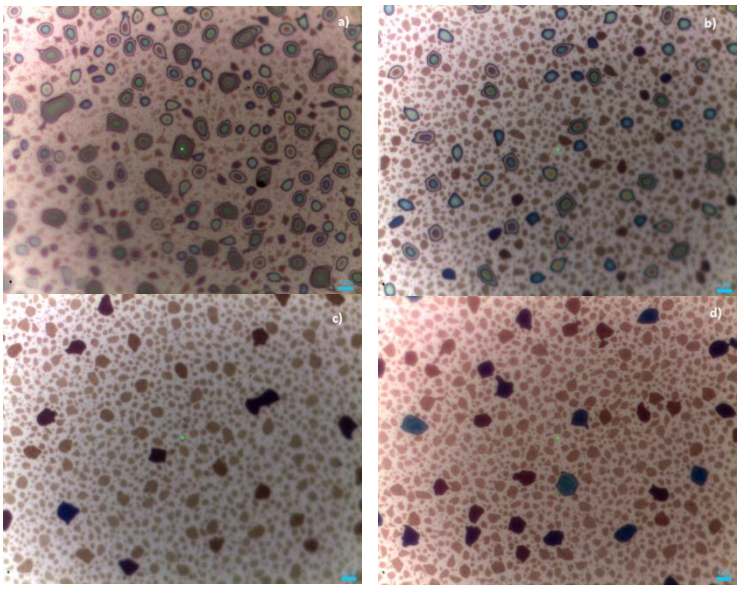

Figure 8. Time evolution of 175-10 A-NR at Day 0(a), Day 1(b), Day 2(c) and Day 90(d). Scale: 4 µm

These two effects are thought to be linked: the reaction between water present in the disappearing light blue domains and the unreacted $FeCl_3$ and iron impurities in the film forms the brown and blue spots. In particular, the proposed reaction path is suggested in Figure 9(68).

$$FeCl_4^- + H_2O + \frac{1}{2}O_2 = Fe(OH)_2 + 2Cl_2 + e^-$$

$$FeCl_3 + H_2O + \frac{1}{2}O_2 = Fe(OH)_2 + \frac{3}{2}Cl_2$$

$$Cl^- + FeCl_3 = FeCl_4^- \xrightarrow{H_2O+\frac{1}{2}O_2} Fe(OH)_2 + 2Cl_2 + e^-$$

Figure 9. Set of reactions responsible for dopant neutralization in PEDOT thin films deposited via oCVD with $FeCl_3$ as oxidant(68)

These are not only responsible for the visual changes undergone by the sample, but also of the neutralization of the dopant counter-anions. This causes the transition from doped quinoid structure to undoped benzoid structure, with degradation of the thin films' conductivity. All of the reactions of Figure 9 contain as reactant both water and oxygen: this is indicative of the fact that the presence of both these molecules is a necessary condition in order for the system to react and degrade. Unfortunately, a viable way to study anhydrous and aerated or de-aerated and humid environments could not be found, not allowing further verification of this concept, proven elsewhere(113). It is important to notice how the film at Day 2 (Figure 8c) and the film at Day 90 (Figure 8d) do not show

significant differences. This evidences the fact that all the species able to react are consumed in the first few days; afterwards the film does not show macroscopic changes.

IV.2.2.AFM

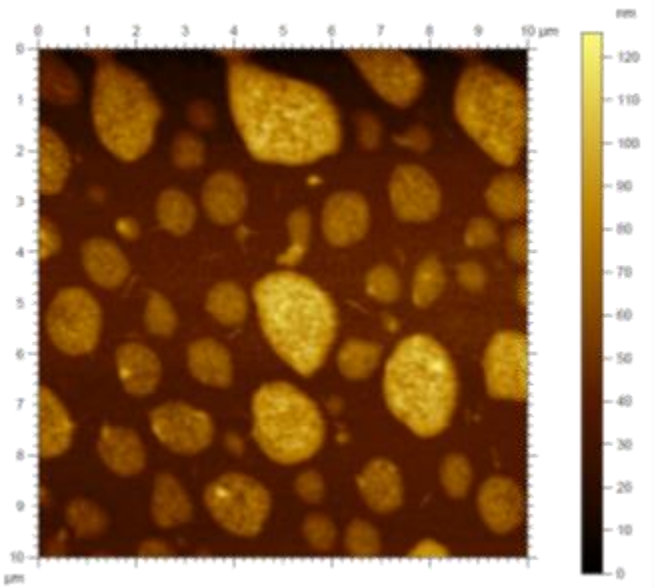

Figure 10. AFM micrograph of 175-10 A-NR

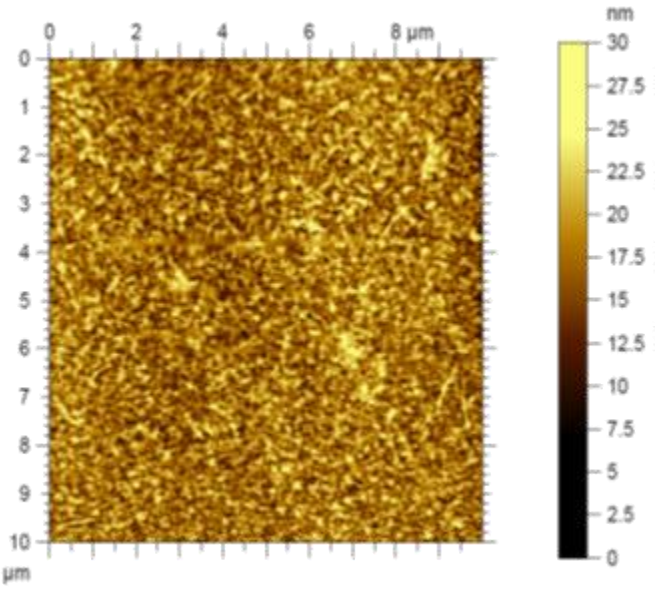

Figure 11. AFM micrograph of 175-10 A-R

Delving deeper towards the micro- and nano- scale, AFM topographic maps in Figure 10 and Figure 11 are presented. These were taken in order to understand the differences between the optical domains and between not rinsed and rinsed samples. The information contained relates to the topography and thus the thickness profile of the samples: the brighter the image, the thicker the film is in that particular area. It immediatly strikes the eye how wide the thickness spread for the non-rinsed sample is: the highest point has a thickness above 70 nm larger than the underlying film. These thick areas are the ones seen in brown and dark blue in Figure 8d. This assumption is confirmed when looking at the rinsed film micrograph: the hills and valleys have disappeared, leaving space to a completely flat and homogeneous area, much like the one seen in Figure 7b. This confirms the previous statement that the colored impurities are lying above an homogeneous thin film and therefore form later in the reaction process and during exposition to oxidative atmosphere. Another important information to be taken is the presence of drag marks left by the cantilever on the very bright areas of Figure 10: this is telling of a soft and viscous rather than solid nature of these parts of the film. This explains why they are not visible at the profilometer: the device uses a stiff stylus which goes right through these non-solid islands. Looking at the rinsed film, no evidence

of similar marks can be found, leading to the assumption that all that is left after rinsing is a solid and uniform PEDOT thin film.

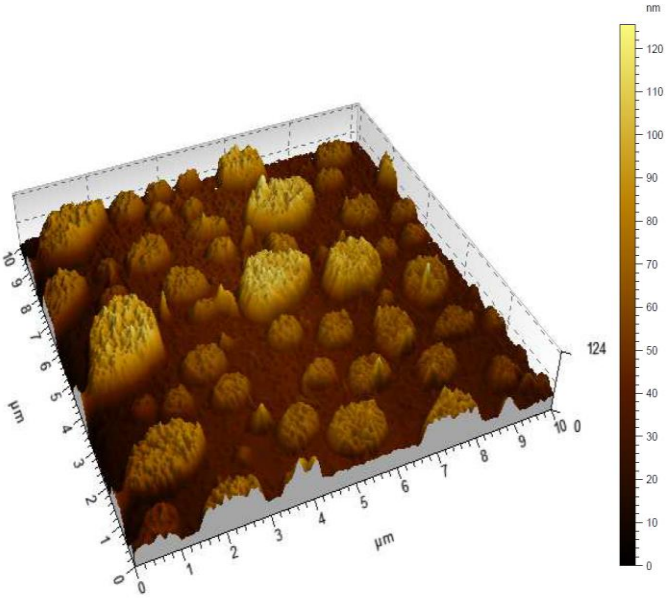

Figure 12. 3D rendering of figure 10.

For clarity, a 3D rendering of Figure 10 is presented: thickness distribution is tight: there are few thick areas and then a lot of less protruding and smaller spots, practically without thicknesses in between. All of these have a common feature in the fact that they have steep walls rather than flatter edges; this is coherent with the assumption of them being originated by reaction of water droplets and oxidant, since PEDOT is hydrophobic and would not allow for spreading of these domains over the surface. No real trend can be identified regarding shape.

IV.2.3.SEM

SEM micrographs of thin films of $FeCl_3$ sublimated in absence of EDOT(Figure 13a), 175-10 A-NR (Figure 13b,c) and 175-10 A-R (Figure 13d,e) are presented at a scale of 500 nm (Figure 13a,c,) and 10 µm (Figure 13b,d).

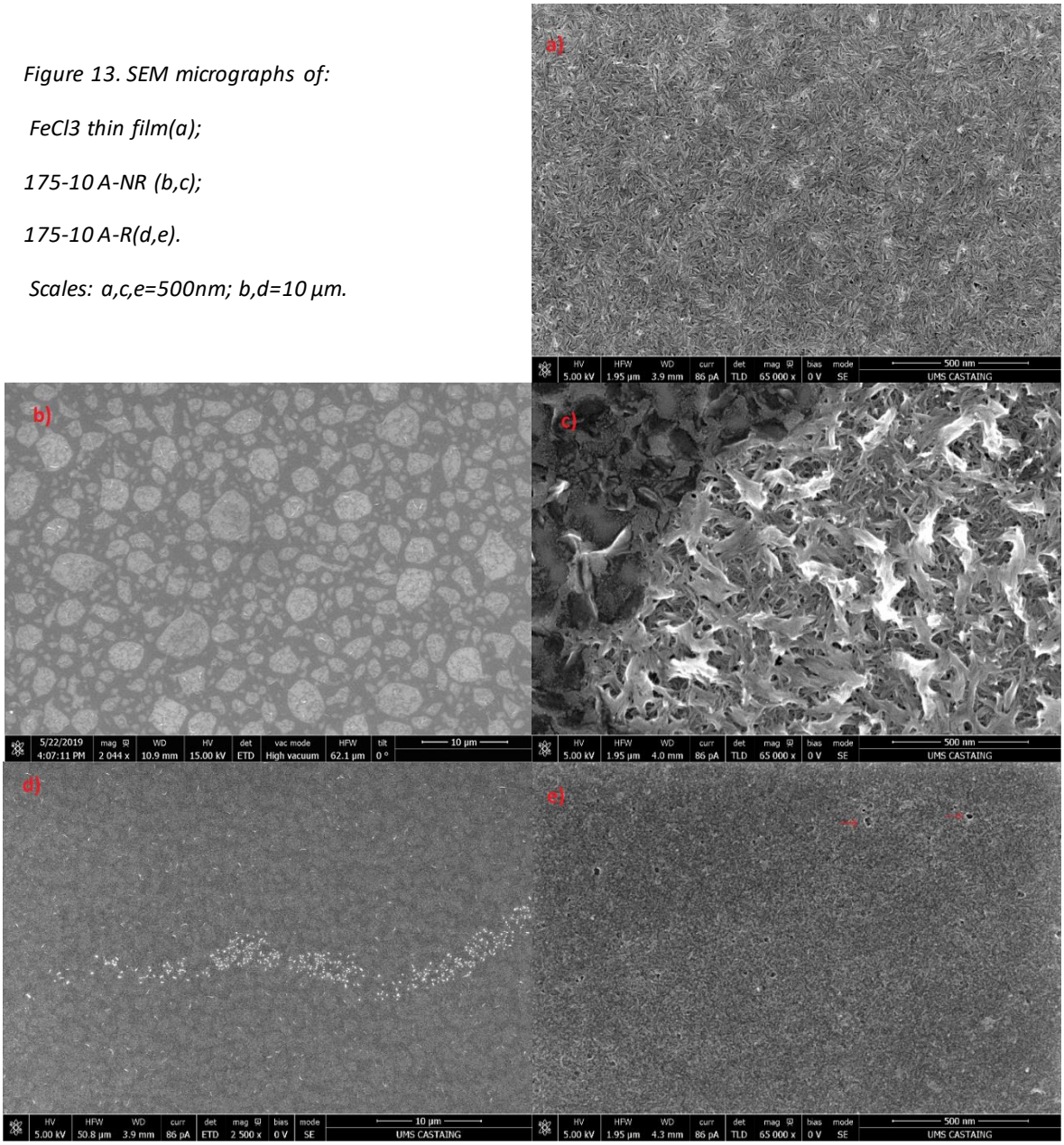

Figure 13. SEM micrographs of:

FeCl3 thin film(a);

175-10 A-NR (b,c);

175-10 A-R(d,e).

Scales: a,c,e=500nm; b,d=10 µm.

It is worth remembering that the strength of the SEM response of a material is related to its proximity to the probe (related to thickness) and its conductivity, both of which increase said response when increasing. A closer (thicker) part of the film could therefore appear brighter when, in fact, being less conductive than another. The first evidence is the extreme complexity of the nanostructure, with no clear ordering and very high porosity of the layer. This is very evident in the non-rinsed sample (Figure 13c), where large leaf-like particles are present all over the surface, with large gaps among and below them. This layer is most likely not formed by long chains of PEDOT since, as we can see from Figure 13e, these structures are completely gone after rinsing and the polymer is not soluble in methanol. It is believed that this leaf-like nanostructure is formed by oligomers and unreacted species. It leaves

space to a much finer nanostructure, which resembles $FeCl_3$'s one (Figure 13a). The similarity between the two leads to the conclusion that the PEDOT thin film is formed above a layer of $FeCl_3$ deposited on the surface before EDOT is injected into the reactor, as described in chapter III.1. This reasoning is sustained by the fact that the good conformity of PEDOT when covering complex shapes is known(114-116). Another important aspect of the small-scale micrographs is the presence of larger pores, some of which marked with red arrows in Figure 13e: these are attributed to degassing of Cl_2, whose production happens as a byproduct of the neutralization reactions described in Figure 9. Moving to the non-rinsed sample, the edge between two different domains is visible in Figure 13c: there is not a remarkable difference in nanostructure. The difference in thickness is evidenced by the bright white of the closest structures in the center-right and, again, no slope is visible, certifying the abrupt ending of the thick domains. These considerations and the ones relate to the similarity between the nanostructures of Figure 13a and Figure 13e confirm once and for all how the deposited thin films are formed in a five steps process:

- $FeCl_3$ sublimates and deposits on the substrate, with formation of an extremely thin film
- EDOT enters the reactor and reaches the substrate, forming a uniform thin film upon reaction
- More $FeCl_3$ reaches the substrate, now covered in PEDOT, some provides further doping, some is left unreacted on the surface
- Freshly injected EDOT reacts only on the surface of the large $FeCl_3$ droplets lying on the film
- Once exposed to oxidative atmosphere, these droplets react with O_2 and H_2O (Figure 9) to form thick iron oxides domains.

Observing the large-scale micrographs, the most relevant information resides in Figure 13d: even on a film that seems homogeneous both optically (Figure 7b) and to AFM (Figure 10), bright and dark spots are visible. This is attributed to the issues discussed in chapter II.4.: doping conductive polymers can not be homogeneous, since steric hindrance limits the dopant to polymeric unit ratio and the dopant molecules are not distributed uniformly among the chains but rather tend to cluster in highly doped sections that are accompanied by almost pristine ones. This results in more (bright) and less (dark) conductive areas spread all over the thin film. This behavior is not visible in the unrinsed film because of the overwhelming thickness differences and the presence of unreacted species and oligomers on the surface, evidence of which is the difference in nanostructures of Figure 13c and Figure 13e.

IV.2.4.EDS

In parallel to SEM, an EDS investigation was performed to have direct confirmation of the presence of some elements in the films. The results are shown in Figure 14. Even if the EDS

signal is stronger for areas situated closer to the probe, *e.g.* thicker, it appears evident how iron and oxygen are more present in certain areas and these are of the exact same shape for the two elements. This reveals that they are present together in the form of iron oxides in the areas that are thicker than the rest of the film. In parallel, the sulphur micrograph shows neither S-rich nor S-poor points anywhere, thus confirming that the brown, thick domains visible at the optical microscope (Figure 8d) are not composed of pure PEDOT, but for the most part of iron oxides. If no PEDOT was present at all, the micrograph would resemble the one in Figure 14d, where the one for silicon can be seen, instead the darker areas in this figure are not visible in Figure 14c. This provides univocal confirmation that the thick brown domains are Fe-rich and O-rich, with only marginal amount of PEDOT in them.

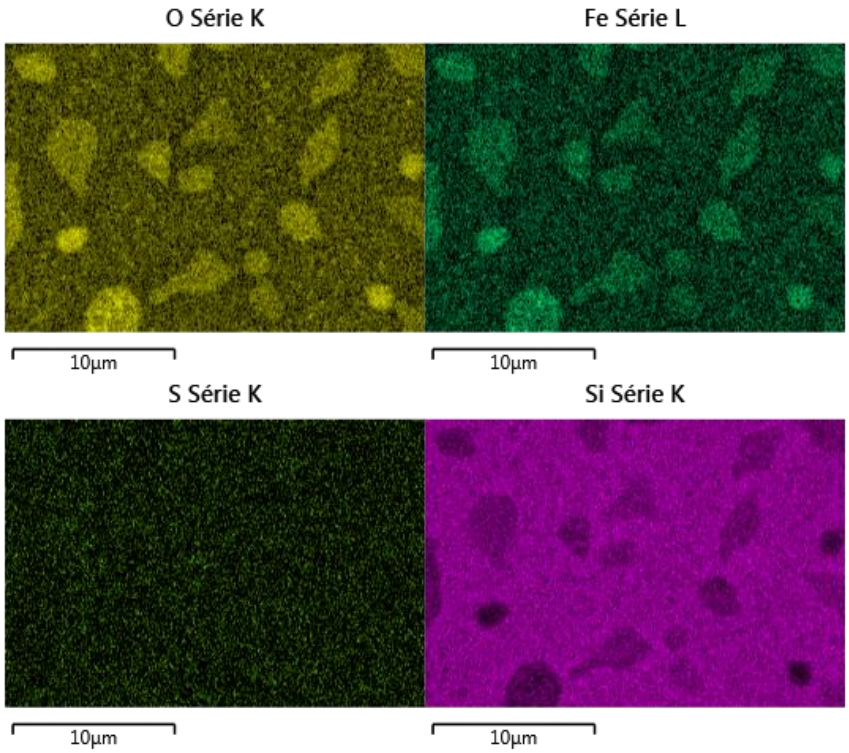

Figure 14. EDS micrographs of 175-10 A-NR for a) Oxygen; b) Iron; c) Sulphur; d) Silicon

IV.2.5.Microscopy conclusions

The in-depth analysis describe above can be summarized in these conclusions:

- Deposition at 240 °C is not possible: the film is not stable due to excess $FeCl_3$
- Thin films are composed of two parts: below is a uniform PEDOT layer and above are thicker domains composed of oligomers, iron oxides and impurities originated by delayed arrival of $FeCl_3$ onto the already formed PEDOT layer
- These domains are removed by methanol rinsing
- In the first two days, unreacted oxidant reacts with water and oxygen to form more of these areas. From AFM they appear soft and viscous, with a thickness over 70 nm larger than the underlying layer
- The films' nanostructure is amorphous and extremely porous. When rinsed it resembles the one of pristine $FeCl_3$ films
- SEM provides evidence of ununiform doping in rinsed films

- EDS confirms that the brown domains are indeed thick and are composed of iron oxides and not PEDOT

While the problem of ununiform doping is intrinsic of conductive polymeric materials, the issue of these macroscopic impurities could be solved by a refinement of the deposition process: a better system for the delivery of $FeCl_3$ is necessary if the rinsing step is to be avoided. This would allow for a quicker, completely dry and less complicated production process that would make upscaling and industrial application more viable.

IV.3.Conductivity

This paragraph delves deep into the discussion on the conductive behavior of the polymeric thin films, with comparative analyses among systems with different process and storage parameters, both at time of deposition and over time. Please note how this work is not about reaching the highest possible conductivity for the material, therefore the absolute values will be well below the maxima reached in other papers(40,70,79-82). The focus must be on the evolutive trends showed by PEDOT and their intensity in relation to the different parameters.

IV.3.1.Time evolution

Conductivity's time evolution for non-rinsed samples (Figure 15) and rinsed samples (Figure 16) is shown below. Time axis is not to scale in order to not lose information on the first days.

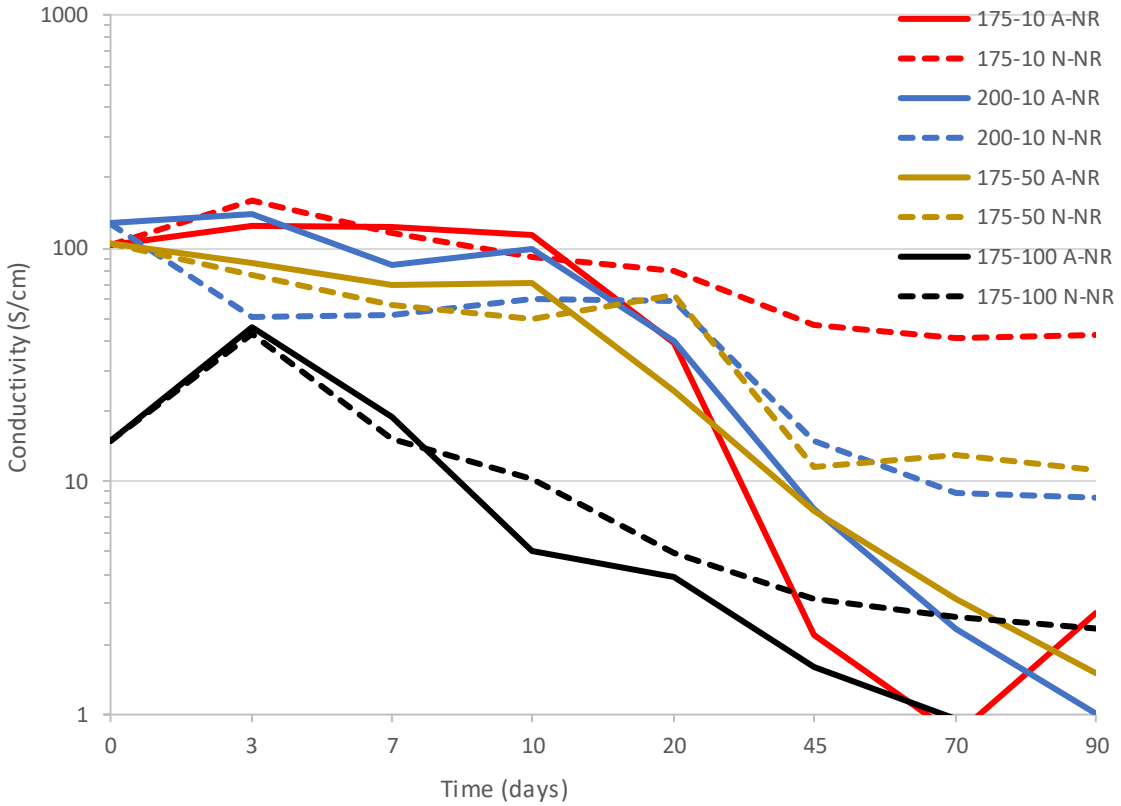

Figure 15. Conductivity evolution for non-rinsed samples

Starting from the non-rinsed samples, we can see a trend: higher EDOT to $FeCl_3$ ratio (Table 2) translates to higher conductivity in the first 10 days, without sizeable differences between 175-10, 200-10 and 175-50 samples. In this time, we also have the highest reported conductivity for non-rinsed samples at 160 S/cm. The 175-100 samples both have lower conductivities, likely due to an excess of $FeCl_3$ at the substrate surface during deposition. Between Day 10 and Day 20, an initial drop happens for the samples stored in air: they lose up to 66% of the initial conductivity (175-10 A-NR). This drop continues over time and does not stop before Day 90, at which the conductivity loss is above 99% (200-10-ANR) and down to around 1 S/cm. This behavior is not unexpected if we consider the reactions described in Figure 9 are responsible for the neutralization of the dopant and, as this happens, PEDOT loses more and more metallic behavior. Remaining on Figure 15, considering the samples stored in argon, a different trend establishes: the samples are stable for longer, since the first drop only happens after Day 20 and, more importantly, is much less pronounced than their air-stored counterparts; third, after Day 45, the samples appear to become stable again. The more stable behavior of these films is expected, given the neutral atmosphere they are conserved in. The cause of the small drop in conductivity after Day 20 can not be identified with pinpoint accuracy, as it may be caused by a human error in the isolation of the storing container or simply exposure to air for the scheduled measurements lasting longer. Both the 175-100 systems not only have lower conductivity, they undergo more gradual degradation than others too. This is attributed to the presence of larger amounts of unreacted oxidant and contaminants on their surface, causing more gradual production of non-conductive species that ruin the films' properties. The takes from this analysis are: oxidative atmosphere does cause problems for the long-term application of $FeCl_3$-doped PEDOT, limiting its lifetime to 10 days; neutral atmosphere improves this lifetime, consolidating the envisioned degradation pathways proposed in Figure 9; major forms of self-induced degradation do not manifest when depositing films with a correct EDOT to $FeCl_3$ ratio, proving that oCVD PEDOT can already be utilized in specific applications in neutral atmosphere. This behavior is coherent with the study by Kawano *et al.*(113), where the effect of hydrated and dehydrated environments on organic solar cells has been studied and it was found that it is enough to decrease RH from 40% to 4% to greatly increase the cells' performance after 10 hours only.

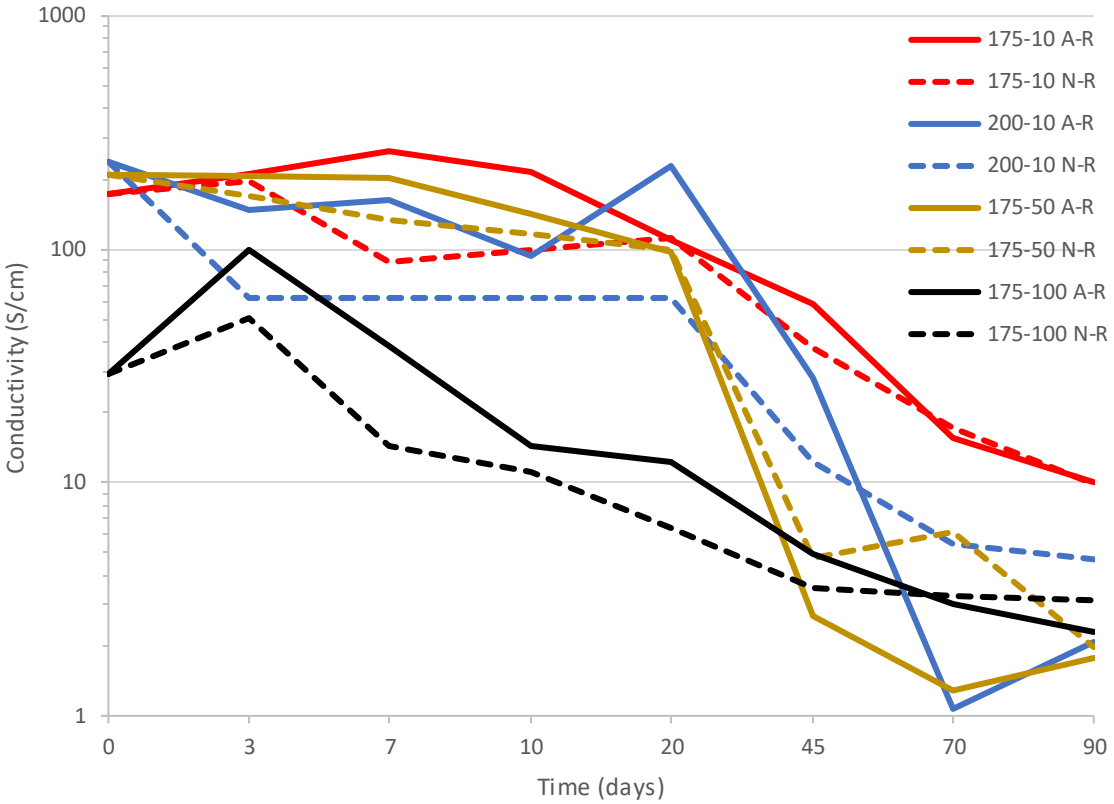

Figure 16. Conductivity evolution for rinsed samples

Inspecting Figure 16, rinsed samples have the same trend regarding the EDOT to $FeCl_3$ ratio: the higher the ratio, the higher the conductivity: with a maximum of 264 S/cm for the 175-10 A-R sample. They show a different behavior when discussing the time evolution: they show higher conductivity in the first days, as expected(21,40,68,70,77) and the conductivity drop happens after Day 20 but, while more gradual, it is more intense compared to the samples stored in argon and non-rinsed. The final conductivity values for the rinsed samples stored in oxidative atmosphere and the ones in neutral atmosphere are similar, unlike in the non-rinsed case; this is indicative of an intrinsic degradation of the film, rather than the formation of impurities related to external contamination explained in Figure 9. The cause of this degradation is attributed to the presence of byproducts and unreacted species from the reaction that progressively form non-conductive species combining with the counter-anions in the film, lowering its properties. While the rinsing process is enacted specifically to prevent this, it is known that methanol is not the best possible solvent for this job, but it is used because of its availability and safeness, when compared to other, better performing, options(40). It is unclear why this intrinsic degradation is less prominent, if not absent, in some unrinsed, argon-stored samples: it is possible that the presence of macroscopic impurities that do not get washed away concentrates the disruptive effect of the contaminants to some more susceptible areas (defects, oligomers, impurities on the surface), *de facto* lowering their influence on the film's overall conductivity. This more generalized degradation is evident when considering that the

highest final conductivity shown by rinsed samples is 10 S/cm by 175-10 A-R and 175-10 N-R (99,4% decrease in 90 days) compared to the 42 S/cm by 175-10 N-NR (60% decrease in 90 days) in non-rinsed samples. If we limit the comparison to samples in oxidative atmosphere, it can be seen how rinsing does have a small beneficial effect for the whole duration of the experimentation: after 90 days, a very small conductivity advantage is retained when rinsing but, at this point, it is hard to consider a success a conductivity of maximum 10 S/cm. Utilization in humid and aerated environment is a major challenge for oCVD PEDOT used depositing $FeCl_3$ even when rinsing but this is to be expected, considering that this process is used to remove excess oxidant and not, of course, counter-anions linked to the chains. As it can be seen in the third reaction in Figure 9, $FeCl_3$ does contribute to the neutralization of counter-anions and this could explain why rinsed samples, which do not incorporate significant amounts of it, retain better conductivity in the long-term. To conclude, while rinsing does have a beneficial effect on conductivity in the first 20 days and prolongs its time-to-drop much like argon-storage does, it is not beneficial in the long run, for motivations that are not completely understood and require a deeper research on the topic. Considering that the conductivity variations between samples are small (two orders of magnitude are not a lot, for a property that, among all materials, spans tens of them) and that some are influenced by thickness and by errors introduced by a characterization method which is not able to provide local measurements, due to size limitations, these conclusions can not be taken as an absolute, but rather contextualized properly.

IV.3.2.Daily comparison

To help visualize better the conclusions obtained so far, the graphs for conductivity at Day 20 (Figure 17) and Day 90(Figure 18) are presented below.

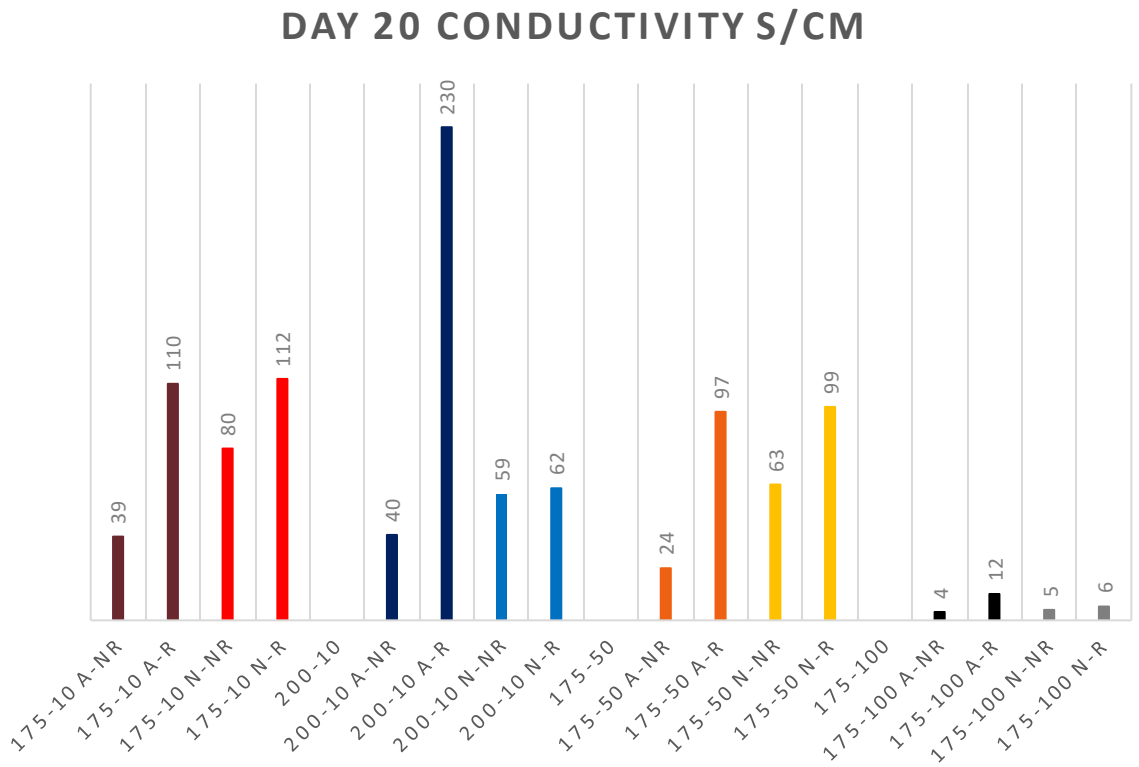

Figure 17. Day 20 conductivity for all investigated samples

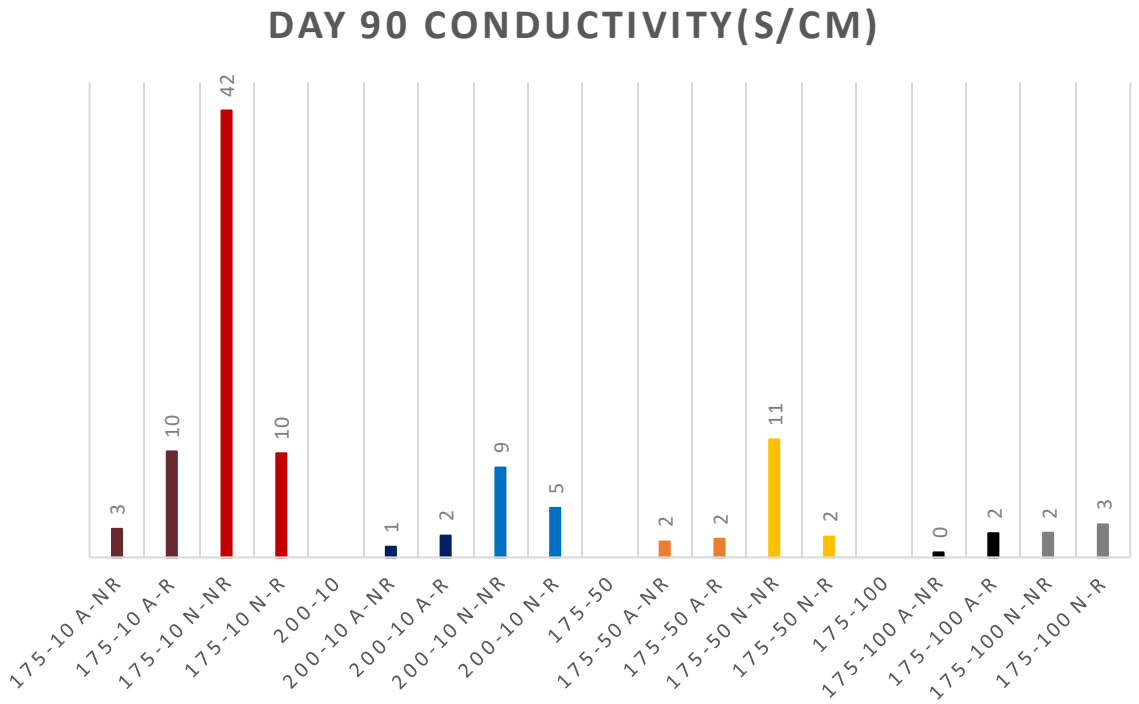

Figure 18. Day 90 conductivity for all investigated samples

At Day 20, non-rinsed samples in oxidative environment already lost most of their performance, therefore it is evident how rinsing still provides a large conductivity gain and the intrinsic degradation spoke of earlier has not kicked in yet, while neutral atmosphere storage has had little to no influence, yet, unlike for non-rinsed samples, where its beneficial effect manifests itself in all the competitive films (175-100 is already weak enough to not show any major discrepancies). The extremely high value of 200-10 A-R is not to be taken too seriously, considering that, as it can be seen in Figure 18, it appears as spike in the graph. The opposite holds true for 175-10 N-NR's value at Day 90 which, even if much higher than all the others, is coherent with the trends in Figure 16 and can be taken as a testament of the positive effect of neutral storage. Figure 17 highlights the aforementioned trend: all the non-rinsed films stored in argon have much higher conductivity than the others in their own deposition conditions. It is worth mentioning after this discussion how, while not the best, the 175-10 sample holds a competitive conductivity in the first 20 days and suffers much less degradation over time, becoming the most performing by quite the margin after 90 days; this is indicative that these deposition conditions are the ones more suited for oCVD deposition of PEDOT with $FeCl_3$ as oxidant. Considering that the deposition parameters originate the highest EDOT to $FeCl_3$ ratio in the reactor, it is worth continuing investigation on even higher ones, in order to optimize the process even more.

IV.4.Raman spectroscopy

Having discussed how the films react to ageing in different environments, it is necessary to understand the reason why they do. The main objective is to either confirm the dopant neutralization theory or find evidence of a different evolution mechanism and explain a plausible new degradation path.

IV.4.1.Acquisition optimization

PEDOT has Raman bands in a very wide spectral range, from 400 cm^{-1} to 1800 cm^{-1} and, beside this, an investigation on the presence of water (band around 3400 cm^{-1}) and iron oxides (down to 100 cm^{-1}) was required, in order to be able to fully understand the films and their development, extending the analysis over almost 4000 cm^{-1} of frequency. On top of this wide spectral range, another issue was the fact that the main band of silicon (520 cm^{-1}) would reach saturation because some films were not thick enough to shield from the signal of the substrate, not allowing for a proper normalization of the spectra. In order to overcome these problems, maintaining reproducibility, two different analysis windows were employed: the first from 100 cm^{-1} to 1200 cm^{-1}, with three accumulations of five seconds each, and the second from 800 cm^{-1} to 3600 cm^{-1}, with three accumulations of thirty seconds each. The overlap made possible the normalization of the two spectra on the silicon peak at around 900 cm^{-1}, allowing for the composition of the full spectrum for every film, overcoming the saturation issue.

IV.4.2.Raman spectroscopy of PEDOT

Raman spectroscopy has been used to characterize materials since its inception in 1928. The first in-depth analysis of PEDOT has been carried out by Tran-Van *et al.* in 2001(29) and has been used as a reference in many papers(37,86,110,117-121). The letter assignation for carbons in the PEDOT molecule is coherent with the one used in the papers listed above in order to allow for an easier comparison; said assignation is shown in Figure 20(37). Note that a benzoid PEDOT molecule Is represented in Figure 19(117) but the nomenclature does not change when transitioning to quinoid or vice-versa. α and α' are the carbons on the polymer backbone, while

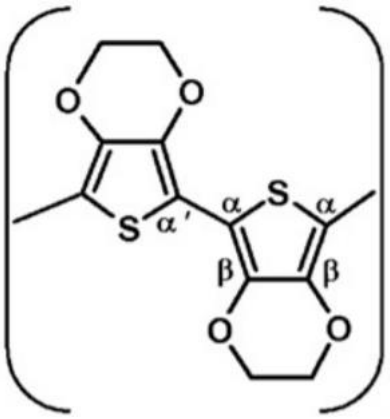

Figure 19. Schematic of a PEDOT molecule with nomenclature for C-atoms identification(117)

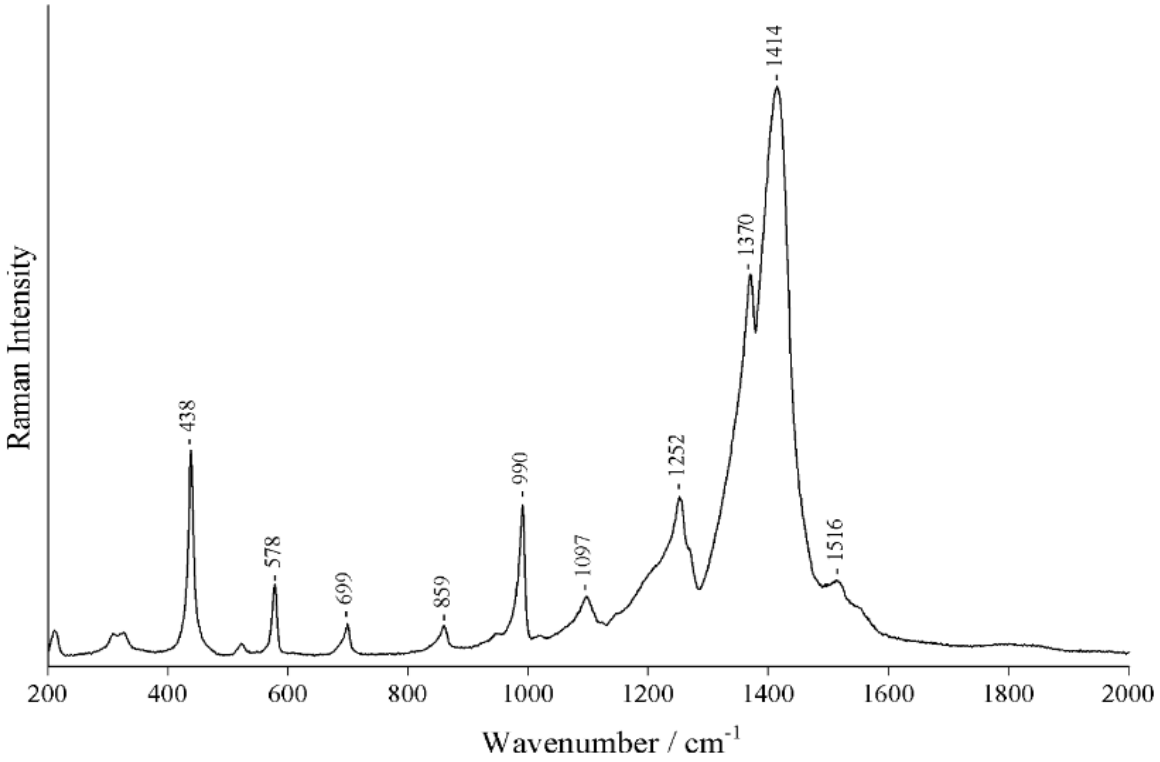

Figure 20. Raman spectrum of PEDOT. Reported wavenumbers are related to the bands attributed to PEDOT(37)

the carbons shared by the thiophenic and dioxyethylenic groups are called β. An example of Raman spectrum of PEDOT between 200 cm^{-1} and 2000 cm^{-1} is shown in Figure 20(37). Please note that this was obtained with a laser wavelength of 785 nm.

The bands identified in this spectrum are the ones directly attributed to PEDOT and the most important ones for this work are explained in Table 5, side by side with attributions from Tran-Van *et al.*(29) and Feng *et al.*(119). Given that these three papers all used different setups, lasers and excitation wavelengths, the common points among them are remarkable and a testament to the reliability that Raman spectroscopy provides to

researchers that want to understand this conductive polymer. The most important bands for the analysis that is going to be developed here are the ones related to the double bonds and the single bonds involved in the backbone (first three rows) since those are the ones that shift when switching from quinoid to benzoid structure and can be used to estimate of the relative amounts of the two in the film.

Table 5. Comparison of the shift of the main bands of PEDOT and their attribution. (29,37,119)

Tran-Van *et al.*	**Chiu *et al.***	**Feng *et al.***	**Attribution**
1509	1516	1508	C=C α=β antisymmetric in plane modes
1444	1414	1429	C=C α=β symmetric in plane modes
1366	1370	1361	C-C β-β stretching in plane modes
1267	1252	1264	C-C α-α inter-ring stretching in plane modes
988	990	990	Oxyethylene ring deformation
440	438	436	C-O-C deformation

IV.4.3.Raman spectroscopy of impurities and contaminants

One of the main objectives of this research was to confirm or dispute the degradation path via dopant neutralization proposed in Figure 9. To do so via Raman, it has been necessary to conduct extensive research on the characteristic bands of not only $Fe(OH)_2$, the proposed final result of the mentioned reactions, but also all the other iron oxides, in order to exclude their presence in the films. It is important to notice that Raman of iron oxides is not a well-studied topic and therefore the sources found rarely had the same excitation wavelength and laser power, not only compared to the one used in this research but also within each other. The reasoning followed here is based on the characteristic bands of the singular oxide which, even when changing intensity, usually do not change in number *e.g.* if Fe_2O_3 has four characteristic bands at 785 nm^{-1} excitation wavelength, it will retain the most relevant bands at any other wavelength. The characteristic spectra of Iron(III) hydroxide(122), magnetite(123,124), goethite(125), hematite1(125) and hematite2(125) are presented respectively in Figure 21 to Figure 24. The graphs are all very different from one another: this is because iron oxides' spectra are very susceptible to an increase in laser power density (PD). A general trend can be identified where at an increase in PD corresponds a sharpening of the bands and a decrease in background noise.

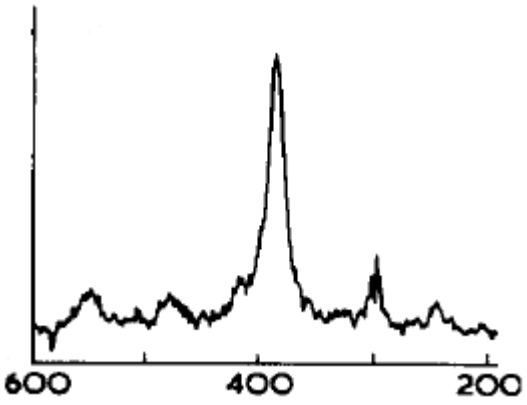

Figure 21. Raman spectrum of pure Fe(III)hydroxide pigment provided by Winsor and Newton. λ_0 = 647,1 nm; integration time = 4s; accumulations = 100(122)

In Figure 22 and Figure 23 the spectra of magnetite and goethite are presented.

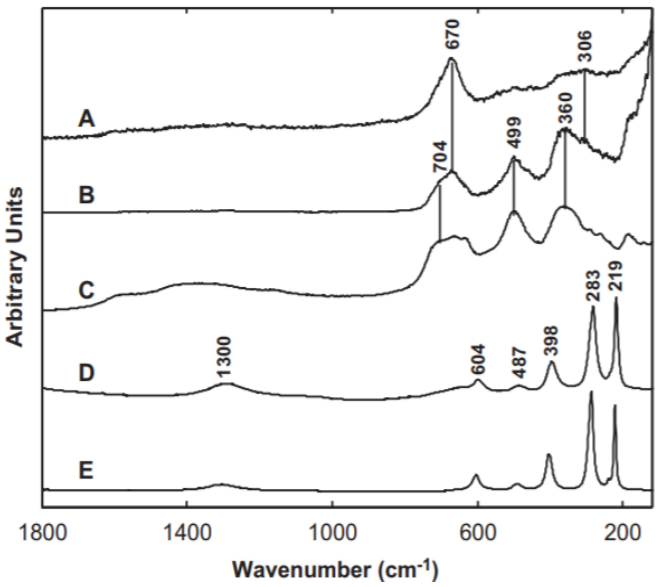

Figure 22. Raman spectra of Fe_3O_4 Magnetic Nanoparticles collected using 0.35mW after exposure for 7 min to different laser powers: (A) 0.35mW; (B) 0.66mW; (C) 2.58mW; (D) 4.93mW; (E) 8.85 mW(125)

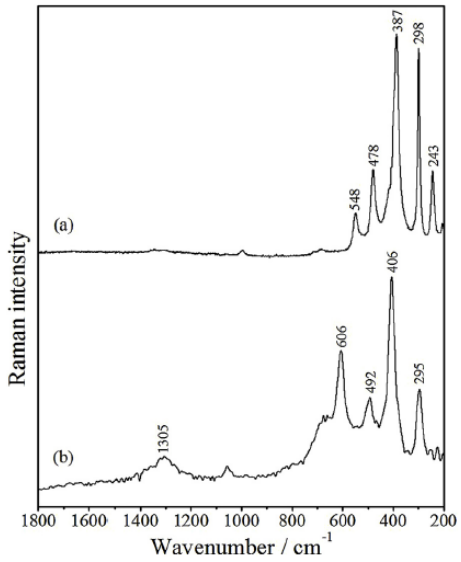

Figure 23. Raman spectra (785 nm) of goethite obtained with: (a) a Renishaw inVia Reflex Raman microscope using 40 mW at the sample (PD = $8*10^4 Wcm^{-2}$) and (b) a portable Raman DeltaNu using ($4*10^2 Wcm^{-2}$)(123)

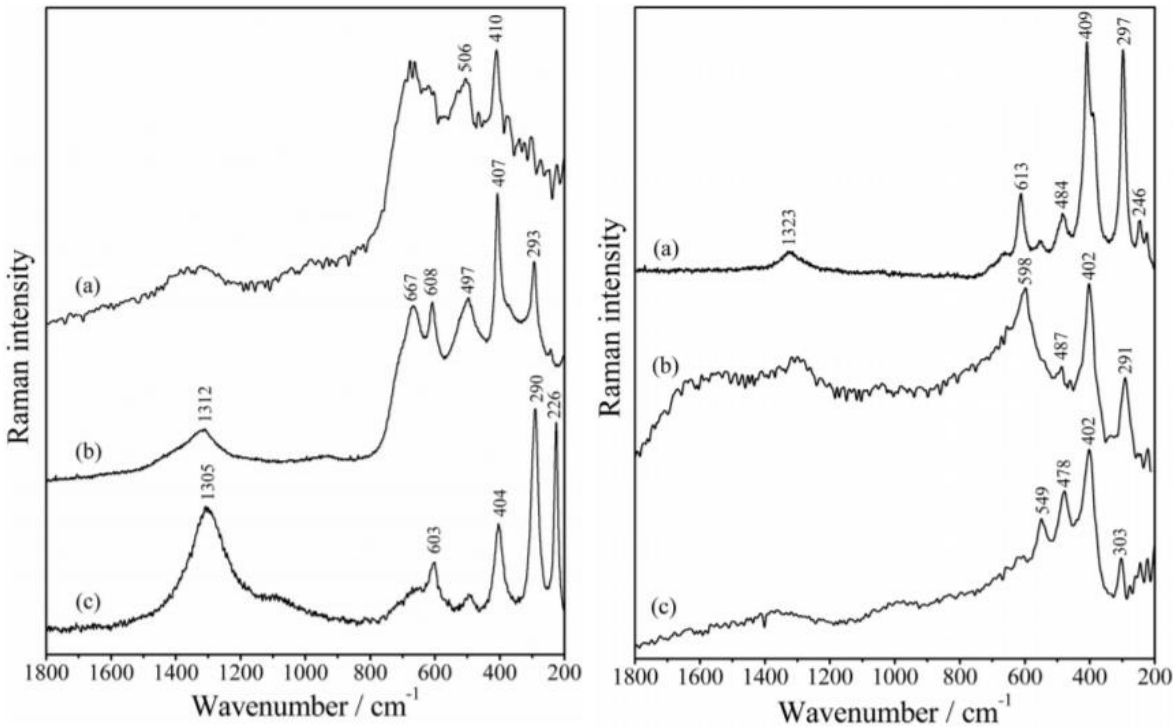

Figure 24. Raman spectra of: I) hem1 obtained in different experimental conditions: (a) with a portable Raman DeltaNu (785 nm and PD = $4*10^2 W\,cm^{-2}$); (b) with a Renishaw inVia Reflex Raman microscope (785 nm and PD = $4*10^3 W\,cm^{-2}$) and (c) with a Renishaw System 3000 (514.5 nm and PD = $1.4*10^3 W\,cm^{-2}$). II) Raman spectra of hem2 obtained (a) with a Renishaw inVia Reflex Raman microscope at PD = $8*10^4 W\,cm^{-2}$ (operating at 785 nm), and with a portable Raman DeltaNu at low laser power where (b) and (c) are different spots (123)

Still, some characteristic bands are present at any PD, see the 295 cm^{-1} one for goethite or

the 402 cm^{-1} one for hematite2. This facilitates their exclusion when looking at the spectra collected in this research for $FeCl_3$ (Figure 25a) and $Fe(OH)_2$ (Figure 25b), focused below 800 cm^{-1}. Please note that for ease of read these graphs were smoothed with a dedicated function of the software LabSpec5®. It can be seen how the two spectra are radically different from each other, this is clear evidence that, during deposition, thus sublimation, the oxidant powder undergoes a radical change: all the four characteristic bands of pristine $FeCl_3$ disappear, leaving space to two main bands, themselves completely different from any of the ones shown in Figure 21 to Figure 24, meaning that the species $FeCl_3$ transforms into are different from any of the iron oxides listed above. Discarding the unlikely discovery of a new iron-based compound, it has to be $Fe(OH)_2$. This result is significative since it confirms the assumptions made elsewhere(68). Being this an intrinsic problem of the oxidant, there is not a real way around it: either a different oxidant is used but it would likely have its own degradation path, or the application of oCVD PEDOT must be limited to de-aerated or dehydrated environments.

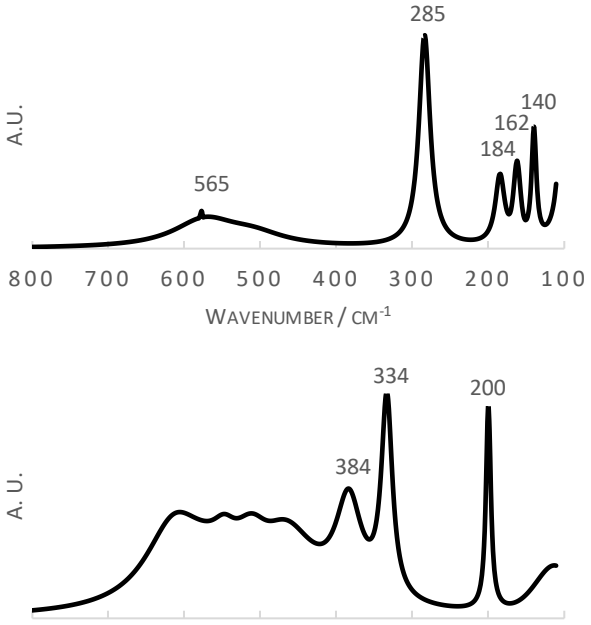

Figure 25. Raman spectrum of a) $FeCl_3$ powder before employment in the polymerization; b) $FeCl_3$ powder after employment in the polymerization. Excitation wavelength = 532 nm; accumulation time = 5s; accumulations = 3

IV.4.4.Raman of PEDOT

The discussion will focus on trends found in all the films, rather than discussing every single spectrum. The effect of time and on the differences between the optical domains shown in Figure 7 will receive particular attention. The analysis will make use of raw spectra to help visualization.

IV.4.4.1.Low wavenumbers

Having discussed the spectra of impurities, it is only logic to start the analysis from the areas of the spectra located at low wavenumbers, since it is the one

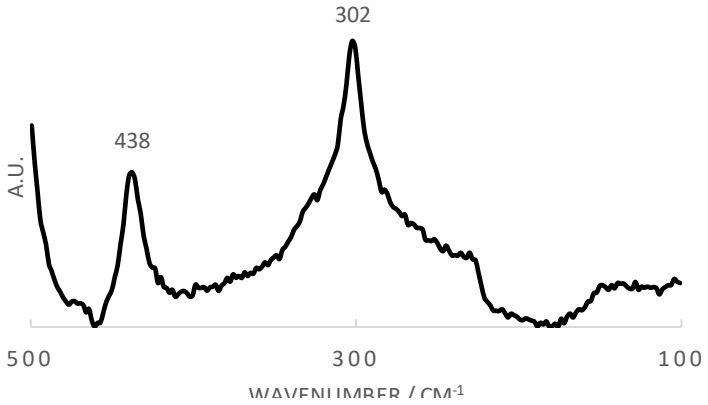

Figure 26. Spectrum of 175-50 A-NR, white optical domain. Excitation length = 532 nm; accumulation time = 5s; accumulations = 3

where they are located. The spectrum of 175-50 A-NR is shown as a reference in Figure 26. The two labelled bands are relative to PEDOT's C-O-C deformation (438 cm^{-1}) and silicon (302 cm^{-1}), no impurity related bands are present, which is coherent with the fact that this is the spectrum of the white domain in Figure 7h. The white domain has been described as a uniform transparent film of pure PEDOT lying in contact with the substrate; being it thin, the intensity of the silicon film is not quenched. The presence of the silicon band makes the normalization of the spectra of the same film collected during the 90 days possible, since it is believed that the thickness does not change over time.

In Figure 27 the evolution of 200-10 N-NR is shown as example. This is done because in all the non-rinsed samples, regardless of the storage, the white optical domain shows the same trend, therefore, for the purpose of simplicity and clarity, the discussion can be done on a singular spectrum. What can be seen is the remarkable stability of the film: normalizing the vertical axis to the silicon peak, almost not evolution is visible, there is only a small increase in intensity and a small shift to higher wavenumber of the band at 440 cm^{-1}, this is attributed to PEDOT's transformation from quinoid to benzoid structure which, together with counter-anion neutralization, modifies the environment around the C-O-C bond in the dioxyethylenic ring.

No impurities formation is visible, with no peak at either 200 cm^{-1} or 330 cm^{-1}, meaning that the film is not extensively contaminated all the way through the experiment. This means that $Fe(OH)_2$, the produce of the reactions in Figure 9 does not reside in the thin transparent film but concentrates in the coloured domains visible at the microscope. This makes sense considering that PEDOT is known for its hydrophobic nature and $Fe(OH)_2$ is characterized by ionic properties very similar to the ones of H_2O, therefore it tends to coalesce in order to reduce surface energy. Other products instead leave the sample entirely (as in the case of gaseous Cl_2 discussed in chapter IV.2.3). Considering the instrumental role of counter-anions on conductivity, another explanation could be that only a small amount of them neutralizes in 90 days without showing in Raman spectroscopy (band remains below the unavoidable background noise) while still degrading the electrical properties of the film.The spectra of the rinsed films are shown in Figure 28. Again, all the rinsed spectra show similar behavior, therefore only one is presented.

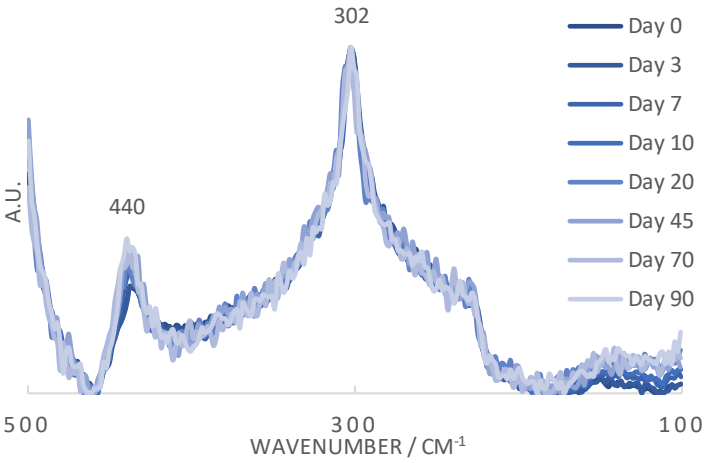

Figure 27. Spectra of 200-10 N-NR, white optical domain. Excitation length = 532 nm; accumulation time = 5s; accumulations = 3

For continuity and direct comparison, the 200-10 N-R sample is provided. As expected, the bands related to PEDOT and Silicon do not show any shift, but the relative intensity of the

PEDOT's one is larger. While it could surprise, considering that after rinsing thickness decreases, as shown in chapter IV.1., it has to be considered that the species removed by rinsing are oligomers, byproducts and contaminants present on the surface, which only act as a barrier between PEDOT and the laser; the Si band would be less influenced by this since its signal already has to go through the whole PEDOT film. Indeed, the higher intensity is likely due to the now unobstructed interaction between the latter and the laser. A significant difference with the non-rinsed samples is the decrease in intensity over time of the band at 441 cm^{-1}: this is attributed to some sort of superficial contamination of the film. It is unclear what could cause this, since the film is stored in neutral atmosphere, but it is deemed the cause of the more dramatic drop in conductivity rinsed films suffer, shown in Figure 16. This point will be further discussed in the following chapter. The most important result shown here is the presence of the bands around 200 cm^{-1} and 330 cm^{-1}. The latter, given its low relative intensity, is almost buried below the silicon's band, but appears as a very slight shoulder, while the former is perfectly visible, although marginally shifted likely due to the different measuring environment. This is proof of the presence of $Fe(OH)_2$ in a PEDOT film deposited via oCVD, a result never reported before in literature. To further cement this, inspecting the 205 cm^{-1} band, it can be seen that its intensity does not change with time and therefore it is not attributable to PEDOT, otherwise it would decrease like the band at 441 cm^{-1}. The intensity's stability tells us that $Fe(OH)_2$ amount increases over time, otherwise it would follow PEDOT's same trend.

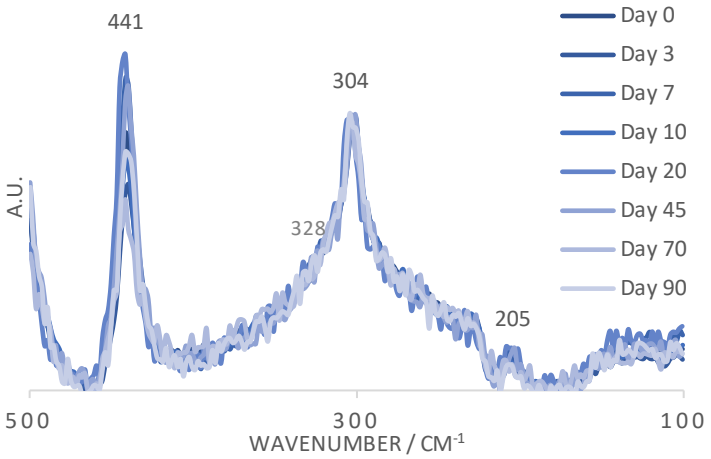

Figure 28. Spectra of 200-10 N-R, white optical domain. Excitation length = 532 nm; accumulation time = 5s; accumulations = 3

Discussed the spectra of the underlying transparent PEDOT film(white optical domain), the investigation turns again to non-rinsed samples, this time regarding the brown domains visible in Figure 8. These were present predominantly in the 175-10 A-NR sample, while in the others their size was too small to allow for their precise Raman investigation, because the laser has a circular shape with a diameter of some micrometers. An investigation of a domain smaller than this would capture informations also on the environment surrounding the target, altering the results. The spectra are shown in Figure 29 and their results reflect the expectations spanning from the discussion of chapter IV.2.2. on AFM: relating to the silicon band (302 cm^{-1}), the thicker brown domains show a much stronger PEDOT band (442 cm^{-1}) and at the same time more intense $Fe(OH)_2$ bands (327 cm^{-1} and 205 cm^{-1}). This is coherent with previous conclusions since the extra thickness is composed mostly of

$Fe(OH)_2$ and PEDOT and this not only increases the intensity of the relative bands but also decreases silicon's one. The large differences shown in the non-normalized bands in different days are caused by the fact that it is impossible to find the exact same spot after days of storage, therefore the different points investigated have different thicknesses, since, as shown, again, in chapter IV.2.2., domains appearing similar at the optical microscope (Figure 8) have a wide thickness distribution. This is particularly clear when looking at the spectra relative to days 7 and 10: both the PEDOT and $Fe(OH)_2$ bands are much weaker than in the other days, indicative of the choice of a much thinner area than the others. Stemming from this is the consideration related to the area around 120 cm^{-1}: it is evident how its evolution follows the one of the two bands considered above. This is telling of the fact that it is not just noise related to the instrument vibration, but rather an effect of other impurities present in the brown domains. It can not attributed neither to PEDOT, because it does not possess a band in the area, nor to $Fe(OH)_2$, because, as it can be seen in Figure 27, 175-50 A-NR is characterized by this band but not by the one at 205 cm^{-1}. The argument relative to the influence of thickness did not present itself in previous analyses since they were related to the underlying transparent PEDOT layer which it has been proved to be uniform and of constant thickness in the chapters on AFM and SEM.

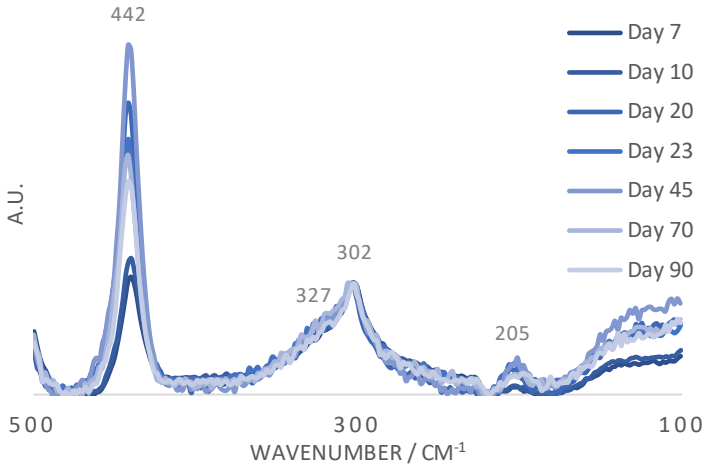

Figure 29. Spectra of 175-10 A-NR, brown optical domain. Excitation length = 532 nm; accumulation time = 5s; accumulations = 3

IV.4.4.2.High wavenumbers

Discussed the influence of impurities on the Raman spectra of oCVD PEDOT, it is time to analyze the wavenumbers from 1200 cm^{-1} to 1700 cm^{-1}, the range in which PEDOT has the bands related to the bonds that contribute to the conjugation length. It was mentioned earlier how, in order to have a conductive PEDOT thin film, it is necessary to dope it to increase the ratio between quinoid and benzoid structure, thereby increasing conjugation length and hole mobility. This has an effect on the shift of the band located around 1430 cm^{-1} as explained by Lee *et al.*(41) and Kaviani *et al.*(38) and Im *et al.(70)*: when the film is doped to a larger extent and, therefore, there is a more widespread presence of quinoid structure, conjugation length increases and the band redshifts. In the first paper, the shift was induced with the formation of crosslinked poly(anthracene-co-EDOT) and poly(biphenyl-co-EDOT) with the aim to increase optical transmittance by tuning the bandgap and as a side effect it was shown how a pristine PEDOT layer has a significant

redshift of the 1430 cm^{-1} band, symptom of longer conjugation which is interrupted by crosslinking in the copolymers. In the second and third paper, the increase in conjugation length was obtained by increasing the substrate temperature from 47 °C to 145 °C, while a further increase up to 180 °C caused degradation of the polymeric chains. The effect described is shown in Figure 30a,b(38,70) respectively. While this could seem small, it is a significant change which allows for clear identification of the better doped films and can provide a motivation as to why some films have better conductivity than others after the ageing period. What is expected is that more conductive samples after 90 days will show a redshift and that over the course of the same period, a blueshift will be visible for every sample that undergoes visible conductivity degradation.

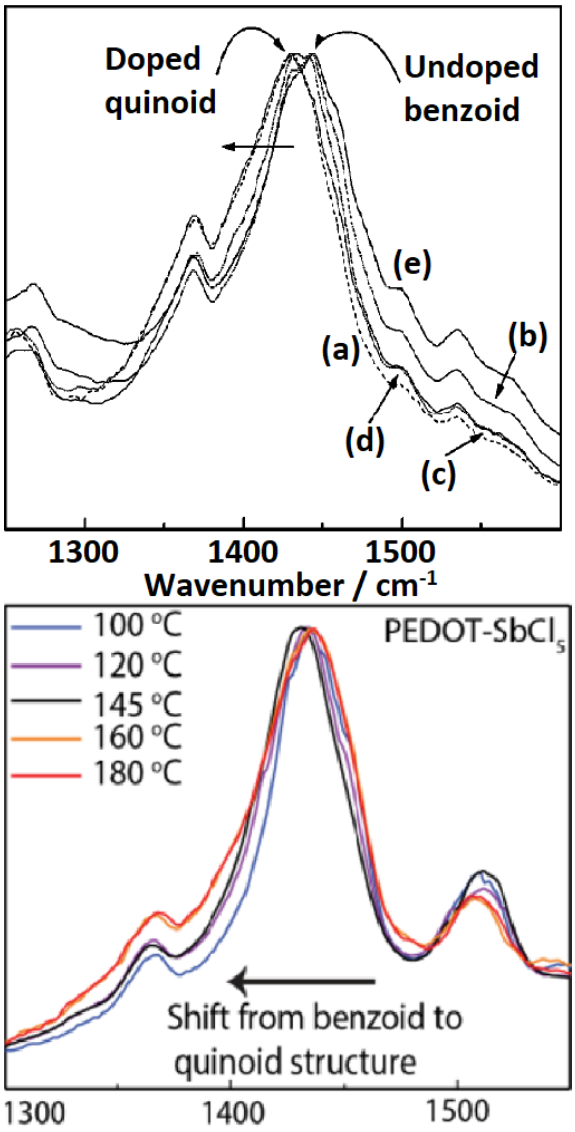

Figure 30. I) From a to e: shift of the 1430 cm^{-1} band when increasing the temperature from 47 °C to 100 °C(75); II) shift of the same band when increasing the temperature from 100 °C to 180 °C(38,70)

To maintain continuity with the previous chapter, the spectra of the same films in Figure 27-30-31 will be shown. The reader is encouraged to refer to Table 5 for the assignation of the bands, if not present the band will be attributed during this discussion. Before presenting the data, it is necessary to mention that, in order to improve readability and collect useful informations from the graphs, they were normalized to the 1430 cm^{-1} band. This was done considering that this band is the sum of two different sub-bands, the one around 1410 cm^{-1} related to quinoid structure and the other around 1440 cm^{-1} related to benzoid structure so, unlike any other, this band is indicative of the total quantity of PEDOT examined, rather than either quinoid or benzoid only. Punctualized this, the first set of spectra is visible in Figure 31. A considerable evolution can be seen from Day 0 to Day 10. First thing first, the main band in this spectra is already shifted heavily towards the quinoid band, residing around 1437 cm^{-1}, a heavy shift from the position reported by Chiu *et al.(37)*, coherent with the low initial conductivity of the samples produced in this work; second, there is a considerable thinning of the main band, which in the first days is clearly split in the two mentioned above and afterwards tends to the single one labelled at 1439 cm^{-1}: this is attributed to the

transition from quinoid to benzoid structure, causing a drastic decrease in the intensity of the relative peak, which "sinks" into the other one, causing also the general downward traslation of the spectra with time.

The shoulder at 1476 cm^{-1} is different because it does not just lose intensity but rather disappears completely, therefore it could be attributed to a vibration exclusive to the

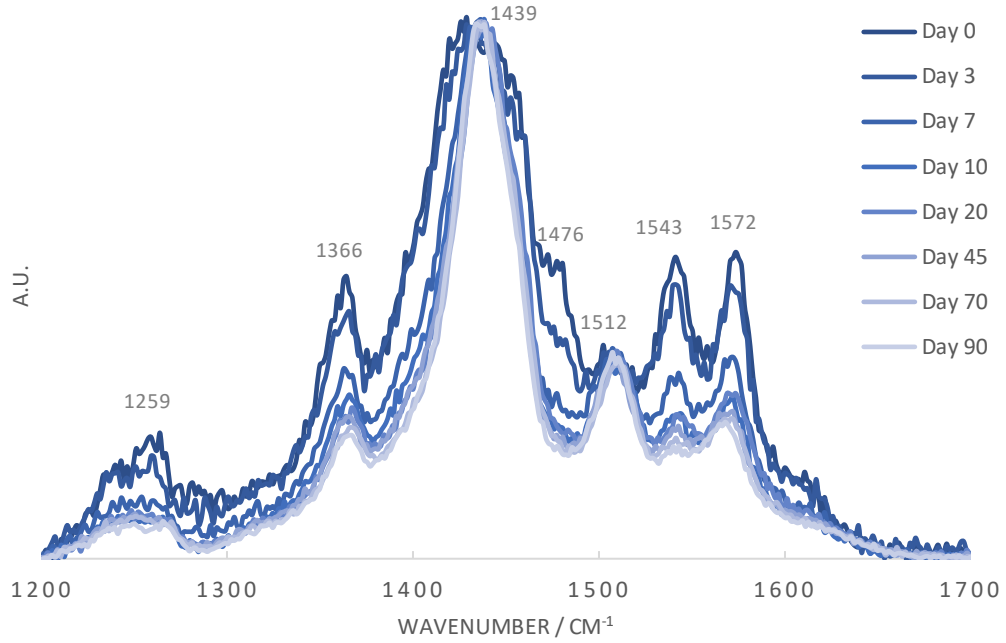

Figure 31. Spectra of 200-10 N-NR, white optical domain. Excitation length = 532 nm; accumulation time = 5s; accumulations = 3

quinoid structure. The band at 1512 cm^{-1} has a trend equal to the one at 1440 cm^{-1}: they do not decrease following the generalized loss of intensity discussed above, instead they remain stable, which means that they actually gain intensity over time. For this very reason they are attributed to vibrations exclusive to the benzoid structure, as suggested elsewhere(38). This confirms that the structures coexist from Day 0 in the film, sustaining the idea that doping efficiency is far from 100% for PEDOT. Investigating the parallel between Figure 31 and Figure 15, it can be seen how the spectra change dramatically in first 10 days, while the conductivity remains stable during this period, just to then drop at Day 45. Considering that the two spectra are only marginally different, the presence of a "doping percentage threshold" is a possible explanation: up to Day 20, while losing counter-anions to neutralization, their distribution in the film still forms long range conductive paths without loss of conjugation but, reached Day 45, even if the greater part of the degradation already happened, the residual loss of dopant causes the interruption of the aforementioned conductive channels, greatly reducing hole mobility and hindering conductivity. This has been presented as a possibility by Noriega *et al.*(126).

Taking a look at the rinsed films' spectra (Figure 32), major differences with Figure 31 appear.

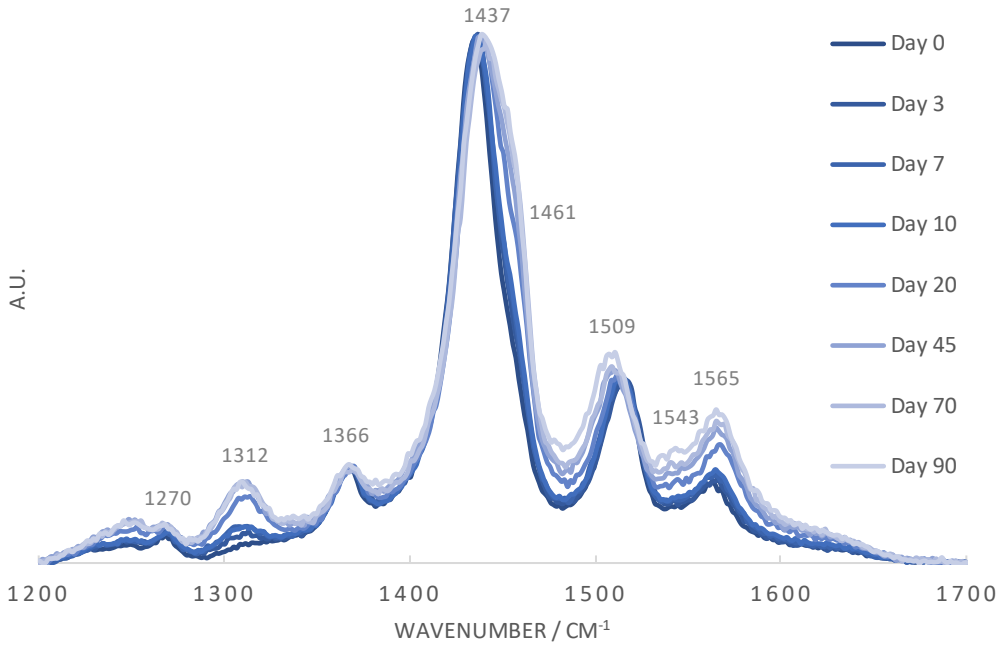

Figure 32. Spectra of 200-10 N-R, white optical domain. Excitation length = 532 nm; accumulation time = 5s; accumulations =

These are attributed to the removal of the superficial oligomers:

- Less noise
- Thinner, more defi-ned bands: less oligomers means less polydispersity index and there-fore bonds will have more similar environments in which they vibrate as the surrounding chains will all have comparable lengths
- Band at 1270 cm^{-1} is from Day 0 shifted like the one at 1259 cm^{-1} in Figure 31 is after 7 days

Significant unrelated evolution is visible: the band at 1437 cm^{-1} continuosly redshifts over the course of the analysis in parallel with the shoulder around 1455 cm^{-1} constantly gaining intensity. This latter band is attributed to CH_2 bending, much like the one at 1565 cm^{-1}(29). Their increase is explained by the uniformation of the film over time which would cause more and more of the PEDOT's CH_2 molecules to oscillate at the same frequency. This change in the surroundings of the CH_2 is also sustained by the shift visible in the 1565 cm^{-1} band, which redshifts up to Day 20 just to then blueshift again from Day 45 onwards. This evolution is enabled by the fact that counter-anions' steric hindrance changes, when they are neutralized, forcing a slow rearrangement over time of the random coil formation of the polymeric chains. The phenomenon described above is present in Figure 31 as well, but it is less noticeable because of the wider bands and higher background noise. The band at 1509 cm^{-1}, which is related to C_α=C_β antisymmetric stretching in plane modes, the opposite of the band at 1437 cm^{-1}, which is symmetric stretching of the same bond, predictably has

the reverse shift compared to the latter, consolidating the idea of a chemically-induced shift, rather than an instrumentally-induced one. Overall, the changes undergone by the rinsed films appear to be less significative than the ones of their non-rinsed counterparts, making it hard to understand why they suffer a much stronger electronic degradation.
This could be explained by the strange band appearing over time at 1312 cm^{-1}: not present at Day 0, it shows up at Day 3, with a continuous increase which has its apex between Day 20 and 45, exactly when the conductivity has the sharpest drop. Its attribution is unknown, and its existence is not mentioned in any paper on Raman spectroscopy of PEDOT. It appears in rinsed samples in any deposition and storage, while it is not visible for non-rinsed films, leading to the belief that it could be related to contamination introduced by the rinsing solution. Still, this is unlikely, since methanol is very volatile and after rinsing the samples are let to dry, even if, given the nanoporosity of the film shown in Figure 13, some could remain trapped in the deeper layers from where it can not evaporate. This band attracts a lot of attention and requires further investigation, although, being this the first work to ever mention its existence and given the intrinsically random nature of oCVD, it is hard to envision a way to systematically reproduce its appearance for further study.
Concluded the discussion on time evolution, it is time to do a direct comparison between non-rinsed and rinsed samples. In order to visualize better the differences, only one spectrum for each class will be used. Days 0, 20 and 90 will be investigated as they are thought to be the most relevant to the discussion. The labels in the pictures are related to pairs of bands related to the same vibrational mode in the two spectra.

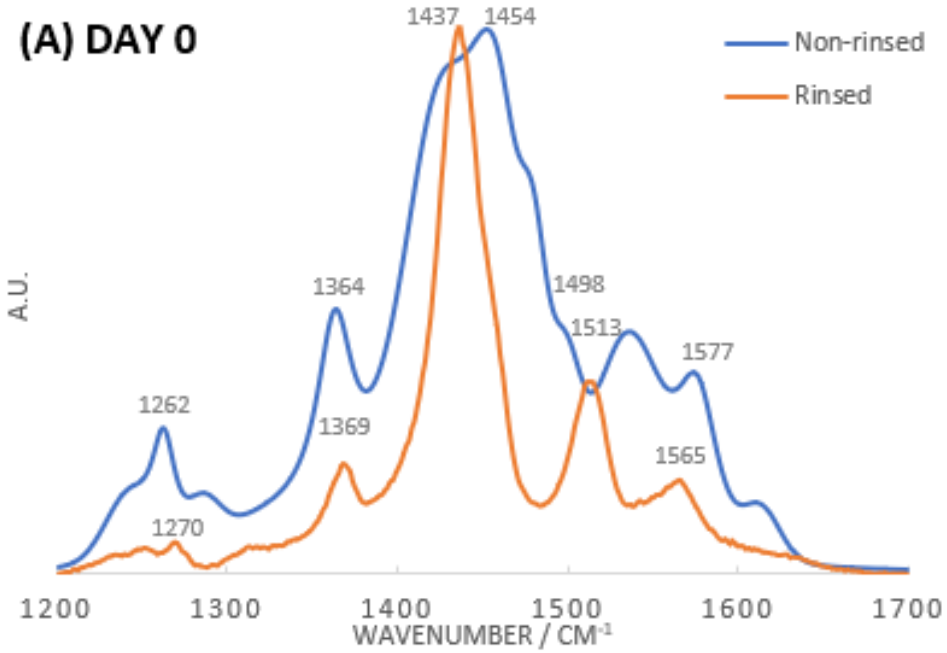

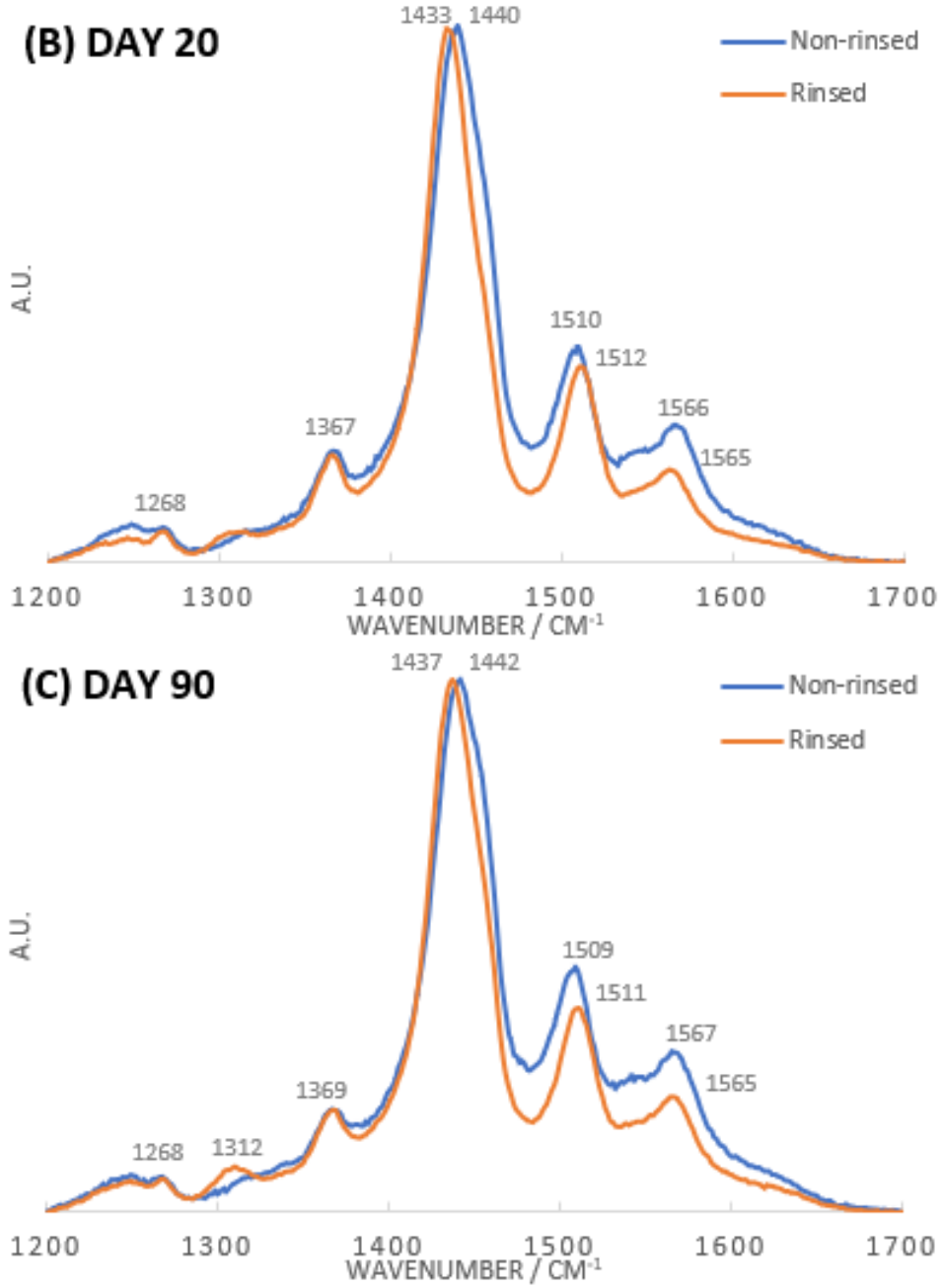

Figure 33. Spectra comparison between 175-10 A-NR and 175-10 A-R at a) Day 0; b) Day 20; c) Day 90

Day 0: immediately after deposition the conductivity for the two samples was 103 S/cm for the non-rinsed one and 174 S/cm for the other. This difference could not only be related to the lower thickness of the rinsed film (Table 4), but also to chemical aspects well visible in Figure 33a: the central band is thinner and has its apex around 1437 cm^{-1} for the rinsed sample, showing only a weak shoulder around 1450 cm^{-1}, where the non-rinsed film instead shows a very strong band attributable to the benzoid structure. This is due to the presence of oligomers, whose shorter chains have intrinsic difficulties to form long conjugation and therefore lower the conductivity. However the it still is relatively high since these short chains are only present on the surface. The oligomers cause not only the broadening of the

bands and the correlated loss of band definition, but also cause the spectrum to appear as if the material was much richer in benzoid structure than what the conductivity measurements evidence, as it can be seen by the significant blueshift of the band at 1498 cm^{-1} compared to its rinsed counterpart. All in all, they differences in electronic performance are marginal when compared to the chemical differences, which is logical, considering that conductive charges, much like water running downhill, will always choose the easiest pathway.

Day 20: after 20 days the conductivity of 175-10 A-NR has already dropped by almost one order of magnitude and sits at 39 S/cm, while the one of 175-10 A-R sits at 110 S/cm, higher than the other's initial value. The rinsed film shows relatively small evolution, with just a marginal redshift of the main band, which would imply an increase in the content of quinoid PEDOT and a subsequent increase in conjugation length. This is not sustained by the macroscopic conductivity measurements, but it is possible that choosing a spot for Raman spectroscopy, the laser was focused in one of the brighter areas evidenced in Figure 13d (invisible at the optical microscope) which, as explained in the same section, are symptom of higher local conductivity, symptom of higher conjugation due to more efficient doping. The non-rinsed spectrum undergoes significant changes, becoming comparable with the rinsed one: the secondary bands at 1268 cm^{-1}, 1366 cm^{-1} and 1510 cm^{-1} shift towards the values seen in the rinsed spectrum, while the central band is shifted right, signaling the presence of a larger amount of benzoid PEDOT, coherently with the conductivity values reported.

Day 90: at this moment, both the films have lost their metallic behavior, with conductivity respectively at 3 S/cm and 10 S/cm. The position of the minor bands is unchanged, while the central one redshifts by 4 cm^{-1} for the rinsed sample; together with the contamination discussed for Figure 32, here visible in the form of the not attributed band at 1312 cm^{-1}, these factors explain the much more intense conductivity decrease of this film, when compared to its counterpart, whose further degradation is explained by the small redshift of the main band since Day 20, evidence of a limited increase in benzoid PEDOT presence.

To conclude, the more messy nature of the spectrum of the non-rinsed samples visible at Day 0 is quenched by the exposure to air which not only increases the amount of $Fe(OH)_2$ present in the film (Figure 29), but also has an effect on the raman spectra comparable to the one rinsing has. It is not certain why this would be, although a possible explanation is that superficial oligomers continue to react with excess oxidant to form longer chains during the first few days; in fact, while part of the oxidant forms $Fe(OH)_2$, it is possible that some remains trapped in the nanopores scattered all over the film, where RH is not high enough to convert it to iron hydroxide. The formation of these longer chains would explain the more and more significant similarity between the two spectra, meanwhile the fact that oligomers are benzoid-rich would explain why, even with further reaction happening over time, this character is retained, as shown by the redshift of the main band in Figure 33b,c.

The comparison just finished can be repeated investigating the effect of storage. Non-rinsed samples will be investigated, since they ultimately yield the best conductivity and therefore are more relevant. For obvious reasons, only Day 20 and Day 90 are investigated in Figure 34a,b respectively.

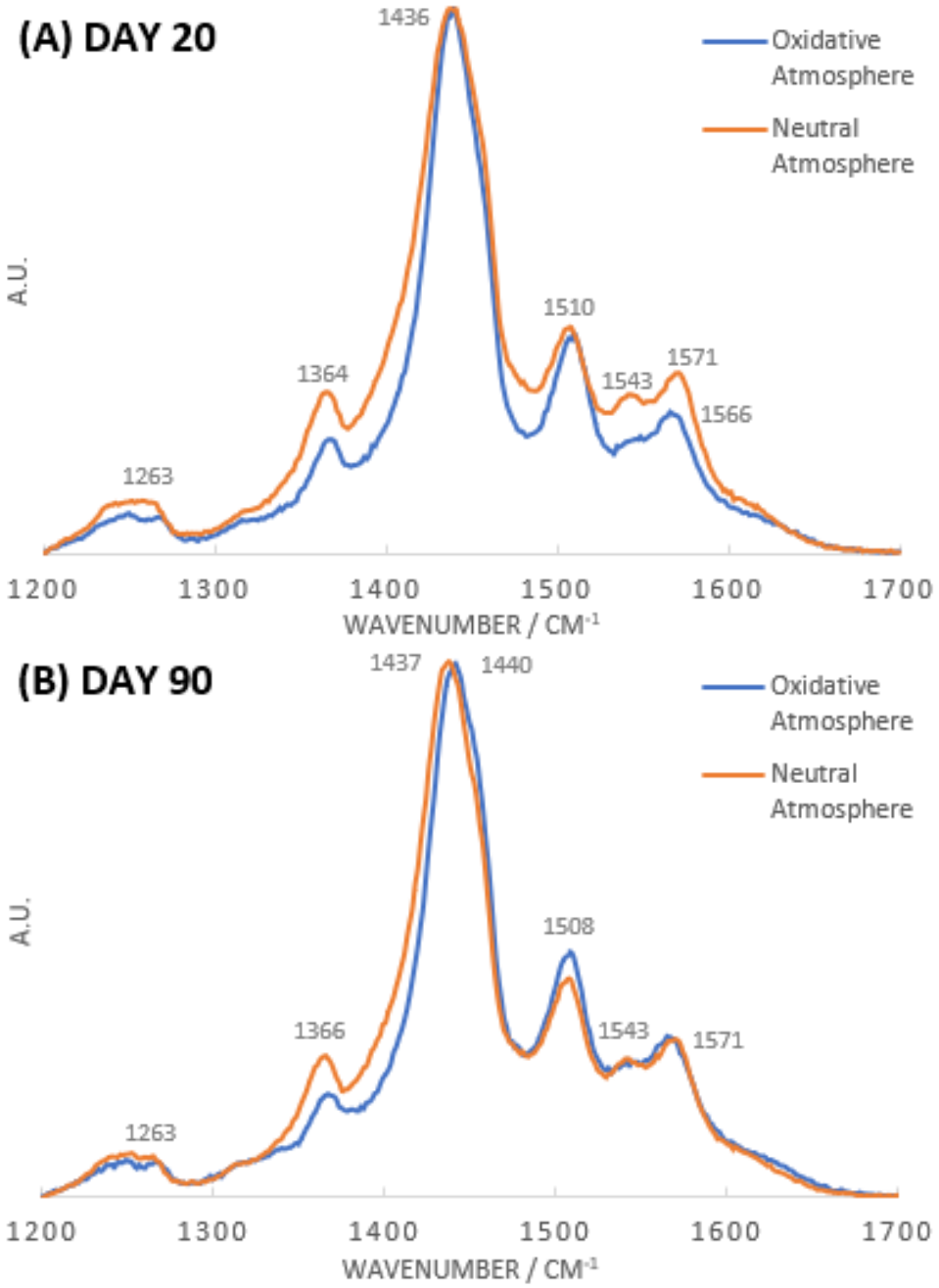

Figure 34. Spectra comparison between 175-10 A-NR and 175-10 N-NR at a) Day 20; b) Day 90

Day 20: at Day 20, 175-10 A-NR and 175-10 N-NR have a conductivity of 39 S/cm and 80 S/cm respectively. Recalling their common Day 0 (Figure 33a), it is evident how the reaction of the oligomers explained above is slower when storing in neutral atmosphere. This is sustained by the increased broadness of the bands caused by the higher polydispersity index. The band at 1543 cm^{-1} could be seen as its "indicator of progress": strongest at Day

0, loses intensity with time, remaining more visible for the sample that evolves the least. Said band is not present in rinsed samples, leading to its attribution to CH_2 bending(29) in short chains located on the surface which, it is important to remember, get washed away by methanol. Considering that the central band has its peak at the same shift for the two, the difference in conductivity can be attributed solely to a lower dopant neutralization ratio in de-aerated atmosphere, in line with the reactions shown in Figure 9. The shift to the CH_2 band at 1571 cm^{-1} seems to confirm the difference in the environments of the two specimens.

Day 90: the conductivity of the two films at this moment was 3 S/cm for 175-10 A-NR and 42 S/cm for 175-10 N-NR. This is justified by the redshift visible for the latter watching the band at 1437 cm^{-1} and the lower intensity of the one at 1508 cm^{-1}, strictly related to the benzoid form of PEDOT. The band at 1543 cm^{-1} is still visible as well, consolidating the assumptions discussed above regarding its role as an indicator of progress for quinoid-benzoid transition in PEDOT caused by dopant neutralization.

IV.4.5.Raman conclusions

The characterization carried out in this work has been very deep, possibly more than any other paper on this subject. It yielded many interesting results that fit correctly into the landscape of PEDOT research, furthering the knowledge of the material the scientific community had and consolidating what were only assumptions and yet, many questions were left unanswered, leaving room for further investigation. To highlight the most relevant conclusions among the many notions discussed above, they are listed here:

- In-depth comparison between bibliography and experimental data showed a chemical reaction involving the oxidant during the deposition process. $FeCl_3$ powder transforms into an iron oxide whose spectrum is different from all the ones shown. Based on bibliography(68), $Fe(OH)_2$ is believed to be that compound
- Evidence of the presence of $Fe(OH)_2$ has been found in the films: in non-rinsed ones it is present in large amount in brown-colored domains (Figure 13 and Figure 14) while not in the white on, while in rinsed films it is present everywhere. This suggests that considerations on interface energy lead to coalescence in spots where the internal energy can be minimized, present in non-rinsed films, while they are not present in rinsed ones, leading to a uniform distribution of $Fe(OH)_2$
- The effect of conjugation length modification on Raman spectra was discussed, with references to study on the matter. The behavior showed by the samples involved in this research was coherent with the electrical conductivity trends shown in chapter IV.3. Conjugation length decreases causing a redshift of the central PEDOT band around 1437 cm^{-1}; in parallel, the benzoid structure-exclusive band at 1508 cm^{-1} increases in intensity

- Dramatic evolution is visible in the first 10 days for non-rinsed specimens, with evidence of considerable transition from quinoid to benzoid structure that culminates in the conductivity drop after Day 10. The fact that this dramatic yet gradual degradation has no significative effect on conductivity before Day 10, leads to the thought that counter-anion neutralization has to reach a threshold before hole mobility drops drastically due to conjugation length reduction; this behavior is attributed to the fact that some conductive channels are retained until the dedoping is extensive enough, *alas* when the threshold is reached
- Bands become thinner with rinsing, symptom of a reduction in polydispersity index caused by the removal of superficial oligomers. Local chain rearrangement is deemed responsible of this effect as well. For non-rinsed films, time evolution has the same effect on Raman spectra, suggesting that spontaneous polymerization continues on the surface of the film, where oligomers combine with each other and with unreacted species to form longer chains. Counter-anion neutralization has a role in this as well, since their evacuation contributes to uniform the chemical environment of the chains, reducing the vibrational frequencies spread
- This last fact is sustained by the comparison between films stored in oxidative atmosphere and ones stored in neutral atmosphere: the latter have thicker bands, symptom of the less homogeneous chemical environment of the molecules and these indeed show better conductivity from Day 20 onwards
- Their better performance is also explained by the blueshift of the central band and the lower intensity of the one at 1510 cm^{-1} which show the presence of less benzoid structure PEDOT
- The band at 1543 cm^{-1}, present at Day 0, has a gradual decline over time in non-rinsed samples, while it does not show in rinsed ones. Its evolution is slower for samples stored in neutral atmosphere. The band's attribution to CH_2 bending(29) leads to the conclusion that these CH_2 are the ones of short superficial chains. Its gradual decrease then consolidates the thought of a spontaneous polymerization occurring over time which is slower under argon storage

These conclusions are of significant importance and could allow this work to establish its role as a reference for future studies on this topic.

Chapter V: Conclusions and perspectives

The aim of the research was double: find the most suitable conditions for the deposition of PEDOT via oxidative Chemical Vapor Deposition with $FeCl_3$ as oxidant and provide a detailed analysis of its degradation mechanism, proposing a degradation path and linking it to the material's electronic behavior. In order to perform an in-depth characterization, process parameters, like oxidant crucible temperature and N_2 (carrier gas), and post-process parameters, like methanol rinsing and storage in oxidative or neutral atmosphere, were investigated. The first allowed to establish the deposition conditions most suitable to the production of highly $FeCl_3$-doped PEDOT; the second allowed to determine the most suitable application conditions for oCVD PEDOT assessing its lifespan as a conductive polymer. Three different oxidant crucible temperatures (175 °C, 200 °C and 240 °C) and three different N_2 flow rates (10 sccm, 50 sccm and 100 sccm) were tested. Lower EDOT/$FeCl_3$ ratio samples, *i.e.* the ones at low T and N_2 flow rate, showed the highest conductivity, with a maximum of 264 S/cm for the 175-10 Air-Rinsed one. However low when compared to other deposition methods, the aim of this study was not to maximize the conductivity but rather verify which of the chosen process conditions would be the best in order to provide a basis for future studies to start from. At the microscope, the films proved to be formed by at least two different structures: common to all, an underlying transparent and homogeneous PEDOT thin film; in the non-rinsed samples, it was surmounted by thick, brown-colored domains. These were not present in the methanol rinsed ones, evidencing their non-PEDOT nature, since the polymer is not soluble in any solvent. From AFM measurements, it was confirmed that the 175-10 Air-Non rinsed (on which the analysis focused due to its better electronic conductivity) film was characterized by a large thickness deviation: the colored domains reached thicknesses above 100 nm, while the transparent layer stood around 45 nm, in line with the profilometry results. Its rinsed counterpart, instead, showed uniform thickness around 33 nm, again in line with profilometry. Thanks to SEM it was possible to identify the amorphous nanostructure of the samples, which showed remarkable differences between non-rinsed and rinsed specimen: in the former, large leaf-like nanostructures dominated the surface regardless of the optical domain inspected, while, in the latter, small rod-like nanostructures were found, similar to the ones seen for pristine $FeCl_3$ films deposited as a reference. This result is in line with the good conformal coverage PEDOT allows, as reported in literature. In parallel to SEM, EDS analyses were performed and it provided with univocal confirmation of the nature of the brown optical domains discussed: it was found that they are composed of a large quantity of Fe and O, while no traces of S were found, confirming the non-PEDOT nature.

This is remarkable since it is testimony of the presence of excess $FeCl_3$ during deposition which, after reacting to form a uniform transparent PEDOT layer, deposits on top of it where, once extracted from the reactor, attracts water due to its hygroscopic nature and reacts to form these iron oxides islands. After analyzing the surface of the films with microscopy, their electronic properties were investigated: for non-rinsed samples stored in air, the conductivity was found to have a dramatic drop after only 10 days from the deposition, while this time extended to 20 days for the rinsed ones and the ones stored in neutral atmosphere. The degradation was attributed to the set of reactions shown in Figure 9: counter-anions neutralization is caused by the presence of both humidity and oxygen and is catalyzed by the presence of unreacted $FeCl_3$ in the films. This explains both why specimens stored in neutral atmosphere (de-aerated, anhydrous storage environment) and rinsed samples (residual $FeCl_3$ is removed) show less degradation and proposes as a final product $Fe(OH)_2$, an iron hydroxide whose formation is coherent with the EDS measurements. To further confirm the proposed degradation path, the final aim of this thesis, Raman spectroscopy was executed all throughout the analysis period. First, spectroscopy of pure $FeCl_3$ and of the powder located in the crucible after deposition were performed; second, extensive research was done to find the spectra of different iron oxides to compare them with: while a $Fe(OH)_2$ spectrum was not found, ones for all other iron oxides (goethite, magnetite, hematite) and iron(II)hydroxide were studied. The difference between $FeCl_3$ powder and the powder after deposition was evident, disguising its oxidation. However, no similarities were found with the other oxides' spectra. The exclusion of all other iron oxides leads to the conclusion that, yes, $FeCl_3$ reacts to form $Fe(OH)_2$. This was confirmed also by the finding of the two bands related to the oxidized powder in the film (Figure 29). They had, however, a complicated phenomenology:

- The bands did not appear in the transparent underlying PEDOT layer in non-rinsed
- The bands were much more intense for the thick, brown domains, proven Fe and O rich
- The bands were present in the uniform PEDOT layer in rinsed samples

These findings have a logical explanation: counter-anion neutralization is a spontaneous process, triggered by the simultaneous presence of H_2O and O_2; once $Fe(OH)_2$ is produced, it tends to coalesce into the brown domains in order to reduce the total energy of the system; in rinsed samples this is not possible, since coalescence centers (impurities, reaction by-products, unreacted species, oligomers) get washed away, and the compound remains distributed evenly in the film. Discussed the evolution of the impurities, the analysis moved to the area of the spectrum where PEDOT has its characteristic bands, in the hope to find a trend coherent with the conductivity degradation evidenced by sheet resistance measurements. PEDOT can show two structures: quinoid, which is conductive and benzoid, which is not. These always coexist in the thin film, since quinoid is obtained

when a counter-anion is in position to dope a determined chain segment, but the maximum doping percentage for PEDOT is 30%. This fact renders non-trivial the evaluation of a typical PEDOT Raman spectrum: the differences in the signal of the two structures are small: the most relevant one is the progressive redshift of the band situated around 1435 cm^{-1} when increasing amounts of benzoid structure are present in the film. This is exactly what can be seen in the spectra obtained: over time, the aforementioned redshift is visible, confirming the evolution from quinoid to benzoid PEDOT, coherently with the conductivity degradation by dopant neutralization described in this work because, once the counter-anion is lost, the chains tend to rearrange to the benzoid structure, which is the more stable of the two in this scenario, diminishing the electronic performance of the thin film. Sustaining this explanation is the progressive blueshift and increase in intensity of the band at 1510 cm^{-1} for all the films since it is attributed solely to benzoid structure's vibrational modes.

This work evidenced some critical drawbacks relative to PEDOT deposited via oCVD using $FeCl_3$ as an oxidant: electronic stability is limited under prolonged exposition to atmosphere, a crucial issue when envisioning applications which require decent properties for more than some days. Even when not exposed to atmospheric conditions for long, the material still undergoes degradation, even if reduced. This is a testament to the steps forward that the deposition process needs to make, in order to obtain stable polymeric thin films. The usage of different oxidants has been tested elsewhere but it was not possible to verify here how they would fare with regard to their stability, further research is therefore required on the matter; other analyses like XPS, GDOES and others could be used.

While other papers already investigated the effects of accelerated ageing, this thesis is the first example of systematic characterization during extended time period; this imposes it as a reference in the research field of PEDOT and conductive polymers in general.

Bibliography

(1) Bolto BA, McNeill R, Weiss DE. Electronic Conduction in Polymers. III. Electronic Properties of Polypyrrole. Aust J Chem 1963;16(6):1090-1103.

(2) Chiang CK, Fincher CR, Park YW, Heeger AJ, Shirakawa H, Louis EJ, et al. Electrical Conductivity in Doped Polyacetylene. Phys Rev Lett 1977 Oct;39(17):1098-1101.

(3) Shirakawa H, Louis EJ, MacDiarmid AG, Chiang CK, Heeger AJ. Synthesis of electrically conducting organic polymers: halogen derivatives of polyacetylene, (CH). J.Chem.Soc.{,} Chem.Commun. 1977(16):578-580.

(4) Maeda R, Kawakami H, Shinohara Y, Kanazawa I, Mitsuishi M. Thermoelectric properties of PEDOT/PSS films prepared by a Gel-film formation process. Materials Letters 2019 15 September 2019;251:169-171.

(5) Fischer R, Gregori A, Sahakalkan S, Hartmann D, Büchele P, Tedde SF, et al. Stable and highly conductive carbon nanotube enhanced PEDOT:PSS as transparent electrode for flexible electronics. Organic Electronics 2018 November 2018;62:351-356.

(6) Subramanyam BVRS, Mahakul PC, Sa K, Raiguru J, Alam I, Das S, et al. Improved stability and performance of organic photovoltaic cells by application of carbon nanostructures and PEDOT:PSS composites as additional transparent electrodes. Solar Energy 2019 1 July 2019;186:146-155.

(7) Lee JJ, Yoo D, Park C, Choi HH, Kim JH. All organic-based solar cell and thermoelectric generator hybrid device system using highly conductive PEDOT:PSS film as organic thermoelectric generator. Solar Energy 2016 September 2016;134:479-483.

(8) Wang X, Meng F, Wang T, Li C, Tang H, Gao Z, et al. High performance of PEDOT:PSS/SiC-NWs hybrid thermoelectric thin film for energy harvesting. Journal of Alloys and Compounds 2018 15 February 2018;734:121-129.

(9) Yamamoto T, Sanechika K, Yamamoto A. Preparation of thermostable and electric-conducting poly(2,5-thienylene). J Polym Sci B Polym Lett Ed 1980 01/01; 2019/11;18(1):9-12.

(10) Li C, Jiang F, Liu C, Liu P, Xu J. Present and future thermoelectric materials toward wearable energy harvesting. Applied Materials Today 2019;15:543.

(11) Ning C, Zhou Z, Tan G, Zhu Y, Mao C. Electroactive polymers for tissue regeneration: Developments and perspectives. Progress in Polymer Science 2018;81:144.

(12) Wang R, Wang J, Tan S, Duan Y, Wang Z, Yang Y. Opportunities and Challenges of Lead-Free Perovskite Optoelectronic Devices. Trends in Chemistry 2019 July 2019;1(4):368-379.

(13) Ghorbani Zamani F, Moulahoum H, Ak M, Odaci Demirkol D, Timur S. Current trends in the development of conducting polymers-based biosensors. TrAC Trends in Analytical Chemistry 2019 September 2019;118:264-276.

(14) Huynh T, Sharma PS, Sosnowska M, D'Souza F, Kutner W. Functionalized polythiophenes: Recognition materials for chemosensors and biosensors of superior sensitivity, selectivity, and detectability. Progress in Polymer Science 2015 August 2015;47:1-25.

(15) van Mullekom HAM, Vekemans JAJM, Havinga EE, Meijer EW. Developments in the chemistry and band gap engineering of donor–acceptor substituted conjugated polymers. Materials Science and Engineering: R: Reports 2001 1 February 2001;32(1):1-40.

(16) Koyama T, Nakamura A, Kishida H. Microscopic Mobility of Polarons in Chemically Doped Polythiophenes Measured by Employing Photoluminescence Spectroscopy. ACS Photonics 2014 08/20;1(8):655-661.

(17) Perepichka I , Perepichka D , Meng H, Wudl F. Light-Emitting Polythiophenes. Adv Mater 2005 10/04; 2019/11;17(19):2281-2305.

(18) Nielsen CB, McCulloch I. Recent advances in transistor performance of polythiophenes. Progress in Polymer Science 2013 December 2013;38(12):2053-2069.

(19) Daoust G, Leclerc M. Structure-property relationships in alkoxy-substituted polythiophenes. Macromolecules 1991 01/01;24(2):455-459.

(20) Heywang G, Jonas F. Poly(alkylenedioxythiophene)s—new, very stable conducting polymers. Adv Mater 1992 02/01; 2019/09;4(2):116-118.

(21) Jonas F, Schrader L. Conductive modifications of polymers with polypyrroles and polythiophenes. Synthetic Metals 1991 6 May 1991;41(3):831-836.

(22) Pei Q, Zuccarello G, Ahlskog M, Inganas O. Electrochromic and highly stable poly(3,4-ethylenedioxythiophene) switches between opaque blue-black and transparent sky blue. Polymer 1994;35(7):1347.

(23) Diaz AF, Kanazawa KK, Gardini GP. Electrochemical polymerization of pyrrole. J Chem Soc , Chem Commun 1979(14):635-636.

(24) Genies EM, Bidan G, Diaz AF. Spectroelectrochemical study of polypyrrole films. Journal of Electroanalytical Chemistry and Interfacial Electrochemistry 1983 8 July 1983;149(1):101-113.

(25) Sadki S, Schottland P, Brodie N, Sabouraud G. The mechanisms of pyrrole electropolymerization. Chem Soc Rev 2000;29(5):283-293.

(26) Kirchmeyer S, Reuter K. Scientific importance, properties and growing applications of poly(3,4-ethylenedioxythiophene). J Mater Chem 2005;15(21):2077-2088.

(27) Lock JP, Im SG, Gleason KK. Oxidative Chemical Vapor Deposition of Electrically Conducting Poly(3,4-ethylenedioxythiophene) Films. Macromolecules 2006 08/01;39(16):5326-5329.

(28) Winther-Jensen B, West K. Vapor-Phase Polymerization of 3,4-Ethylenedioxythiophene: A Route to Highly Conducting Polymer Surface Layers. Macromolecules 2004 06/01;37(12):4538-4543.

(29) Tran-Van F, Garreau S, Louarn G, Froyer G, Chevrot C. Fully undoped and soluble oligo(3,4-ethylenedioxythiophene)s: spectroscopic study and electrochemical characterization. J.Mater.Chem. 2001;11(5):1378-1382.

(30) Howden RM, Flores EJ, Bulović V, Gleason KK. The application of oxidative chemical vapor deposited (oCVD) PEDOT to textured and non-planar photovoltaic device geometries for enhanced light trapping. Organic Electronics 2013 September 2013;14(9):2257-2268.

(31) Jonas F, Morrison JT. 3,4-polyethylenedioxythiophene (PEDT): Conductive coatings technical applications and properties. Synthetic Metals 1997 15 March 1997;85(1):1397-1398.

(32) Hui Y, Bian C, Xia S, Tong J, Wang J. Synthesis and electrochemical sensing application of poly(3,4-ethylenedioxythiophene)-based materials: A review. Analytica Chimica Acta 2018 31 August 2018;1022:1-19.

(33) Dietrich M, Heinze J, Heywang G, Jonas F. Electrochemical and spectroscopic characterization of polyalkylenedioxythiophenes. Journal of Electroanalytical Chemistry 1994 16 May 1994;369(1):87-92.

(34) Ahonen HJ, Lukkari J, Kankare J. n- and p-Doped Poly(3,4-ethylenedioxythiophene): Two Electronically Conducting States of the Polymer. Macromolecules 2000 09/01;33(18):6787-6793.

(35) Gustafsson H, Kvarnström C, Ivaska A. Comparative study of n-doping and p-doping of poly(3,4-ethylenedioxythiophene) electrosynthesised on aluminium. Thin Solid Films 2008 28 November 2008;517(2):474-478.

(36) Kvarnström C, Neugebauer H, Ivaska A, Sariciftci NS. Vibrational signatures of electrochemical p- and n-doping of poly(3,4-ethylenedioxythiophene) films: an in situ attenuated total reflection Fourier transform infrared (ATR-FTIR) study In honour of

Professor Giu0seppe Zerbi on the occasion of his 65th birthday. Journal of Molecular Structure 2000 28 March 2000;521(1):271-277.

(37) Chiu WW, Travaš-Sejdić J, Cooney RP, Bowmaker GA. Studies of dopant effects in poly(3,4-ethylenedi-oxythiophene) using Raman spectroscopy. J Raman Spectrosc 2006 12/01; 2019/06;37(12):1354-1361.

(38) Kaviani S, Mohammadi Ghaleni M, Tavakoli E, Nejati S. Electroactive and Conformal Coatings of Oxidative Chemical Vapor Deposition Polymers for Oxygen Electroreduction. ACS Appl Polym Mater 2019 03/08;1(3):552-560.

(39) Rudd S, Murphy PJ, Evans DR. Diffusion controlled vapour deposition of mixed doped PEDOT. Synthetic Metals 2018 August 2018;242:61-66.

(40) Howden RM, McVay ED, Gleason KK. oCVD poly(3,4-ethylenedioxythiophene) conductivity and lifetime enhancement via acid rinse dopant exchange. J.Mater.Chem.A 2013;1(4):1334-1340.

(41) Lee S, Gleason KK. Enhanced Optical Property with Tunable Band Gap of Cross-linked PEDOT Copolymers via Oxidative Chemical Vapor Deposition. Adv Funct Mater 2015 01/01; 2019/06;25(1):85-93.

(42) Piro B, Mattana G, Zrig S, Anquetin G, Battaglini N, Capitao D, et al. Fabrication and Use of Organic Electrochemical Transistors for Sensing of Metabolites in Aqueous Media. Applied Sciences 2018 06;8:928.

(43) Tenhaeff WE, Gleason KK. Initiated and Oxidative Chemical Vapor Deposition of Polymeric Thin Films: iCVD and oCVD. Adv Funct Mater 2008 04/11; 2019/11;18(7):979-992.

(44) Meng Q, Jiang Q, Cai K, Chen L. Preparation and thermoelectric properties of PEDOT:PSS coated Te nanorod/PEDOT:PSS composite films. Organic Electronics 2019 January 2019;64:79-85.

(45) Liu S, Li H, He C. Simultaneous enhancement of electrical conductivity and seebeck coefficient in organic thermoelectric SWNT/PEDOT:PSS nanocomposites. Carbon 2019 August 2019;149:25-32.

(46) Stepien L, Roch A, Tkachov R, Leupolt B, Han L, van Ngo N, et al. Thermal operating window for PEDOT:PSS films and its related thermoelectric properties. Synth Met 2017 March 2017;225:49-54.

(47) Zhang L, Harima Y, Imae I. Highly improved thermoelectric performances of PEDOT:PSS/SWCNT composites by solvent treatment. Organic Electronics 2017 December 2017;51:304-307.

(48) Zhu Z, Liu C, Jiang F, Xu J, Liu E. Effective treatment methods on PEDOT:PSS to enhance its thermoelectric performance. Synth Met 2017 March 2017;225:31-40.

(49) Hareesh K, Shateesh B, Joshi RP, Dahiwale SS, Bhoraskar VN, Haram SK, et al. PEDOT:PSS wrapped NiFe2O4/rGO tertiary nanocomposite for the super-capacitor applications. Electrochim Acta 2016 20 May 2016;201:106-116.

(50) Lee S, Eom T, Kim M, Yang S, Shim BS. Durable soft neural micro-electrode coating by an electrochemical synthesis of PEDOT:PSS / graphene oxide composites. Electrochim Acta 2019 1 August 2019;313:79-90.

(51) Patil DS, Pawar SA, Shin JC. Silver decorated PEDOT:PSS wrapped MnO2 nanowires for electrochemical supercapacitor applications. Journal of Industrial and Engineering Chemistry 2018 25 June 2018;62:166-175.

(52) Zhou Q, Zhu D, Ma X, Mo D, Jiang F, Xu J, et al. PEDOT:PSS-assisted polyindole hollow nanospheres modified carbon cloth as high performance electrochemical capacitor electrodes. Electrochim Acta 2016 10 September 2016;212:662-670.

(53) Sun K, Zhang S, Li P, Xia Y, Zhang X, Du D, et al. Review on application of PEDOTs and PEDOT:PSS in energy conversion and storage devices. J Mater Sci : Mater Electron 2015 07/01;26(7):4438-4462.

(54) Lv D, Chen W, Shen W, Peng M, Zhang X, Wang R, et al. Enhanced flexible room temperature ammonia sensor based on PEDOT: PSS thin film with FeCl3 additives prepared by inkjet printing. Sensors Actuators B: Chem 2019;298:126890.

(55) Manivannan K, Sivakumar M, Cheng C, Lu C, Chen J. An effective electrochemical detection of chlorogenic acid in real samples: Flower-like ZnO surface covered on PEDOT:PSS composites modified glassy carbon electrode. Sensors Actuators B: Chem 2019;301:127002.

(56) Song S, Wang K, Zhang Y, Wang Y, Zhang C, Wang X, et al. Self-assembly of graphene oxide/PEDOT:PSS nanocomposite as a novel adsorbent for uranium immobilization from wastewater. Environmental Pollution 2019;250:196.

(57) Baruah B, Kumar A. PEDOT:PSS/MnO2/rGO ternary nanocomposite based anode catalyst for enhanced electrocatalytic activity of methanol oxidation for direct methanol fuel cell. Synth Met 2018;245:74.

(58) Baruah B, Kumar A, Umapathy GR, Ojha S. Enhanced electrocatalytic activity of ion implanted rGO/PEDOT:PSS hybrid nanocomposites towards methanol electro-oxidation in direct methanol fuel cells. J Electroanal Chem 2019;840:35.

(59) Syed Zainol Abidin,Shariffah Nur Jannah, Mamat MS, Rasyid SA, Zainal Z, Sulaiman Y. Electropolymerization of poly(3,4-ethylenedioxythiophene) onto polyvinyl alcohol-

graphene quantum dot-cobalt oxide nanofiber composite for high-performance supercapacitor. Electrochimica Acta 2018 20 January 2018;261:548-556.

(60) Ellis H, Vlachopoulos N, Häggman L, Perruchot C, Jouini M, Boschloo G, et al. PEDOT counter electrodes for dye-sensitized solar cells prepared by aqueous micellar electrodeposition. Electrochim Acta 2013 30 September 2013;107:45-51.

(61) Fonseca SM, Moreira T, Parola AJ, Pinheiro C, Laia CAT. PEDOT electrodeposition on oriented mesoporous silica templates for electrochromic devices. Solar Energy Materials and Solar Cells 2017 January 2017;159:94-101.

(62) Kim J, Kim E, Won Y, Lee H, Suh K. The preparation and characteristics of conductive poly(3,4-ethylenedioxythiophene) thin film by vapor-phase polymerization. Synthetic Metals 2003 5 September 2003;139(2):485-489.

(63) Madl CM, Kariuki PN, Gendron J, Piper LFJ, Jones WE. Vapor phase polymerization of poly (3,4-ethylenedioxythiophene) on flexible substrates for enhanced transparent electrodes. Synthetic Metals 2011 July 2011;161(13):1159-1165.

(64) Metsik J, Timusk M, Käämbre T, Mändar H, Umalas M, Kuus A, et al. Stability of poly(3,4-ethylenedioxythiophene) thin films prepared by vapor phase polymerization. Polymer Degradation and Stability 2016 April 2016;126:170-178.

(65) Padmalekha KG, Admassie S. Electrochromic, magnetotransport and AC transport properties of vapor phase polymerized PEDOT (VPP PEDOT). Synthetic Metals 2009 September 2009;159(17):1885-1889.

(66) Alf ME, Asatekin A, Barr MC, Baxamusa SH, Chelawat H, Ozaydin-Ince G, et al. Chemical Vapor Deposition of Conformal, Functional, and Responsive Polymer Films. Adv Mater 2010 05/11; 2019/10;22(18):1993-2027.

(67) Fabretto M, Zuber K, Hall C, Murphy P, Griesser HJ. The role of water in the synthesis and performance of vapour phase polymerised PEDOT electrochromic devices. J Mater Chem 2009;19(42):7871-7878.

(68) Lee S, Paine DC, Gleason KK. Heavily Doped poly(3,4-ethylenedioxythiophene) Thin Films with High Carrier Mobility Deposited Using Oxidative CVD: Conductivity Stability and Carrier Transport. Advanced Functional Materials 2014;24(45):7187-7196.

(69) Arnold SP, Harris JK, Neelamraju B, Rudolph M, Ratcliff EL. Microstructure-dependent electrochemical properties of chemical-vapor deposited poly(3,4-ethylenedioxythiophene) (PEDOT) films. Synth Met 2019 July 2019;253:26-33.

(70) Im SG, Olivetti EA, Gleason KK. Systematic control of the electrical conductivity of poly (3,4-ethylenedioxythiophene) via oxidative chemical vapor deposition (oCVD). Surface and Coatings Technology 2007 25 September 2007;201(22):9406-9412.

(71) Lock JP, Lutkenhaus JL, Zacharia NS, Im SG, Hammond PT, Gleason KK. Electrochemical investigation of PEDOT films deposited via CVD for electrochromic applications. Synth Met 2007 November 2007;157(22):894-898.

(72) Brooke R, Cottis P, Talemi P, Fabretto M, Murphy P, Evans D. Recent advances in the synthesis of conducting polymers from the vapour phase. Progress in Materials Science 2017 May 2017;86:127-146.

(73) Hojati-Talemi P, Simon GP. Electropolymerization of Polypyrrole/Carbon Nanotube Nanocomposite Films over an Electrically Nonconductive Membrane. J Phys Chem C 2010 08/26;114(33):13962-13966.

(74) Vepřek S. Plasma-induced and plasma-assisted chemical vapour deposition. Thin Solid Films 1985 16 August 1985;130(1):135-154.

(75) Chrisey DB, Piquè A, McGill RA, Horwitz JS, Ringeisen BR, Bubb DM, et al. Laser Deposition of Polymer and Biomaterial Films. Chem Rev 2003 02/01;103(2):553-576.

(76) Cho B, Park KS, Baek J, Oh HS, Koo Lee Y, Sung MM. Single-Crystal Poly(3,4-ethylenedioxythiophene) Nanowires with Ultrahigh Conductivity. Nano Lett 2014 06/11;14(6):3321-3327.

(77) Chelawat H, Vaddiraju S, Gleason K. Conformal, Conducting Poly(3,4-ethylenedioxythiophene) Thin Films Deposited Using Bromine as the Oxidant in a Completely Dry Oxidative Chemical Vapor Deposition Process. Chem Mater 2010 05/11;22(9):2864-2868.

(78) Chen R, Sun K, Zhang Q, Zhou Y, Li M, Sun Y, et al. Sequential Solution Polymerization of Poly(3,4-ethylenedioxythiophene) Using V2O5 as Oxidant for Flexible Touch Sensors. iScience 2019 22 February 2019;12:66-75.

(79) Bubnova O, Khan ZU, Wang H, Braun S, Evans DR, Fabretto M, et al. Semi-metallic polymers. Nature Materials 2013 12/08;13:190.

(80) Nielsen CB, Giovannitti A, Sbircea D, Bandiello E, Niazi MR, Hanifi DA, et al. Molecular Design of Semiconducting Polymers for High-Performance Organic Electrochemical Transistors. J Am Chem Soc 2016 08/17;138(32):10252-10259.

(81) Rudd S, Franco-Gonzalez J, Kumar Singh S, Ullah Khan Z, Crispin X, Andreasen JW, et al. Charge transport and structure in semimetallic polymers. J Polym Sci Part B: Polym Phys 2018 01/01; 2019/10;56(1):97-104.

(82) Wang X, Zhang X, Sun L, Lee D, Lee S, Wang M, et al. High electrical conductivity and carrier mobility in oCVD PEDOT thin films by engineered crystallization and acid treatment. Science advances 2018 09/14;4(9):eaat5780-eaat5780.

(83) Abdah MAAM, Azman NHN, Kulandaivalu S, Sulaiman Y. Review of the use of transition-metal-oxide and conducting polymer-based fibres for high-performance supercapacitors. Materials & Design 2019 Available online 13 September 2019:108199.

(84) Long Y, Li M, Gu C, Wan M, Duvail J, Liu Z, et al. Recent advances in synthesis, physical properties and applications of conducting polymer nanotubes and nanofibers. Progress in Polymer Science 2011 October 2011;36(10):1415-1442.

(85) Yoo J, Kim J, Kim YS. Liquid electrolyte-free cylindrical Al polymer capacitor review: Materials and characteristics. Journal of Power Sources 2015 15 June 2015;284:466-480.

(86) Rajesh M, Justin Raj C, Kim BC, Manikandan R, Kim KH, Park SY, et al. Evaporative successive ionic layer adsorption and reaction polymerization of PEDOT: a simple and cost effective technique for binder free supercapacitor electrodes. Electrochimica Acta 2017 20 June 2017;240:231-238.

(87) Rivnay J, Inal S, Salleo A, Owens R, Berggren M, Malliaras GG. Organic electrochemical transistors. Nature Reviews Materials 2018 01/16;3(2):17086.

(88) Chung DDL. Thermoelectric polymer-matrix structural and nonstructural composite materials. Advanced Industrial and Engineering Polymer Research 2018;1(1):61.

(89) Li Y, Du Y, Dou Y, Cai K, Xu J. PEDOT-based thermoelectric nanocomposites - A mini-review. Synth Met 2017;226:119.

(90) Wang H, Yu C. Organic Thermoelectrics: Materials Preparation, Performance Optimization, and Device Integration. Joule 2019 16 January 2019;3(1):53-80.

(91) Ahmed U, Alizadeh M, Rahim NA, Shahabuddin S, Ahmed MS, Pandey AK. A comprehensive review on counter electrodes for dye sensitized solar cells: A special focus on Pt-TCO free counter electrodes. Solar Energy 2018 1 November 2018;174:1097-1125.

(92) Murakami TN, Grätzel M. Counter electrodes for DSC: Application of functional materials as catalysts. Inorganica Chimica Acta 2008 15 February 2008;361(3):572-580.

(93) Xia J, Yanagida S. Strategy to improve the performance of dye-sensitized solar cells: Interface engineering principle. Solar Energy 2011 December 2011;85(12):3143-3159.

(94) Barr MC, Rowehl JA, Lunt RR, Xu J, Wang A, Boyce CM, et al. Direct Monolithic Integration of Organic Photovoltaic Circuits on Unmodified Paper. Adv Mater 2011;23(31):3500-3505.

(95) Pitchaiya S, Natarajan M, Santhanam A, Asokan V, Yuvapragasam A, Madurai Ramakrishnan V, et al. A review on the classification of organic/inorganic/carbonaceous hole transporting materials for perovskite solar cell application. Arabian Journal of Chemistry 2018 Available online 28 June 2018.

(96) Bae J, Shin K, Kwon OS, Hwang Y, An J, Jang A, et al. A succinct review of refined chemical sensor systems based on conducting polymer–cyclodextrin hybrids. Journal of Industrial and Engineering Chemistry 2019 25 November 2019;79:19-28.

(97) Uppalapati D, Boyd BJ, Garg S, Travas-Sejdic J, Svirskis D. Conducting polymers with defined micro- or nanostructures for drug delivery. Biomaterials 2016;111:149.

(98) Talikowska M, Fu X, Lisak G. Application of conducting polymers to wound care and skin tissue engineering: A review. Biosensors and Bioelectronics 2019 15 June 2019;135:50-63.

(99) Walker BW, Lara RP, Mogadam E, Yu CH, Kimball W, Annabi N. Rational design of microfabricated electroconductive hydrogels for biomedical applications. Progress in Polymer Science 2019;92:135.

(100) Alegret N, Dominguez-Alfaro A, Salsamendi M, Gomez IJ, Calvo J, Mecerreyes D, et al. Effect of the fullerene in the properties of thin PEDOT/C60 films obtained by co-electrodeposition. Inorg Chim Acta 2017 1 November 2017;468:239-244.

(101) Lete C, Marin M, Anghel EM, Preda L, Matei C, Lupu S. Sinusoidal voltage electrodeposition of PEDOT-Prussian blue nanoparticles composite and its application to amperometric sensing of H2O2 in human blood. Materials Science and Engineering: C 2019 September 2019;102:661-669.

(102) Paterakis G, Raptis D, Ploumistos A, Belekoukia M, Sygellou L, Ramasamy MS, et al. N-Doped graphene/PEDOT composite films as counter electrodes in DSSCs: Unveiling the mechanism of electrocatalytic activity enhancement. Appl Surf Sci 2017 30 November 2017;423:443-450.

(103) Sun D, Li H, Li M, Li C, Dai H, Sun D, et al. Electrodeposition synthesis of a NiO/CNT/PEDOT composite for simultaneous detection of dopamine, serotonin, and tryptophan. Sensors Actuators B: Chem 2018 15 April 2018;259:433-442.

(104) Ni D, Song H, Chen Y, Cai K. Significantly enhanced thermoelectric performance of flexible PEDOT nanowire film via coating Te nanostructures. Journal of Materiomics 2019 Available online 3 July 2019.

(105) Xiao Y, Wu J, Yue G, Lin J, Huang M, Lan Z, et al. Electrodeposition of high performance PEDOT/Ti counter electrodes on Ti meshes for large-area flexible dye-sensitized solar cells. Electrochim Acta 2012 15 December 2012;85:432-437.

(106) Alkhazaili A, Hamasha MM, Choi G, Lu S, Westgate CR. Reliability of thin films: Experimental study on mechanical and thermal behavior of indium tin oxide and poly(3,4-ethylenedioxythiophene). Microelectronics Reliability 2015 February–March 2015;55(3):538-546.

(107) Verge P, Vidal F, Aubert P, Beouch L, Tran-Van F, Goubard F, et al. Thermal ageing of poly(ethylene oxide)/poly(3,4-ethylenedioxythiophene) semi-IPNs. European Polymer Journal 2008 November 2008;44(11):3864-3870.

(108) Vitoratos E, Sakkopoulos S, Dalas E, Paliatsas N, Karageorgopoulos D, Petraki F, et al. Thermal degradation mechanisms of PEDOT:PSS. Organic Electronics 2009 February 2009;10(1):61-66.

(109) Bontapalle S, Varughese S. Understanding the mechanism of ageing and a method to improve the ageing resistance of conducting PEDOT:PSS films. Polymer Degradation and Stability 2020 January 2020;171:109025.

(110) Zanfrognini B, Colina A, Heras A, Zanardi C, Seeber R, Lòpez-Palacios J. A UV-Visible/Raman spectroelectrochemical study of the stability of poly(3,4-ethylendioxythiophene) films. Polym Degrad Stab 2011;96(12):2112.

(111) Winter I, Reese C, Hormes J, Heywang G, Jonas F. The thermal ageing of poly(3,4-ethylenedioxythiophene). An investigation by X-ray absorption and X-ray photoelectron spectroscopy. Chemical Physics 1995 1 May 1995;194(1):207-213.

(112) Winther-Jensen B, West K. Stability of highly conductive poly-3,4-ethylene-dioxythiophene. Reactive and Functional Polymers 2006 May 2006;66(5):479-483.

(113) Kawano K, Pacios R, Poplavskyy D, Nelson J, Bradley DDC, Durrant JR. Degradation of organic solar cells due to air exposure. Solar Energy Materials and Solar Cells 2006 15 December 2006;90(20):3520-3530.

(114) Madhan Kumar A, Adesina AY, Hussein MA, Ramakrishna S, Al-Aqeeli N, Akhtar S, et al. PEDOT/FHA nanocomposite coatings on newly developed Ti-Nb-Zr implants: Biocompatibility and surface protection against corrosion and bacterial infections. Materials Science and Engineering: C 2019 May 2019;98:482-495.

(115) Nakova A, Ilieva M, Boijadjieva-Scherzer T, Tsakova V. Glycerol oxidation on Pd nanocatalysts obtained on PEDOT-coated graphite supports. Electrochimica Acta 2019 20 May 2019;306:643-650.

(116) Zhuzhelskii DV, Tolstopjatova EG, Eliseeva SN, Ivanov AV, Miao S, Kondratiev VV. Electrochemical properties of PEDOT/WO3 composite films for high performance supercapacitor application. Electrochimica Acta 2019 10 March 2019;299:182-190.

(117) Tamburri E, Sarti S, Orlanducci S, Terranova ML, Rossi M. Study of PEDOT conductive polymer films by admittance measurements. Materials Chemistry and Physics 2011 15 February 2011;125(3):397-404.

(118) Szkoda M, Nowaczyk G, Lisowska-Oleksiak A, Siuzdak K. The influence of polarization of titania nanotubes modified by a hybrid system made of a conducting

polymer PEDOT and Prussian Blue redox network on the Raman spectroscopy response and photoelectrochemical properties. Electrochim Acta 2018;279:34.

(119) Feng Z, Wu J, Cho W, Leach MK, Franz EW, Naim YI, et al. Highly aligned poly(3,4-ethylene dioxythiophene) (PEDOT) nano- and microscale fibers and tubes. Polymer 2013;54(2):702.

(120) Garcìa-Barberà A, Culebras M, Roig-Sànchez S, Gòmez CM, Cantarero A. Three dimensional PEDOT nanowires network. Synth Met 2016;220:208.

(121) Augusto T, Neto ET, Neto AAT, Vichessi R, Vidotti M, Torresi SICd. Electrophoretic deposition of Au@PEDOT nanoparticles towards the construction of high-performance electrochromic electrodes. Solar Energy Mater Solar Cells 2013;118:72.

(122) Clark RJH, Curri ML. The identification by Raman microscopy and X-ray diffraction of iron-oxide pigments and of the red pigments found on Italian pottery fragments. Journal of Molecular Structure 1998 1 January 1998;440(1):105-111.

(123) Li Y, Church JS, Woodhead AL. Infrared and Raman spectroscopic studies on iron oxide magnetic nano-particles and their surface modifications. Journal of Magnetism and Magnetic Materials 2012 April 2012;324(8):1543-1550.

(124) Lübbe M, Gigler AM, Stark RW, Moritz W. Identification of iron oxide phases in thin films grown on Al2O3(0001) by Raman spectroscopy and X-ray diffraction. Surface Science 2010 15 April 2010;604(7):679-685.

(125) dos Santos IFS, Hutchinson I, Ingley R, Edwards HGM, de Faria DLA. Amorphous iron oxides investigated by portable and bench-top Raman spectrometers: An extraterrestrial analytical perspective. Vibrational Spectroscopy 2016 November 2016;87:20-26.

(126) Noriega R, Rivnay J, Vandewal K, Koch FPV, Stingelin N, Smith P, et al. A general relationship between disorder, aggregation and charge transport in conjugated polymers. Nature Materials 2013 11/01;12(11):1038-1044.